

UNIVERSITY OF KWA-ZULU NATAL



UNIVERSITY OF  
KWAZULU-NATAL

**Uncoded Space-Time Labelling Diversity:  
Data Rate & Reliability Enhancements and Application to  
Real-World Satellite Broadcasting**

by

Sulaiman Saleem Patel

Supervised by:

Dr Tahmid Quazi

Prof. Hongjun Xu

A thesis submitted in fulfillment for the degree of  
Doctor of Philosophy in Electronic Engineering

in the

Discipline of Electrical, Electronic and Computer Engineering,  
College of Agriculture, Engineering and Science,  
University of Kwa-Zulu Natal, Durban, South Africa

March 2019

# Declaration of Authorship

I, **Sulaiman Saleem Patel**, declare that this thesis titled, ‘**Uncoded Space-Time Labelling Diversity: Data Rate & Reliability Enhancements and Application to Real-World Satellite Broadcasting**’ and the work presented in it are my own. I confirm that:

- The research reported in this thesis, except where otherwise indicated, is my original work.
- This thesis has not been submitted for any degree or examination at any other university.
- This thesis does not contain other persons data, pictures, graphs or other information, unless specifically acknowledged as being sourced from other persons.
- This thesis does not contain other persons writing, unless specifically acknowledged as being sourced from other researchers. Where other written sources have been quoted, then: i) their words have been re-written but the general information attributed to them has been referenced and ii) where their exact words have been used, their writing has been placed inside quotation marks, and referenced.
- Where I have reproduced a publication of which I am an author, co-author or editor, I have indicated in detail which part of the publication was written by myself alone and have fully referenced such publications.
- This thesis does not contain text, graphics or tables copied and pasted from the Internet, unless specifically acknowledged, and the source being detailed in the thesis and in the References sections.

Signed:

---

Date:

---

As the candidate’s supervisor, I, **Tahmid Quazi**, agree to the submission of this thesis.

Signed:

---

Date:

---

UNIVERSITY OF KWA-ZULU NATAL

## *Abstract*

Doctor of Philosophy in Electronic Engineering

**Uncoded Space-Time Labelling Diversity:**

**Data Rate & Reliability Enhancements and Application to Real-World Satellite Broadcasting**

by Sulaiman Saleem Patel

Satellite broadcasting is among the key technologies considered to enable Internet access for the worlds least developed economies. Recent studies have considered designing multiple-input, multiple-output (MIMO) satellite broadcasting schemes based on their terrestrial variants. The research presented in this thesis proposes enhancements to the recent terrestrial Uncoded Space-Time Labelling Diversity (USTLD) scheme, and its adaptation to satellite systems. The first extension to the original USTLD model that is presented enhances its spectral efficiency by utilising more transmit antennas. This leads to two key challenges when considering implementation: exponentially increased detection complexity, which results in higher latencies, and antenna correlation in devices with limited available space. To combat the increased detection complexity, existing low-complexity detection algorithms (LCDAs) based on QR decomposition (QRD) are adapted and applied to USTLD systems. The existing LCDAs are found to not achieve optimal detection accuracy when benchmarked with maximum-likelihood detection (MLD), which achieves optimal detection accuracy but incurs high complexity. Thus, a new QRD-based LCDA designed specifically for USTLD systems is developed. Results show that the new LCDA achieves the same detection accuracy as MLD with a complexity reduction of 79.75% and 92.53% for the USTLD systems investigated.

The effect of antenna correlation is then studied for harsh fading channels with no line-of-sight between transmitter and receiver. By using the Kronecker correlation model to consider transmit and receive antenna correlation independently, it is found that USTLD systems are more sensitive to correlation at the transmitter than at the receiver. It is shown that USTLD systems are more susceptible to correlation than comparable Alamouti space-time block coded systems. The results show that an antenna spacing of  $0.4\lambda$  is optimal, where  $\lambda$  is the transmission carrier wavelength.

The second extension to the USTLD model considered is to further improve its link reliability by incorporating polarisation diversity. These uncoded space-time-polarisation-labelling diversity (STPLD) systems are studied in the context of MIMO satellite broadcasting, using modulation schemes from the DVB-S2X satellite broadcasting standard.

To produce mappers that achieve labelling diversity for these modulation schemes, a genetic algorithm is designed and implemented. Results show that these novel mappers result in a gain in the range of 5dB to 7dB. Additionally, the polarisation diversity allows the STPLD system to achieve twice the diversity order of the original USTLD system. The effects of inter-antenna and inter-beam correlation in STPLD systems are also studied. It is found that transmit-side correlation causes the greatest performance degradation of the STPLD system. It is also observed that the STPLD system is more sensitive to inter-beam correlation than inter-antenna correlation.

## *Acknowledgements*

This work would not have been possible without the exemplary support of my those around me. Thank you to Dr Quazi and Prof. Xu, for their guidance and unwavering faith in my ability. Thank you to the family and friends who unknowingly inspire and motivate me to reach for new heights every day. Most of all, I give thanks to God Almighty for granting me the strength to overcome the challenges I faced, and for blessing me in more ways than I will ever know.

*“Knowledge is the life of the mind.”*

~ Abu Bakr as-Siddiq (R.A.)

*“If you trust in yourself. . . and believe in your dreams. . . and follow your star. . . you’ll still get beaten by people who spent their time working hard and learning things and weren’t so lazy.”*

~ Terry Pratchett

# Contents

<b>Declaration of Authorship</b>	<b>i</b>
<b>Abstract</b>	<b>ii</b>
<b>Acknowledgements</b>	<b>iv</b>
<b>List of Figures</b>	<b>vii</b>
<b>List of Tables</b>	<b>ix</b>
<b>Abbreviations</b>	<b>x</b>
<b>1 Research Background</b>	<b>1</b>
1.1 Introduction . . . . .	1
1.1.1 Motivation and Context . . . . .	1
1.1.1.1 The Internet as a Human Right and the Digital Divide . . . . .	1
1.1.1.2 Wireless Communication Systems for Developed & Developing Nations	2
1.1.2 Technical Overview of Wireless Communication Systems . . . . .	2
1.1.2.1 Link Reliability and Diversity . . . . .	2
1.1.2.2 Spectral Efficiency and Data Rate . . . . .	6
1.1.2.3 Challenges for Real-World Implementation . . . . .	7
1.2 Research Objectives . . . . .	9
1.2.1 The Original Uncoded Space-Time Labelling Diversity System . . . . .	9
1.2.2 Proposed Enhancements . . . . .	10
1.3 Contributions . . . . .	11
<b>2 Journal Article 1</b>	<b>22</b>
2.1 Abstract . . . . .	23
2.2 Introduction . . . . .	24
2.3 System Model . . . . .	28
2.3.1 Transmission Model . . . . .	28
2.3.2 Detection Model . . . . .	29
2.3.2.1 Maximum Likelihood Detection . . . . .	29
2.3.2.2 Standard QR Decomposition and QRD-m . . . . .	30
2.3.2.3 QR-QL Parallel Searching . . . . .	33
2.3.2.4 Extended QR-QL Parallel Searching Algorithm . . . . .	34

2.3.2.5	Proposed LCDA: Multiple Stage Reduced Set Detection for USTLD	35
2.4	Performance Analysis	38
2.4.1	Average Bit Error Probability for High-Rate USTLD	38
2.4.2	Analytical Evaluation of Algorithmic Complexity	39
2.5	Results and Discussion	41
2.6	Conclusion	47
2.7	Appendix: Derivations of Complexity in Terms of Effective Real Operations	48
2.7.1	MLD Derivation	48
2.7.2	QRD, QRD-m and QRLPSA Derivations	48
2.7.3	Extended QRLPSA Derivation	50
2.7.4	MSRSD-USTLD Derivation	50
<b>3</b>	<b>Journal Article 2</b>	<b>54</b>
3.1	Abstract	55
3.2	Introduction	56
3.3	System Model	59
3.3.1	Transmission Model	59
3.3.2	Correlation Model	60
3.3.3	Detection	61
3.4	Error Performance Analysis	62
3.4.1	Uncorrelated Nakagami-q Error Performance	62
3.4.2	Correlated Nakagami-q Error Performance	64
3.5	Results and Discussion	66
3.6	Conclusion	72
3.7	Appendix: Details of Uncorrelated Nakagami-q Derivation	73
<b>4</b>	<b>Journal Article 3</b>	<b>80</b>
4.1	Abstract	81
4.2	Introduction	82
4.3	System Model	85
4.3.1	Space, Time, Polarisation and Labelling Diversity	85
4.3.2	Modulation Scheme	86
4.3.3	Transmission and Detection Models of Proposed System	87
4.3.4	Correlation Model	89
4.4	Analysis of Error Performance	92
4.4.1	Uncorrelated Error Performance	92
4.4.2	Correlated Error Performance	96
4.5	Mapper Design to achieve Labelling Diversity	100
4.5.1	Description of Genetic Algorithm for Secondary Mapper Design	101
4.5.1.1	Genes, Chromosomes and the Population	102
4.5.1.2	Imitating ‘Evolution’	102
4.5.1.3	Evaluating Candidate Secondary Mappers	103
4.5.2	Designed Mappers for STPLD System	106
4.6	Results and Discussion	110
4.6.1	Error Performance of Proposed System	110
4.6.2	Correlation Study	114
4.7	Conclusion	118
<b>5</b>	<b>Concluding Remarks</b>	<b>124</b>

# List of Figures

1.1	Illustration of Detection without Labelling Diversity . . . . .	5
1.2	Illustration of Joint Detection with Labelling Diversity . . . . .	5
1.3	Block Diagram of a USTLD Transmitter . . . . .	9
2.1	16QAM Binary Constellation Mapping, Key: $\Omega_1/\Omega_2$ . . . . .	28
2.2	Illustration of a QRD Search Tree . . . . .	30
2.3	Illustration of a QRD-m Search Tree . . . . .	33
2.4	Block Diagram of Extended QRLPSA . . . . .	34
2.5	Block Diagram of MSRS-D-USTLD . . . . .	35
2.6	Analytical ABEP converging to simulated results using ML Detection . . . . .	41
2.7	Bit Error Rate Comparison of Uncoded Systems with Equal Data Rate . . . . .	42
2.8	Comparison of LCDA Accuracy for $4 \times 4$ 16QAM HR-USTLD . . . . .	44
2.9	Comparison of LCDA Accuracy for $4 \times 5$ 16PSK HR-USTLD . . . . .	45
3.1	16QAM Binary Constellation Mapping. Key: $\Omega_1/\Omega_2$ . . . . .	59
3.2	Comparison of Theoretical and Simulated Results: $2 \times 3$ 16QAM USTLD . . . . .	66
3.3	Comparison of Theoretical and Simulated Results: $2 \times 3$ 16PSK USTLD . . . . .	67
3.4	Comparison of Theoretical and Simulated Results: Different USTLD Systems with Transmit and Receive Antenna Correlation . . . . .	67
3.5	Effect of Fading Parameter $q$ at 20dB. . . . .	68
3.6	Comparing the Effects of Transmit and Receive Antenna Correlation at 15dB ( $q = 0.2$ ) . . . . .	69
3.7	Comparing the Performance of USTLD and Alamouti-Coded Systems at 13dB ( $q = 0.7$ ) . . . . .	70
4.1	Illustration of the proposed STPLD system . . . . .	88
4.2	High-Level Illustration of Genetic Algorithm . . . . .	101
4.3	Simplified Illustration of “Evolution and Natural Selection” during each Iteration of the Genetic Algorithm . . . . .	106
4.4	8APSK Constellation Mappings . . . . .	107
4.5	16APSK Constellation Mappings . . . . .	108
4.6	32APSK Constellation Mappings . . . . .	108
4.7	64APSK Constellation Mappings . . . . .	109
4.8	BER Performance of $2 \times 2$ 16APSK OSTBC, OSTPBC, USTLD and STPLD Systems, $q = 0.3$ . . . . .	111
4.9	BER Performance of $2 \times 4$ 32APSK OSTBC, OSTPBC, USTLD and STPLD Systems, $q = 0.3$ . . . . .	112
4.10	BER Performance of $2 \times 2$ 64APSK OSTBC, OSTPBC, USTLD and STPLD Systems, $q = 0.7$ . . . . .	113
4.11	Validation of (4.34) for $2 \times 3$ 8APSK STPLD Systems with Transmit-Side and Receive-Side Correlation, $q = 0.5$ . . . . .	114

---

4.12	Validation of (4.34) for $2 \times 3$ 8APSK STPLD Systems with Inter-Antenna and Inter-Beam Interference, $q = 0.5$ . . . . .	115
4.13	Effect of Transmit-Side IAI and IBI on $2 \times 3$ 8APSK, $q = 0.5$ , $\gamma = 25\text{dB}$ . . . . .	115
4.14	Effect of Receive-Side IAI and IBI on $2 \times 3$ 8APSK, $q = 0.5$ , $\gamma = 25\text{dB}$ . . . . .	116
4.15	Effect of Transmit-Side and Receive-Side IAI and IBI on $2 \times 3$ 8APSK, $q = 0.5$ , $\gamma = 25\text{dB}$ . . . . .	116

# List of Tables

1.1	Key Concepts for understanding labelling diversity . . . . .	4
2.1	Algorithm for generating lookup table entries of $\xi_i^\lambda, i \in [1 : M]$ . . . . .	37
2.2	Complexity Comparison of LCDAs in terms of Number of Candidate Label Vectors .	40
2.3	Complexity Comparison of LCDAs in terms of Effective Real Operations . . . . .	40
2.4	Diversity Order Comparison of Systems in Figure 2.7 . . . . .	42
2.5	Comparison of LCDA Complexity for HR-USTLD System in Figure 2.8 . . . . .	44
2.6	Comparison of LCDA Complexity for HR-USTLD System in Figure 2.9 . . . . .	45
3.1	Simulation Parameters for Figures 3.2 to 3.4 . . . . .	68
4.1	Nomenclature for describing systems with Labelling Diversity . . . . .	86
4.2	Description of APSK Constellations . . . . .	87
4.3	Details of Parameters used in implementing Genetic Algorithm . . . . .	107
5.1	Summary of Key Results . . . . .	125

# Abbreviations

<b>ABEP</b>	<b>A</b> verage <b>B</b> it <b>E</b> rror <b>P</b> robability
<b>APSK</b>	<b>A</b> mplitude <b>P</b> hase <b>S</b> hift <b>K</b> eying
<b>AWGN</b>	<b>A</b> dditive <b>W</b> hite <b>G</b> aussian <b>N</b> oise
<b>BICSS-ID</b>	<b>B</b> it- <b>I</b> nterleaved <b>C</b> oded <b>S</b> ystems with <b>I</b> terative <b>D</b> ecoding
<b>ECM</b>	<b>E</b> xponential <b>C</b> orrelation <b>M</b> odel
<b>ED</b>	<b>E</b> uclidean <b>D</b> istance
<b>GA</b>	<b>G</b> enetic <b>A</b> lgorithm
<b>GRV</b>	<b>G</b> aussian <b>R</b> andom <b>V</b> ariable
<b>HR-USTLD</b>	<b>H</b> igh- <b>R</b> ate <b>U</b> ncoded <b>S</b> pace- <b>T</b> ime <b>L</b> abelling <b>D</b> iversity
<b>IAI</b>	<b>I</b> nter- <b>A</b> ntenna <b>I</b> nterference
<b>IBI</b>	<b>I</b> nter- <b>B</b> eam <b>I</b> nterference
<b>i.i.d.</b>	<b>i</b> ndependent and <b>i</b> dentically <b>d</b> istributed
<b><math>\mathcal{K}</math>-HSX</b>	<b><math>\mathcal{K}</math></b> -point <b>H</b> ypersphere <b>S</b> wap <b>C</b> rossover
<b>LCDA</b>	<b>L</b> ow- <b>C</b> omplexity <b>D</b> etection <b>A</b> lgorithm
<b>LDC</b>	<b>L</b> east <b>D</b> eveloped <b>C</b> ountry
<b>MGF</b>	<b>M</b> oment <b>G</b> enerating <b>F</b> unction
<b>MIMO</b>	<b>M</b> ultiple- <b>I</b> nter <b>M</b> ultiple- <b>O</b> utput
<b>MLD</b>	<b>M</b> aximum- <b>L</b> ikelihood <b>D</b> etection
<b>MSRSD-USTLD</b>	<b>M</b> ultiple <b>S</b> tage <b>R</b> educed <b>S</b> et <b>D</b> etection for <b>U</b> STLD
<b>ODP</b>	<b>O</b> rthogonally <b>D</b> ual- <b>P</b> olarised
<b>OSTBC</b>	<b>O</b> rothogonal <b>S</b> pace- <b>T</b> ime <b>B</b> lock <b>C</b> ode
<b>OSTPBC</b>	<b>O</b> rothogonal <b>S</b> pace- <b>T</b> ime- <b>P</b> olarisation <b>B</b> lock <b>C</b> ode
<b>PEP</b>	<b>P</b> airwise <b>E</b> rror <b>P</b> robability
<b>PSK</b>	<b>P</b> hase <b>S</b> hift <b>K</b> eying
<b>Q-STBC</b>	<b>Q</b> uasi-orthogonal <b>S</b> pace- <b>T</b> ime <b>B</b> lock <b>C</b> ode
<b>QAM</b>	<b>Q</b> uadrature <b>A</b> mplitude <b>M</b> odulation

---

<b>QAP</b>	<b>Q</b> uadratic <b>A</b> ssignment <b>P</b> roblem
<b>QLD</b>	<b>Q</b> L <b>D</b> ecomposition
<b>QRD</b>	<b>Q</b> R <b>D</b> ecomposition
<b>QRLPSA</b>	<b>Q</b> R- <b>Q</b> L <b>P</b> arallel <b>S</b> earching <b>A</b> lgorithm
<b>RV</b>	<b>R</b> andom <b>V</b> ariable
<b>SD</b>	<b>S</b> pherical <b>D</b> etection
<b>SNR</b>	<b>S</b> ignal-to- <b>N</b> oise <b>R</b> atio
<b>SSG</b>	<b>S</b> ingle- <b>S</b> ided <b>G</b> aussian
<b>STBC</b>	<b>S</b> pace- <b>T</b> ime <b>B</b> lock <b>C</b> ode
<b>STPLD</b>	<b>S</b> pace- <b>T</b> ime- <b>P</b> olarisation- <b>L</b> abelling <b>D</b> iversity
<b>USTLD</b>	<b>U</b> ncoded <b>S</b> pace- <b>T</b> ime <b>L</b> abelling <b>D</b> iversity
<b>V-BLAST</b>	<b>V</b> ertical- <b>B</b> ell Laboratories <b>L</b> ayered <b>S</b> pace- <b>T</b> ime

# Chapter 1

## Research Background

### 1.1 Introduction

#### 1.1.1 Motivation and Context

##### 1.1.1.1 The Internet as a Human Right and the Digital Divide

The Internet has revolutionised the way humans interact with each other and the world around them, making it arguably the most important innovation in mankind's history. As of 30 June 2018, it has been reported that there are over 4.2 billion Internet users across the world – signifying a 1066% growth since the year 2000 [1]. Technologies such as instant messaging and social media have become ingrained in the daily lives of individuals from all demographics throughout the world, revolutionising how humans interact and communicate with each other [2, 3]. Considering a broader perspective, the Internet has also shaped the modern socio-economic landscape by serving as a catalyst for human rights movements, disseminating information regarding global challenges (such as climate change) and improving access to international markets for businesses of different scales [4–6]. Due to the wide-scale benefits of the Internet, 83% of respondents in the Global Internet Survey 2012 indicated that Internet access should be considered a basic human right [7]. A similar sentiment was shared by the United Nations Human Rights Council, which recognised the Internet as a tool for allowing individuals to exercise their right to freedom of speech [6].

However, there is an evident disparity in Internet access between developed and developing nations. Internet World Stats [1] reflects that only 55.1% of the world's population had access to the Internet as of 30 June 2018. More strikingly, Internet access had only penetrated to 36.1% and 49.0% of the African and Asian populations respectively. By comparison, the Internet penetration rate for North America and Europe were respectively reported as 95.0% and 85.2% [1]. These statistics highlight the digital divide that exists between developing nations and the first-world [9].

### 1.1.1.2 Wireless Communication Systems for Developed & Developing Nations

Wireless communication systems have emerged as a core technology to facilitate Internet access for societies in both developed and developing nations. Key advantages of wireless systems over their wired counterparts include: i) allowing the use of mobile devices within the network, ii) increased flexibility for selecting network topology, iii) ease of deployment and iv) extended coverage and range through the use of multi-hop networks and/or satellite broadcasting.

For developed nations and regions with a high Internet penetration rate, the next generation of wireless communication systems aim to provide users with better access to content. Emerging technologies like the Internet of Things [10], ultra-high definition video streaming [11] and real-time augmented reality systems [12, 13] are expected to place severe strain on the existing network infrastructure. Thus, next-generation wireless communication systems for these regions require lower latencies, improved device interconnectivity, ubiquitous access, higher data rates and better link reliability [14].

For developing nations, wireless communication systems are expected to play a key role in providing Internet access to rural areas. In particular, satellite broadcasting has been identified as viable means of facilitating Internet access to remote regions where there is limited telecommunication infrastructure [15–17]. There have already been a variety of successfully implemented projects that have used satellite broadcasting technology to provide services such as e-health and Internet-based education to rural areas [18–20].

## 1.1.2 Technical Overview of Wireless Communication Systems

### 1.1.2.1 Link Reliability and Diversity

The reliability of the link between transmitter and receiver is among the most important considerations when designing a wireless communication system. At the physical layer, link reliability is primarily determined by the robustness of the system in the presence of two sources of interference: noise and multipath fading [21, 22]. Noise arises from various natural phenomenon, such as the fluctuation of electrical characteristics in physical components due to temperature (thermal noise) and black body noise from celestial sources like the Sun [21]. Noise can also originate from man-made sources, such as: power lines, medical equipment, internal-combustion engines, electricity generators and other telecommunication systems [23, 24]. Each of these noise components are typically modelled by random variables that are assumed to follow Gaussian distribution. By the central limit theorem, their cumulative effect is also Gaussian distributed [21, 22]. Furthermore, the effect of noise is assumed to be ‘white’, indicating that it is not frequency-selective, and is modelled at the receiver as another signal superimposed on what was transmitted. This leads to the common acronym AWGN, which stands for additive white Gaussian noise. Noise can also be modelled to also

contain an impulsive component, which is usually done when considering dense urban areas with large volumes of man-made noise sources [23, 24].

Multipath fading accounts for the effects of reflection, refraction and scattering that occur during the course of transmission [21, 22]. The effect of fading introduces both amplitude distortion and phase delay to the transmitted symbol, and it is thus represented by a complex coefficient to the transmitted symbol. There exist multiple models to represent amplitude distribution of this fading coefficient; the most common of which is the Rayleigh fading model [21, 22, 25]. Rayleigh fading assumes that there is no direct line-of-sight path between the transmitter and receiver, which often provides a prudent estimate of the worst-case performance of the system. The Rayleigh fading distribution models the in-phase and quadrature components of the fading as independent and identically distributed (i.i.d.) Gaussian random variables [25]. Another well-established model of fading amplitude is the Nakagami- $q$ , or Hoyt, fading model [25–28]. Nakagami- $q$  fading models the in-phase and quadrature components of the fading as independent Gaussian random variables with different variances, which are related by the fading parameter ( $q$ ) [26]. It has been shown by Chytil that this model provides a good fit for modelling signal propagation in satellite links subjected to strong ionospheric scintillation [28]. Additionally, the Nakagami- $q$  fading model is able to represent harsher fading environments than Rayleigh model [25]. Thus, the Nakagami- $q$  model allows for better insight into the worst-case performance of the system than the Rayleigh model.

A popular technique to improve link reliability in the presence of fading is to include diversity in the system, specifically microdiversity [22, 29]. Wireless communication systems achieve diversity by sending the same information across multiple independent transmission paths, and considering multiple received signals carrying the same information concurrently during detection. The traditional mechanisms of achieving diversity may be grouped into seven categories [29]: i) time, ii) antenna, iii) frequency, iv) field, v) polarisation, vi) angle and vii) multipath. Of these mechanisms, this thesis focusses on time, antenna and polarisation diversity.

Time diversity protects against burst errors by transmitting the same information across multiple time slots [22]. As a consequence, systems employing time diversity have reduced spectral efficiency. Antenna diversity is achieved by adopting a multiple-input, multiple-output (MIMO) structure with multiple transmit and receive antennas, creating many signal paths between transmitter and receiver. These paths should ideally be i.i.d. to maximise diversity gain [22, 25]. Theoretically, the use of a large number of antennas allows for high antenna diversity gains. However, when implementing real-world wireless communication systems, physical space on devices is often limited. For example, handheld devices require a small form factor to ensure mobility and smaller multi-antenna satellites are often limited to only two antennas [77]. Increasing the number of antennas in a constrained space leads to the distance between antennas decreasing, resulting in spatial correlation [31, 32]. Spatial correlation causes a degradation in error performance and loss of diversity due to inter-antenna interference (IAI) [31–35]. To achieve polarisation diversity, literature shows that it is necessary to introduce orthogonally dual-polarised (ODP) antennas to the system [36–38, 77]. There are two

common configurations to ensure that antennas are ODP [77]. The first is to utilise linear polarisations (i.e. a horizontal/vertical polarisation pair) and the second is to utilise circular polarisations (i.e. a left/right hand circular polarisation pair). Since the polarisations are orthogonal, each polarisation from a single antenna can be considered as a separate transmission (or reception) stream. In other words, a linearly ODP antenna can either transmit or receive statistically independent signals from the horizontally and vertically polarised streams. Similar reasoning holds for a left/right hand circular polarisation pair. By increasing the number of transmission and reception streams, the use of ODP antennas at the transmitter and receiver introduces polarisation diversity to the system [36, 37]. An important consideration for systems with polarisation diversity is the effect of inter-beam interference (IBI) [77]. A possible cause of IBI is manufacturing imperfections that may result in antennas not being perfectly ODP.

Another diversity mechanism that is of importance for the research presented in this thesis is labelling diversity (also referred to as ‘constellation reassignment’ and ‘mapping diversity’ in literature) [39–50]. Labelling diversity was originally applied to bit-interleaved coded systems with iterative decoding [39–43]. However, the use of convolutional encoding and decoding in these systems incurs high detection complexity, resulting in higher latencies [21]. This has led to studies which apply labelling diversity to uncoded systems, which are typically more cost-effective and simpler to implement. Examples of these uncoded systems are: i) decode-and-forward relay systems [44], ii) multi-packet data transmissions with automatic repeat requests [46], iii) space-time block coded systems [47, 51], iv) space-time block coded systems with spatial modulation [52] and v) space-time block coded systems with channel modulation using radio frequency mirrors [53].

When discussing systems that achieve labelling diversity, it is important to have a clear understanding of the nomenclature associated with them. For this reason, Table 1.1 provides brief definitions of key concepts related to labelling diversity systems. In these systems, different bit-to-symbol mappers

TABLE 1.1: Key Concepts for understanding labelling diversity

Term	Description
Symbol	A symbol represents the magnitude and phase used when modulating the transmission carrier in order to transmit information codewords. This is represented by a complex number.
Constellation	A constellation refers to the set of all possible symbols that may be used to encode information codewords. Constellations are commonly represented with a scatter plot of points on the complex plane, where each point represents a unique symbol.
Label	The label assigned to a symbol is the information codeword associated with that symbol. Although information codewords are binary, it is common to represent labels in decimal form for brevity.
Mapping Mapper	Mapping is the process of assigning labels to symbols using a predefined function. A mapper is the mapping function which assigns labels to symbols within a constellation. The input to a mapper is the label to be assigned, and its output is the corresponding encoded symbol.

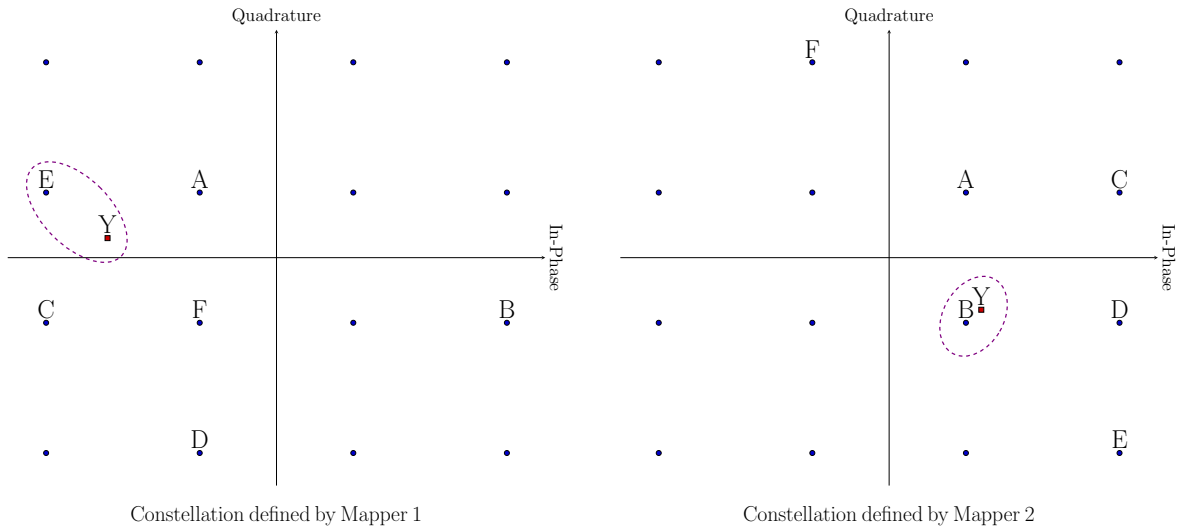


FIGURE 1.1: Illustration of Detection without Labelling Diversity

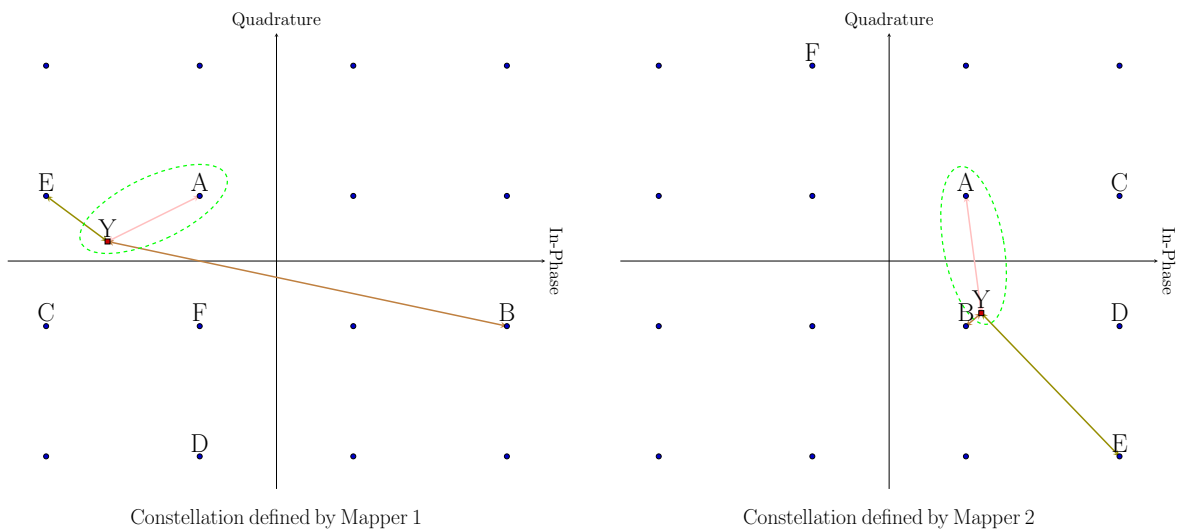


FIGURE 1.2: Illustration of Joint Detection with Labelling Diversity

are used to encode the same information prior to transmission. The mappers are designed such that the symbol corresponding to a given label has different neighbours when mapped by each mapper [47]. Thus, for a labelling diversity system utilizing  $x$  mappers, each label is represented as a point in a  $2x$ -dimensional hyperspace. The objective of mapper design is to maximise the distance between points corresponding to each label in this hyperspace. The constellation represented by each mapper is then simply a plane within the  $2x$ -dimensional hyperspace. A strict constraint of the labelling diversity technique is that the symbols on each constellation remain the same, regardless of the label assigned to them [47].

The mechanics by which labelling diversity is able to improve error performance is easiest to observe by use of an example. Consider the transmission of a single information codeword, A, which can be mapped to symbols using one of two binary mappers. The received signal, Y, is shown on constellation represented by each mapper in Figures 1.1 and 1.2. From the illustrations provided, the following is noted:

- Labels A, C, E and F are closest to the received signal Y on the constellation defined by Mapper 1.
- Labels A, B, C and D are closest to the received signal Y on the constellation defined by Mapper 2.
- An MLD detector would estimate that the symbol closest to the received signal was transmitted.

Hence, codeword E would be detected using only the constellation defined by Mapper 1, which is incorrect. Similarly, codeword B would be detected using only the constellation defined by Mapper 2. This is illustrated in Figure 1.1. However, when considering both constellations concurrently, it is evident that the average distance between A and Y when considering both constellations is the least, as illustrated in Figure 1.2. Thus, in terms of the 4-dimensional hyperspace defined by both constellations, A is the point closest to Y. As such, joint detection using MLD, considering both constellations concurrently, will correctly determine that codeword A was transmitted.

### 1.1.2.2 Spectral Efficiency and Data Rate

An alternative metric to evaluate wireless communication systems is spectral efficiency, which relates to the data rate or throughput achievable by the system [21, 22]. As discussed by Lee *et al.* [54] and Huawei [14], the efficient use of available frequency spectra is among the key challenges for next-generation wireless communication systems. Typically, coded systems require a wider bandwidth than uncoded systems, which makes them less spectrally efficient. Coding compensates for this by offering improved link reliability [21, 22, 29, 37]. The trade-off between reliability and spectral efficiency is inherent to most MIMO systems.

Possibly the simplest means to improve spectral efficiency is to increase the order of the modulation scheme used to encode information bits [21, 29]. Higher modulation orders allow more information bits to be encoded into a single symbol prior to transmission [21, 22, 29]. However, this typically reduces the spacing between symbols on a normalised constellation representation of the symbol set, indicating a degradation in error performance.

Another means to improve spectral efficiency is to multiplex data over separate spatial streams. In a MIMO system, such as that used by the Vertical-Bell Laboratories Layered Space-Time (V-BLAST) architecture [55], this is typically achieved by simultaneously transmitting symbols carrying different information bits from each antenna. In this way, higher data rates are achievable by introducing more transmit antennas to the system. There are many cases where physical space is constrained at the transmitter of a system, such as mobile devices and smaller satellites (as mentioned in Section 1.1.2.1). Thus, spatial correlation and IAI are practical challenges when increasing the number of transmit antennas in the system. Furthermore, the algorithmic complexity of recovering the transmitted information using the optimal, maximum-likelihood detection (MLD) method increases

exponentially with the number of transmit antennas [55, 56]. This leads to challenges in designing receiver hardware when implementing the system [57].

A further means of improving the spectral efficiency of MIMO systems is to encode information in domains other than the signal domain prior to transmission. One such example is the spatial modulation technique [52, 58]. Spatial modulation systems use information bits to select a single transmit antenna from the MIMO configuration to be active during transmission [58]. The advantage of this technique is that it avoids the problem of IAI at the transmitter, which was a concern in the V-BLAST architecture. However, for the same number of transmit antennas and signal modulation order, the V-BLAST architecture is capable of achieving higher data rates. Other techniques similar to spatial modulation include polarisation modulation [59] and channel modulation [53, 60].

### 1.1.2.3 Challenges for Real-World Implementation

The preceding discussions in Sections 1.1.2.1 and 1.1.2.2 indicated two challenges that arise when implementing real-world wireless communication systems: correlation and detection complexity. It is important to consider the effects of these challenges when studying wireless systems to predict the real-world performance of the systems.

As mentioned previously, the effect of correlation is observed by a degradation in error performance. There are two widely-adopted models used when predicting the effects of correlation on MIMO systems. The first model is the separable model, also referred to as the Kronecker model, which is commonly used to study error performance [33–35, 65–67]. The second model is the non-separable model, which is often used when studying channel capacity [61–64]. Lin *et al.* [66] and Moustakas *et al.* [67] have previously shown that the non-separable model reduces to the Kronecker model for systems that achieve antenna diversity. As such, the research presented in this thesis focusses on applying the Kronecker model to the systems considered. The mathematical framework for analysing the error performance of space-time block coded MIMO systems in the presence of correlation was developed by Hedayet *et al.* [35]. By using the Kronecker model, Hedayet *et al.* showed that the identical correlated channels of MIMO systems may be modelled as eigenvalue-weighted, uncorrelated channels for statistical analysis [35].

The computational complexity of detection algorithms does not directly affect either the link reliability or spectral efficiency of a MIMO system. However, high detection complexity results in increased power consumption, as well as higher latencies and hardware requirements (in terms of processing power and memory). These factors have prompted studies into low-complexity detection algorithms (LCDAs) for MIMO systems [45, 51, 57, 68–75]. LCDAs are typically benchmarked against MLD, which achieves optimal detection accuracy but incurs high complexity [56]. Thus, the two factors considered when evaluating an LCDA are accuracy and complexity. Many LCDAs present a trade-off between these factors [45, 70–75]

To evaluate detection complexity, there are a variety of approaches found in literature. In some works, the proposed LCDA is implemented in hardware and its performance is evaluated in terms of the search latencies experienced [57]. Alternatively, it is possible to analyse complexity in terms of the size of the search space considered by an LCDA. Peer *et al* [69]. Another method to determine complexity is to determine the number of mathematical operations performed by receiver hardware during detection [53].

Existing LCDAs for MIMO systems may be divided into two broad classes: linear detection schemes, and search-based detection schemes. Linear detection schemes, such as zero forcing [70] and minimum mean squared error equalising [71], perform linear matrix operations during the detection process, incurring a lower complexity cost than MLD. However, these schemes are unable to fully capture the receive diversity of the MIMO system, leading to reduced detection accuracy and a degradation in error performance [72, 73]. For this reason, the research in this thesis focusses on considering search-based LCDAs.

Search-based detection schemes are often based on QR Decomposition (QRD), which transforms the detection problem into a tree search. In this way, detection is done one information codeword at a time. Spherical detection (SD) [74] is a popular scheme that has been combined with QRD to reduce complexity. This is achieved by reducing the search space at each layer of the search to only those symbols within a predefined hypersphere of the received signal. Another important improvement to the standard QRD approach is QRD- $m$ , where the  $m$  best paths are considered while traversing each layer of the search tree [75]. More recently, Radosavljevic *et al.* [57] and Peer *et al.* [69], developed LCDAs that improved upon QRD with SD by simultaneously considering the equivalent QL Decomposition (QLD) search tree. The QRD search tree is based on an upper, right triangular structure; whereas the QLD search tree is based on a lower, left triangular structure. As such, the order in which symbols are detected is reversed depending on the search tree structure used. By performing partial, parallel searches through both trees, only half of each individual tree need be traversed to obtain estimates for all symbols, thereby reducing complexity [57, 69].

A further challenge considered in this thesis is that of MIMO satellite broadcast systems [76]. As documented by Arapoglou *et al.* [77, 78], adopting a MIMO structure for satellite systems is a non-trivial task due to limitations in the physical space available on smaller satellites. Schwartz *et al.* [79] have addressed this limitation by proposing to use two single-antenna satellites in conjunction to act as a single dual-antenna node in the system. Another technique that has been considered is the use of dual-polarised antennas [80, 81]. If the polarisation streams are perfectly orthogonal, a system using 1 dual-polarised transmit antenna and 1 dual-polarised receive antenna is equivalent to a  $2 \times 2$  single-polarised antenna system [80]. Preliminary studies on the feasibility of MIMO satellite broadcasting have been positive. As recently as 2016, Hofmann *et al.* [82] and Byman *et al.* [83] documented results of implementing real-world MIMO satellite broadcast systems using each of the aforementioned configurations.

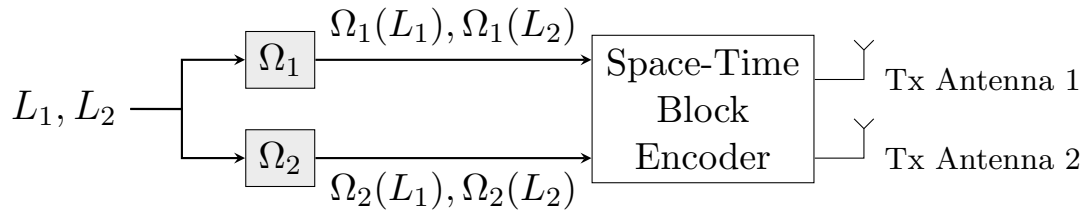


FIGURE 1.3: Block Diagram of a USTLD Transmitter

## 1.2 Research Objectives

### 1.2.1 The Original Uncoded Space-Time Labelling Diversity System

Uncoded Space-Time Labelling Diversity (USTLD) is a recent space-time block coded system that was proposed in 2016 by Xu *et al.* [47] as a direct extension of the Alamouti space-time block code [84]. The original USTLD system was thus proposed with a MIMO configuration consisting of two antennas at the transmitter and any arbitrary  $N_{\text{Rx}}$  antennas at the receiver. To achieve time and labelling diversity, two information codewords,  $L_1$  and  $L_2$ , are transmitted across two time slots using two mappers, denoted  $\Omega_1$  and  $\Omega_2$ . The symbols resulting from mapping the labels  $L_1$  and  $L_2$  using  $\Omega_1$  and  $\Omega_2$  are denoted  $\Omega_1(L_1)$ ,  $\Omega_1(L_2)$ ,  $\Omega_2(L_1)$  and  $\Omega_2(L_2)$ . This system is illustrated in Figure 1.3.

The design of the mappers  $\Omega_1$  and  $\Omega_2$  determines the extent to which a system is able to achieve labelling diversity [40, 43–47, 51]. For a constellation with modulation order  $M$ , there are  $M!$  possible designs for each mapper. Hence, there are  $(M!)^2$  possible designs for the mapper pair  $\Omega_1$  and  $\Omega_2$  in a USTLD system. Even for a relatively low modulation order of  $M = 8$ , this results in more than  $1.62 \times 10^9$  candidate designs for the mapper pair. Due to the vastness of the candidate mapper pair design space, proving the optimality of a pair of mappers remains an open research problem [47]. From literature [46, 47], the best attempt at determining optimal mapper pair designs was done by Samra *et al.* [46]. Samra *et al.* implemented an algorithm to search through the candidate mapper design space, which produced optimised mapper designs for modulation orders of  $M = 8$  and  $M = 16$ . However, this approach could not be scaled to higher order modulations due to the high computational cost of the algorithm. Other works have exploited the symmetry of points within the constellation to devise heuristic approaches to mapper design [44, 47]. These geometric heuristics are not constrained by the size of the constellation, but rather by their shape and symmetry. Depending on the choice of the heuristic, the geometric approach may not produce good mapper pair designs which is difficult to determine by inspection.

The focus of the research presented in this thesis is to enhance the original USTLD model by proposing modifications to improve its spectral efficiency and link reliability. Additionally, the effects of correlation and detection complexity are studied for the proposed systems to provide better insight into their real-world application.

### 1.2.2 Proposed Enhancements

The first proposed enhancement to the original USTLD system in this thesis is to increase its spectral efficiency by adding more transmission streams. Drawing inspiration from the V-BLAST architecture, this is to be accomplished by utilising more transmit antennas [55]. The use of more antennas in a MIMO system is feasible for next-generation terrestrial systems in developed countries, where technologies such as Massive MIMO are being considered for next-generation systems [14, 85].

As discussed in Section 1.1.2.2, the addition of more transmit antennas causes an increase in detection complexity. Thus, the research in this thesis will study the application of LCDAs to USTLD systems. For the reasons outlined in Section 1.1.2.3, the focus is on search-based LCDAs that utilise QRD and its enhancements [57, 69, 75]. As will be shown in Section 2.5, direct application of existing LCDAs do not perform as well as MLD in terms of detection accuracy. Thus, a new LCDA for USTLD systems is to be developed. The proposed LCDA is to achieve optimal detection accuracy while incurring a lower computational cost than MLD.

Section 1.1.2.2 also indicates that the addition of more transmit antennas to the USTLD system can lead to antenna correlation. Therefore, this thesis will study the effect of antenna correlation on the error performance of USTLD systems. To do this, the Kronecker correlation model [65] and correlation analysis techniques [35] discussed in Section 1.1.2.3 will be applied to USTLD systems. This study will also focus on modelling the USTLD system in a Nakagami- $q$  fading environment to provide insight into the worst-case error performance.

The second enhancement to the USTLD system in this thesis will be to improve link reliability by incorporating polarisation diversity. As detailed in Section 1.1.2.1, a consequence of polarisation diversity is that inter-beam interference occurs in the system. The effects of both IAI and IBI will thus be studied using the correlation analysis techniques derived by Hedayet *et al* [35]. This system will be developed for satellite broadcasting, targeting developing countries. Satellite broadcasting systems favour the use of circular constellations with high modulation orders when encoding information, such as those detailed in the latest DVB-S2X standard [86]. To design mappers that achieve labelling diversity for these constellations, a new approach to mapper design that can be applied to generic constellations of any size or shape will be developed. This will be done using an iterative heuristic search in the form of a genetic algorithm [87].

### 1.3 Contributions

The research conducted in the preparation of this thesis has contributed directly to eight research articles: 3 conference papers and 5 journal papers. The title, authors, article type, publication status and a brief summary of each article is provided.

Latter chapters of this thesis present only the 3 journal articles for which the candidate is listed as the primary author (i.e. Articles 1, 3 and 7).

#### Article 1

Title	High-Rate Uncoded Space-Time Labelling Diversity with Low-Complexity Detection
Authors	Sulaiman Saleem Patel, Tahmid Quazi and Hongjun Xu
Type	Journal Article
Status	Provisionally Accepted for Publication in <i>Transactions on Emerging Telecommunications Technologies</i>
Summary	This journal article extends the existing USTLD model to allow for higher achievable data rates. The proposed high-rate USTLD (HR-USTLD) model improves the data rate by allowing more than 2 transmit antennas to be used (i.e. an $N_{Tx} \times N_{Rx}$ USTLD model is considered). The use of more transmit antennas exponentially increases the complexity of codeword detection at the receiver. Hence, a study of existing low-complexity detection algorithms (LCDAs) and their application to the HR-USTLD system is conducted. The existing LCDAs are found to exhibit poor detection accuracy for HR-USTLD, and hence, a new LCDA is developed. The proposed LCDA achieves optimal detection accuracy at significantly reduced complexity when benchmarked with maximum-likelihood detection.

#### Article 2

Title	Performance of Uncoded Space-Time Labelling Diversity in Dual-Correlated Rayleigh-Fading Channels
Authors	Sulaiman Saleem Patel, Tahmid Quazi and Hongjun Xu
Type	Conference Article
Status	Published in <i>Proceedings of the Southern Africa Telecommunication Networks and Applications Conference (SATNAC) 2017</i> , Sep. 2017
Summary	This conference article develops a model for $2 \times 2$ USTLD systems affected by correlation in Rayleigh fading channels. The study is constrained to spatially correlated receive antennas. Results are presented to show that USTLD systems are more susceptible to correlation than the comparable MIMO systems investigated.

**Article 3**

- Title** Error performance of Uncoded Space Time Labeling Diversity in spatially correlated Nakagami-q channels
- Authors** Sulaiman Saleem Patel, Tahmid Quazi and Hongjun Xu
- Type** Journal Article
- Status** Published in the *International Journal of Communication Systems*, 2018, vol 31, no.12, e-Locator e3720. DOI: 10.1002/dac.3720.
- Summary** This journal article expands the study done in Article 2 from a  $2 \times 2$  to an  $N_{Tx} \times N_{Rx}$  USTLD system (i.e. the HR-USTLD system proposed in Article 1). USTLD systems are modelled in the presence of Nakagami-q fading for both spatially correlated and uncorrelated systems, as the Nakagami-q model allows for better insight into the worst-case error performance of the system. Correlation at both the transmitter and receiver are considered. It is shown that transmit antenna correlation degrades the error performance of USTLD more than receive antenna correlation. An optimal antenna spacing is determined, providing insight into practical considerations when implementing USTLD systems. Finally, USTLD systems are found to be more susceptible to correlation than comparable Alamouti space-time block coded systems.

**Article 4**

- Title** Optimal Antenna Spacings for Uncoded Space-Time Labelling Diversity Systems with Linear and Non-Linear Antenna Configurations
- Authors** Sulaiman Saleem Patel, Tahmid Quazi and Hongjun Xu
- Type** Conference Article
- Status** Published in *Proceedings of the Southern Africa Telecommunication Networks and Applications Conference (SATNAC) 2018*, Sep. 2018
- Summary** The studies in Article 3 are presented assuming that antennas are linearly arranged at both the transmitter and receiver. This conference article compares the performance of  $N_{Tx} \times N_{Rx}$  USTLD systems using linear and non-linear antenna arrangements. It is found that the non-linear arrangements considered (dense antenna arrays and equispaced antennas) allow lower optimal distances to be achieved. Hence, they allow for smaller achievable form factors when implementing USTLD systems. The equispaced antenna configuration is found to be the most optimal. As in Article 3, the system is studied in Nakagami-q fading.

**Article 5**

- Title** USTLD Mapper Design for APSK Constellation over Satellite Channels
- Authors** Tahmid Quazi and Sulaiman Saleem Patel
- Type** Journal Article
- Status** Published in *Transactions on Emerging Telecommunications Technologies*. 2019, e-Locator e3586. DOI: 10.1002/ett.3586.
- Summary** This journal article extends the existing USTLD system to a satellite context by considering M-ary APSK constellations from the latest DVB-S2X satellite broadcasting standard. The challenge of mapper design for these constellations is highlighted, and heuristic designs for a subset of the constellations within DVB-S2X are developed. Additionally, a two-stage analytical method to evaluate and compare mapper designs (for any modulation scheme) is developed. The two-stage approach is shown to give a fair estimation of the extent to which a pair of designed mappers achieves labelling diversity. The system is modelled in Nakagami-q fading, as literature shows the Nakagami-q distribution is appropriate for modelling satellite systems subject to high ionospheric scintillation.

**Article 6**

- Title** A Genetic Algorithm for Designing Uncoded Space-Time Labelling Diversity Mappers
- Authors** Sulaiman Saleem Patel, Tahmid Quazi and Hongjun Xu
- Type** Conference Article
- Status** Published in *Proceedings of the IEEE International Workshop on Signal Processing Systems (SiPS) 2018*, Oct. 2018. DOI: 10.1109/SiPS.2018.8598435
- Summary** The most critical aspect of developing a USTLD system is the design of the binary mappers used to encode information. Existing design techniques are limited; as they either rely on symmetry-based heuristics, or constrain the size of the constellation due to high computational costs. This conference article proposes a new genetic algorithm for labelling diversity mapper design, which is applicable to constellations of any shape or size. The proposed algorithm is tested on both symmetric and asymmetric constellations, and up to 64-ary modulation orders. The mappers produced by the genetic algorithm are shown to perform as well as, or better than, existing mapper design techniques in all test cases.

**Article 7**

Title	A MIMO Satellite Broadcasting System with Space, Time, Polarisation and Labelling Diversity
Authors	Sulaiman Saleem Patel, Tahmid Quazi and Hongjun Xu
Type	Journal Article
Status	Prepared for Submission to the <i>International Journal of Satellite Communications and Networking</i>
Summary	This journal article proposes a novel (STPLD) system for MIMO satellite broadcasting. The STPLD system considered constellations from the latest DVB-S2X satellite broadcasting standard. To design mappers that achieve labelling diversity for these constellations, the genetic algorithm developed in Article 6 is enhanced by using the two-stage mapper evaluation approach developed in Article 5. As in Article 5, the STPLD system is modelled in Nakagami-q fading, as literature shows the Nakagami-q distribution is appropriate for modelling satellite systems subject to high ionospheric scintillation. The inclusion of polarisation diversity in the STPLD system comes at the expense of increased inter-beam interference, which is a form of correlation. The affects of correlation, in terms of both inter-beam and inter-antenna interference, are studied using the correlation analysis techniques developed in Article 3.

**Article 8**

Title	Performance analysis of M-APSK Generalised Spatial Modulation with constellation reassignment
Authors	Ahmad Khalid, Tahmid Quazi, Hongjun Xu and Sulaiman Saleem Patel
Type	Journal Article
Status	Provisionally Accepted for Publication by the <i>International Journal of Communication Systems</i>
Summary	Constellation reassignment is a scheme which applies the concept of labelling diversity to systems that transmit information over a single time slot. This journal article studies generalised spatial modulation systems with constellation reassignment, and focusses on M-ary APSK constellations. A key challenge for these systems is the design of mappers for the APSK constellations studied that achieve labelling diversity. To address this challenge, this journal article modifies the genetic algorithm developed in Article 6 for the constellation reassignment context. The modified genetic algorithm is then implemented to design mappers that achieve labelling diversity.

## References

- [1] Miniwatts Marketing Group. Internet Usage Statistics: The Internet Big Picture. [Online Resource] 2018. <https://www.internetworldstats.com/stats.htm>. Accessed November 20, 2018.
- [2] Pew Research Centre. *Social Media Use in 2018*. [Online Report] 2018. <http://www.pewinternet.org/wp-content/uploads/sites/9/2018/02/PI.2018.03.01.Social-Media.FINAL.pdf>. Accessed November 20, 2018.
- [3] Pew Research Centre. *Social Media Use in 2018*. [Online Report] 2018. [http://www.pewglobal.org/wp-content/uploads/sites/2/2018/06/Pew-Research-Center\\_Global-Tech-Social-Media-Use\\_2018.06.19.pdf](http://www.pewglobal.org/wp-content/uploads/sites/2/2018/06/Pew-Research-Center_Global-Tech-Social-Media-Use_2018.06.19.pdf). Accessed November 20, 2018.
- [4] The International Telecommunications Union. *ICT Facts and Figures 2017*. [Online Report] 2017. <https://www.itu.int/en/ITU-D/Statistics/Documents/facts/ICTFactsFigures2017.pdf>. Accessed August 4, 2018.
- [5] The Internet Society. *2017 Internet Society Global Internet Report; Paths to our Digital Future*. [Online Report] 2017. <https://future.internetsociety.org/wp-content/uploads/2017/09/2017-Internet-Society-Global-Internet-Report-Paths-to-Our-Digital-Future.pdf>. Accessed August 3, 2018.
- [6] The United Nations General Assembly. *Report of the Special Rapporteur on the promotion and protection of the right to freedom of opinion and expression, Frank La Rue*. [Online Report] A/HRC/17/27; 2011. [https://www2.ohchr.org/english/bodies/hrcouncil/docs/17session/A.HRC.17.27\\_en.pdf](https://www2.ohchr.org/english/bodies/hrcouncil/docs/17session/A.HRC.17.27_en.pdf). Accessed November 20, 2018.
- [7] The Internet Society. *Global Internet User Survey Summary Report*. [Online Report] 2012. <http://wayback.archive-it.org/9367/20170907075228/https://www.internetsociety.org/sites/default/files/rep-GIUS2012global-201211-en.pdf>. Accessed June 26, 2018.
- [8] The United Nations General Assembly. *Transforming our world: the 2030 Agenda for Sustainable Development*. [Online Report] A/RES/70/1; 2015. [http://www.un.org/ga/search/view\\_doc.asp?symbol=A/RES/70/1&Lang=E](http://www.un.org/ga/search/view_doc.asp?symbol=A/RES/70/1&Lang=E). Accessed August 5, 2018.
- [9] Cabral A, Moodley L, Yeboah-Amankwah S. *Digital Divide: The impact of closing Africa's Internet gap*. [Online Report] McKinsey & Company; 2018. <https://www.mckinsey.com/business-functions/marketing-and-sales/our-insights/digital-divide-the-impact-of-closing-africas-internet-gap>. Accessed August 5, 2018.
- [10] Čolaković A, Hadžialić M. Internet of Things (IoT): A review of enabling technologies, challenges, and open research issues. *Computer Networks*. 2018; 144: 17–39. DOI: 10.1016/j.comnet.2018.07.017.

- [11] Zhang W, Wu Y, Hur N, Ikeda T, Xia P. FOBTv: Worldwide Efforts in Developing Next-Generation Broadcasting System. *IEEE Trans. Broadcast.* 2014; 60(2): 154–159. DOI: 10.1109/TBC.2014.2310067 .
- [12] Yovcheva Z, Buhalis D, Gatzidis C. Smartphone Augmented Reality Applications for Tourism. *e-Review of Tourism Research (eRTR)*, 2012; 10(2): 63–66.
- [13] Chi H-L, Kang S-C, Wang X. Research trends and opportunities of augmented reality applications in architecture, engineering, and construction. *Automation in Construction.* 2013; 33: 116–122. DOI: 10.1016/j.autcon.2012.12.017.
- [14] Huawei. *5G: A Technology Vision*. [Online Report] 2013. [https://www.huawei.com/ilink/en/download/HW\\_314849](https://www.huawei.com/ilink/en/download/HW_314849). Accessed November 20, 2018.
- [15] Conte R. Satellite rural communications: telephony and narrowband networks. *Int. J. Satellite Communic. and Networking.* 2005; 23(5): 307–321.
- [16] Iqbal MK, Iqbal MB, Shamoon S, Bhatti M. Future of satellite broadband Internet services and comparison with terrestrial access methods e.g. DSL and cable modem. In: 3rd IEEE Int. Conf. on Computer, Control and Communic., Karachi (Pakistan); 2013: 1–5.
- [17] Yesufu, AK. Possible use of satellites in rural telecommunications in Africa. In: 2nd Int. Conf. on Rural Telecomm., London (England); 1990: 156–159.
- [18] Tomassini D, Ginati A, Feliciani F, Deconick F, Gaudio V, Cuccarese F, Recchia F, Bove A, Cabanas F, Mathee B, Halloway L, Richardson P, Francis I. Space4edu: Satellite technology for smart rural schools in South Africa. In: 64th Int. Astronautical Congress, Beijing (China); 2013: 4472–4479.
- [19] Olla P. Exploiting satellite radio technology to create an African satellite health education infrastructure. In: 57th Int. Astronautical Congress, Valencia (Spain); 2006: 8955–8961.
- [20] Martín-de-Mercado G, Horsch A, Parentela G, Mancini P, Ginati A. Satellite-enhanced telemedicine and eHealth for sub-saharan Africa: A development opportunity. In: 62nd Int. Astronautical Congress, Cape Town (South Africa); 2011: 4320–4327.
- [21] Haykin S, Moher M. *Communication Systems*, 5th ed. John Wiley & Sons, Inc.; 2010.
- [22] Goldsmith A. *Wireless Communications*. Cambridge (USA): Cambridge University Press; 2005.
- [23] Bianchi C, Meloni A. Natural and man-made terrestrial electromagnetic noise: an outlook. *Ann. Geophys.* 2007; 50(3): 435–445
- [24] Leferink F, Silva F, Catrysse J, Batterman S, Beauvois V, Roc’h A. Man-Made Noise in Our Living Environments. *URSI Radio Science Bulletin* (September 2010); 2010(334): 49–57. DOI: 10.23919/URSIRSB.2010.7911080.

- [25] Simon MK, Alouini M-S. *Digital Communication over Fading Channels: A Unified Approach to Performance Analysis*. New York (USA): John Wiley & Sons, Inc.; 2000.
- [26] Romero-Jerez JM, Lopez-Martinez FJ. A New Framework for the Performance Analysis of Wireless Communications Under Hoyt (Nakagami-q) Fading. *IEEE Trans. Inf. Theory*. 2017; 63(3): 1693–1702.
- [27] Amol R, Kaur K. Performance Analysis of Hoyt Fading Channel for M-ary and Monte Carlo Simulation. *Int. J. of Adv. Computronics and Management Studies*. 2016; 1(3): 13–19.
- [28] Chytil B. The distribution of amplitude scintillation and the conversion of scintillation indices. *J. Atmospheric and Terrestrial Phys.* 1967; 29(9): 1175–1177.
- [29] Stüber GL. *Principles of Mobile Communication*, 2nd ed. Kluwer Academic Publishers; 2002.
- [30] Arapoglou P-D, Burzigotti P, Bertinelli M, Bolea Alamanac A, De Gaudenzi R. To MIMO or Not To MIMO in Mobile Satellite Broadcasting Systems. *IEEE Trans. Wireless Commun.* 2011; 10(9): 2807–2811.
- [31] Ebrahimi-Tofghi N, Ardebilipour M, Shahabadi M. Receive and Transmit Array Antenna Spacing and Their Effect on the Performance of SIMO and MIMO Systems by using an RCS Channel Model. *Int. J. of Elec., Comp., Energetic, Electronic and Commun. Eng.* 2007; 1(12): 1732–1736.
- [32] Akoun PO, Xu H. Optimal error analysis of receive diversity schemes on arbitrarily correlated Rayleigh fading channels. *IET Commun.* 2016; 10(7): 854–861.
- [33] Khumbani B, Mohandas VK, Singh RP, Kabra S, Kshetrimayum RS. Analysis of Space-Time Block Coded Spatial Modulation in Correlated Rayleigh and Rician Fading Channels. In: IEEE Conf. on DSP, Singapore (Singapore); 2015: 516–520.
- [34] Varshney N, Goel A, Jagannatham AK. Cooperative communication in spatially modulated MIMO systems. In: IEEE Wireless Commun. and Networking Conf. (WCNC), Doha (Qatar); 2016.
- [35] Hedayet A, Shah H, Nosratinia A. Analysis of Space-Time Coding in Correlated Fading Channels. *IEEE Trans. on Wireless Commun.* 2005; 4(6): 2882–2891.
- [36] Vaughan RG. Polarization diversity in mobile communications. *IEEE Trans. Vehicular Tech.* 1990; 39(3): 177–186. DOI: 10.1109/25.130998.
- [37] Raoof K, Zid MB, Prayongpun N, Bouallegue A. Advanced MIMO Techniques: Polarization Diversity and Antenna Selection. In: Bizaki HK, ed. *MIMO Systems, Theory and Applications*. Rijeka: IntechOpen 2011. DOI: 10.5772/14375.
- [38] Wysocki BJ, Wysocki TA. On an Orthogonal Space-Time-Polarization Block Code. *J. of Commun.* 2009; 4(1): 20–25.

- [39] Huang Y, Ritcey JA. Improved 16-QAM constellation labelling for BI-STCM-ID with the Alamouti scheme. *IEEE Commun. Letters*. 2005; 9(2): 157–159.
- [40] Huang Y, Ritcey JA. Optimal constellation labelling for iteratively decoded bit-interleaved space-time coded modulation. *IEEE Trans. Inf. Theory*. 2005; 51(5): 1865–1871.
- [41] Krasicki M. Improved labelling diversity for iteratively-decoded multiantenna systems. In: Proc. 7th Int. Conf. on Wireless Commun. and Mobile Computing (IWCMC), Istanbul (Turkey); 2011: 359–364.
- [42] Krasicki M. Essence of 16-QAM labelling diversity. *IET Electronics Lett*. 2013; 49(8): 567–569.
- [43] Krasicki M. Algorithm for Generating All Optimal 16-QAM BI-STCM-ID Labelings. *Wireless Personal Commun*. 2015; 83: 873–894.
- [44] Seddik KG, Ibrahim AS, Liu KJR. Trans-Modulation in Wireless Relay Networks. *IEEE Commun. Lett*. 2008; 12(3): 170–172.
- [45] Naidoo NR. *Enhanced performance and efficiency schemes for Generalised Spatial Modulation*. Doctoral Thesis, University of Kwa-Zulu Natal, 2017.
- [46] Samra H, Ding Z, Hahn P. Symbol Mapping Diversity Design for Multiple Packet Transmissions. *IEEE Trans. Commun*. 2005; 53(5): 810–817.
- [47] Xu H, Govindasamy K, Pillay N. Uncoded Space-Time Labeling Diversity. *IEEE Commun. Lett*. 2016; 20(8): 1511–1514.
- [48] Dlodlo B, Xu H. Trellis code-aided high-rate M-QAM space-time labeling diversity using a unitary expansion. *Int. J. Commun. Syst*. 2018; 31(11): e3590. DOI: 10.1002/dac.3590.
- [49] Ejaz S, Yang F, Xu H. Labeling Diversity for  $2 \times 2$  WLAN Coded-Cooperative Networks. *Radioengineering*. 2015; 24(2): 470480.
- [50] Zhao Z, Zhou L, Zheng X, Park S-E. Enhanced Constellation Rearrangement for HARQ with Symbol Combining. In: IEEE Mobile WiMax Symp. (MWS), Napa Valley, CA(USA); 2009.
- [51] Ayanda D, Xu H, Pillay N. Uncoded M-ary quadrature amplitude modulation space-time labeling diversity with three transmit antennas. *Int. J. Commun. Syst*. 2018:e3818. DOI: 10.1002/dac.3818.
- [52] Govindasamy K, Xu H, Pillay N. Space-time block coded spatial modulation with labeling diversity. *Int. J. Commun. Syst*. 2017:e3395. DOI: 10.1002/dac.3395.
- [53] Pillay N, Xu H. Uncoded Space-Time Labeling Diversity – Application of Media-based Modulation with RF Mirrors. *IEEE Commun. Lett*. 2017. DOI: 10.1109/LCOMM.2017.2770145.

- [54] Lee J, Tejedor E, Ranta-aho K, Wang H, Lee K-T, Semaan E, Mohyeldin E, Song J, Bergljung C, Jung S. Spectrum for 5G: Global Status, Challenges, and Enabling Technologies. *IEEE Commun. Magazine*. 2018; 56(3): 12–18. DOI: 10.1109/MCOM.2018.1700818.
- [55] Wolniansky PW, Foschini GJ, Golden GD, Valenzuela RA. V-BLAST: an architecture for realizing very high data rates over the rich-scattering wireless channel. In: Proc. 1998 URSI Int. Symp. on Sig., Syst. and Electronics, Pisa (Italy); 1998. DOI: 10.1109/ISSSE.1998.738086.
- [56] Fincke U, Pohst M. Improved Methods for Calculating Vectors of Short Length in a Lattice. *Math. of Computation*. 1985; 44(170):463–471.
- [57] Radosavljevic P, Kim KJ, Shen H, Cavallaro JR. Parallel Searching-Based Sphere Detector for MIMO Downlink OFDM Systems. *IEEE Trans. Signal Process.* 2012; 60(6): 3240–3252.
- [58] Mesleh RY, Haas H, Sinanovic S, Ahn CW, Yun S. Spatial Modulation. *IEEE Trans. Vehicular Tech.* 2008; 57(4): 2228–2241. DOI: 10.1109/TVT.2007.912136.
- [59] Abidin Z, Xiao P, Amin M, Fusco V. Circular Polarization Modulation for digital communication systems. In: 8th Int. Symp. Commun. Syst., Networks & Dig. Sig. Process. (CSNDSP), Poznan(Poland).; 2012. DOI: 10.1109/CSNDSP.2012.6292758.
- [60] Basar E, Altunbas I. Space-Time Channel Modulation. *IEEE Trans. Vehicular Tech.* 2017; 66(8): 7609–7614.
- [61] Weichselberger W, Herdin M, Ozelik H and Bonek E. A stochastic MIMO channel model with joint correlation of both link ends. *IEEE Trans. Wireless Commun.* 2006; 5(1): 90–100.
- [62] Tulino AM, Lozano A and Verdú S. Impact of antenna correlation on the capacity of multi-antenna channels. *IEEE Trans. Inf. Theory*. 2005; 51(7): 2491–2509.
- [63] Lin C, Veeravalli VV. Optimal linear dispersion codes for correlated MIMO channels. *IEEE Trans. Wireless Commun.* 2008; 7(2): 657–666.
- [64] Raghavan V, Sayeed AM and Veeravalli VV. Semiunitary Precoding for Spatially Correlated MIMO Channels. *IEEE Trans. Inf. Theory*. 2011; 57(3): 1284–1298.
- [65] Kermoal JP, Schumacher L, Pedersen KI, Mogensen PE, Frederiksen F. A stochastic MIMO radio channel model with experimental validation. *IEEE J. on Sel. Areas in Commun.* 2002; 20(6): 1211–1226.
- [66] Lin C, Raghavan V, Veeravalli VV. To Code or Not to Code Across Time: Space-Time Coding with Feedback. *IEEE J. on Sel. Areas in Commun.* 2008; 26(8): 1588–1598.
- [67] Moustakas A, Baranger H, Balents L, Sengupta A and Simon S. Communication through a diffusive medium: Coherence and capacity. *Science*. 2000; 287: 287–290.

- [68] Dai Y, Sun S, Lei Z. A Comparative Study of QRD-M Detection and Sphere Decoding for MIMO-OFDM Systems. In: Proc. IEEE Int. Symp. Pers., Indoor and Mobile Radio Commun. Syst., Berlin (Germany); 2005:186–190.
- [69] Peer N, Murin Y, Dabora R. Improved QRD-QLD Algorithm for Low Complexity MIMO Decoding. *IEEE Commun. Lett.* 2014;18(10):1703–1706.
- [70] Xu R, Lau FCM. Performance analysis for MIMO systems using zero forcing detector over fading channels. *IEE Proc. Commun.* 2006;153(1):74–80.
- [71] Prasad S, Sur SN. Lattice Reduction Aided Detection Techniques for MIMO Systems. *Int. Research Jour. of Eng. and Tech.* 2016; 3(3):1496–1502.
- [72] Jiang Y, Varanasi MK, Li J. Performance analysis of ZF and MMSE equalizers for MIMO systems: An in-depth study of the high SNR regime. *IEEE Trans. Inf. Theory.* 2011;57(4):2008–2026.
- [73] Neinavaie M, Derakhtian M. ML Performance Achieving Algorithm with the Zero-Forcing Complexity at High SNR Regime. *IEEE Trans. Wireless Commun.* 2016;15(7):4651–4659.
- [74] Vikalo H, Hassibi B. On the sphere-decoding algorithm II. Generalizations, second-order statistics, and applications to communications. *IEEE Trans. Signal Process.* 2005; 53(8):2819–2834.
- [75] Kim, KJ, Yue J, Iltis RA, Gibson JD. A QRD-D/Kalman Filter-Based Detection and Channel Estimation Algorithm for MIMO-OFDM Systems. *IEEE Trans. Wireless Commun.* 2005;4(2):710–721.
- [76] Kyröläinen J, Hulkkonen A, Ylitalo J, Byman A, Shankar B, Arapoglou P-D, Grotz J. Applicability of MIMO to satellite communications. *Int. J. Satellite Communic. and Networking.* 2014; 32: 343–357.
- [77] Arapoglou P-D, Burzigotti P, Bertinelli M, Bolea Alamanac A, De Gaudenzi R. To MIMO or Not To MIMO in Mobile Satellite Broadcasting Systems. *IEEE Trans. Wireless Commun.* 2011; 10(9): 2807–2811.
- [78] Arapoglou P-D, Liolis K, Bertinelli M, Panagopoulos A, Cottis P, De Gaudenzi R. MIMO over Satellite: A Review. *IEEE Commun. Surveys & Tutorials.* 2011; 13(1): 27–51.
- [79] Schwartz RT, Knopp A, Ogermann D, Hofmann CA, Lankl B. Optimum-capacity MIMO satellite link for fixed and mobile services. In: Int. ITG Workshop on Smart Antennas, Vienna (Austria); 2008: 209–216.
- [80] Zorba N, Realp M, Lagunas MA, Pérez-Neira AI. Dual Polarization for MIMO processing in Multibeam Satellite Systems. In: 10th Int. Workshop on Sig. Process. for Space Communic., Rhodes Island (Greece); 2008: 1–7.

- 
- [81] Arapoglou P-D, Burzigotti P, Bolea Alamanac A, De Gaudenzi R. Capacity potential of mobile satellite broadcasting systems employing dual polarization per beam. In: 5th Adv. Satellite Multimedia Syst. Conf. and the 11th Sig. Process. for Space Commun. Workshop, Cagliari (Italy); 2010: 213–220.
- [82] Hofmann C, Storek K-U, Schwartz RT, Knopp A. Spatial MIMO over Satellite: A Proof of Concept. In: IEEE Int. Conf. on Commun., Kuala Lumpur (Malaysia); 2016: 1–6.
- [83] Byman A, Hulkkonen A, Arapoglou P-D, Bertinelli M, De Gaudenzi R. MIMO for Mobile Satellite Digital Broadcasting: From Theory to Practice. *IEEE Trans. Vehic. Tech.* 2016; 65(7): 4839–4853.
- [84] Alamouti SM. A Simple Transmit Diversity Technique for Wireless Communications. *IEEE J. on Sel. Areas in Commun.* 1998; 16(8): 1451–1458.
- [85] Albdran S, Alshammari A, Matin MA. Spectral and energy efficiency for massive MIMO systems using exponential correlation model. In: IEEE 7th Annual Comp. and Commun. Workshop and Conf. (CCWC), Las Vegas, NV (USA); 2017.
- [86] Digital Video Broadcasting. Second generation framing structure, channel coding and modulation systems for Broadcasting, Interactive Services, News Gathering and other broadband satellite applications; Part 2: DVB-S2 Extensions (DVB-S2X). *European Telecomm. Standards Inst.* 2014; EN 302 307-2 V1.1.1.
- [87] Ahmed ZH. An Improved Genetic Algorithm using Adaptive Mutation Operator for the Quadratic Assignment Problem. In Proc. 38th Int. Conf. Telecomm. and Sig. Process., Prague (Czech Republic); 2015. DOI: 10.1109/TSP.2015.7296481.

## Chapter 2

### Journal Article 1

# High-Rate Uncoded Space-Time Labelling Diversity with Low-Complexity Detection

Sulaiman Saleem Patel, Tahmid Quazi, Hongjun Xu  
Provisionally Accepted for Publication: *Transactions on Emerging  
Telecommunications Technologies*

## 2.1 Abstract

Uncoded space-time labelling diversity (USTLD) is a recent scheme that improved the error performance compared to conventional multiple-input, multiple-output systems. Thus far USTLD has suffered from limited achievable data rates, as the original model uses only two transmit antennas. This motivates for the work in this paper, where the USTLD model is extended to allow for any desired number of transmit antennas. An analytical bound for the average bit error probability of this high-rate USTLD (HR-USTLD) system is derived. This expression is verified using the results of Monte Carlo simulations, which show a tight fit in the high signal-to-noise ratio region. The increased data rates associated with larger transmit antenna arrays in HR-USTLD systems come at the cost of increased detection complexity. Therefore, this paper studies the application of low-complexity detection algorithms based on the popular QR decomposition technique, and proposes a new algorithm specifically designed for HR-USTLD systems. Analysis of this algorithm in terms of accuracy and computational complexity is also provided and benchmarked against maximum-likelihood detection (MLD). It is shown that the proposed algorithm achieves near-MLD accuracy, while reducing complexity by 79.75% and 92.53% for the respective  $4 \times 4$  16QAM and  $4 \times 5$  16PSK HR-USTLD systems investigated.

## 2.2 Introduction

### Context of Research

The inclusion of diversity in wireless communication systems allows for many potential benefits, such as protection against burst errors and improved robustness in the presence of multipath fading or co-channel interference [1]. Uncoded space-time labelling diversity (USTLD) [2–4] is a recent scheme which achieves three levels of diversity: antenna diversity, time diversity and labelling diversity. Antenna diversity is achieved by adopting a multiple-input, multiple-output (MIMO) system model. The inclusion of multiple antennas at both the transmitter and receiver generates more signal paths, increasing the likelihood of correct detection [1, 5]. The original work on USTLD describes a MIMO system of two transmit antennas and any arbitrary  $N_{\text{Rx}}$  receive antennas [2]. To achieve time diversity, symbols representing the same binary data are transmitted in two time slots. To achieve labelling diversity, symbols are selected from constellations with different binary mappings in each time slot. The design and selection of mappers aims to maximise the minimum product Euclidean distance (ED) between symbol pairs in each constellation. Stated differently, adjacent symbols in the constellation defined by the primary mapper are spaced further apart in the constellations defined by subsequent mappers. By following this approach, detection is done based on symbol pairs, instead of individual symbols. Due to difficulties in designing labelling diversity mappers, Xu *et al.* [2] constrained their studies to  $M$ -ary quadrature amplitude modulation (MQAM) and  $M$ -ary phase shift keying (MPSK) modulation schemes.

A drawback of the USTLD scheme is that transmitting symbols containing the same information across two time slots halves the effective data rate of the system. In general, two approaches to improving the data rate of uncoded MIMO systems, such as USTLD, are to either increase the modulation order,  $M$ , or to increase the number of transmission streams. Higher modulation orders allow the system to transmit larger codewords in each instance, i.e. the number of bits per codeword is increased. To increase the number of transmission streams, MIMO systems typically increase the number of transmit antennas,  $N_{\text{Tx}}$ , and transmit independent symbols from each antenna simultaneously [1, 5]. This increases the number of codewords transmitted during a single time slot. It is possible to increase either  $M$  or  $N_{\text{Tx}}$  in USTLD systems, however they also result in increasing the complexity of detection for receiver hardware. The algorithmic complexity of performing maximum-likelihood detection (MLD or ML detection) on an  $N_{\text{Tx}} \times N_{\text{Rx}}$  USTLD system with modulation order  $M$  is  $\mathcal{O}(N_{\text{Tx}}N_{\text{Rx}}M^{N_{\text{Tx}}})$ , where  $\mathcal{O}(\cdot)$  is the ‘order of’ operator used in complexity analysis [6]. This is derived in the Appendix of this paper in terms of real operations, the metric suggested by Pillay and Xu [4]. The high complexity of MLD motivates for the development of low-complexity detection algorithms (LCDAs), with the goal of achieving near-ML accuracy at significantly reduced complexity [7].

The current work on USTLD systems [2] only allows for increasing the data rate by using higher modulation orders, as  $N_{\text{Tx}}$  in the system is fixed at only two transmit antennas. This is because

the original USTLD system model [2] was conceived as a direct extension of the Alamouti space-time block code [8] to improve its bit error rate (BER). Since the structure proposed by Alamouti constrains the system to only two transmit antennas [8], the same constraint was applied to the original USTLD model [2].

However, as discussed in literature [1, 5], the data rate of uncoded MIMO systems increases logarithmically with  $M$  and linearly with  $N_{\text{Tx}}$ . Thus, the improvement in data rate as  $M$  increases is hyperbolic and becomes negligible as  $M \rightarrow \infty$ . By contrast, increasing  $N_{\text{Tx}}$  provides constant data rate improvement. Another drawback to increasing modulation order is that the average ED between constellation points for normalised constellations decreases as  $M$  increases, resulting in inferior error performance. It is also noted that increasing the modulation order above  $M = 16$  presents difficulties in designing optimal mappers to achieve labelling diversity [2, 3, 9]. For these reasons, this paper proposes to increase the achievable data rates of USTLD systems by extending the existing model to allow for more than two transmit antennas. To distinguish between such a system and the existing USTLD model, this paper adopts the term ‘high-rate USTLD’ (HR-USTLD) to describe the  $N_{\text{Tx}} \times N_{\text{Rx}}$  USTLD model proposed. It is further noted that Ayanda *et al.* [10] have also extended the original USTLD model to allow for the use of 3 transmit antennas and 3 labelling diversity mappers. However, the system proposed by Ayanda *et al.* also uses a third transmission time slot, and thus achieves the same data rate as the original USTLD model [2, 10]. Thus, the HR-USTLD system presented in this paper is capable of achieving higher data rates than the 3 mapper USTLD system.

As mentioned previously, HR-USTLD incurs high detection complexity. Existing LCDAs for MIMO systems may be divided into two broad classes: linear detection schemes, and search-based detection schemes. Linear detection schemes, such as zero forcing [11] and minimum mean squared error equalising [12], perform linear matrix operations during the detection process, incurring a lower complexity cost than MLD. However, these schemes are unable to fully capture the receive diversity of the MIMO system, leading to reduced detection accuracy and a degradation in error performance [13, 14]. For this reason, this paper focuses on applying search-based LCDAs to the systems investigated.

Search-based detection schemes are often based on QR Decomposition (QRD), which transforms the detection problem into a tree search. In this way, detection is done one information codeword at a time. Spherical detection (SD) [15] is a popular scheme that has been combined with QRD to reduce complexity. This is achieved by constraining the search space at each layer of the search to only those symbols within a predefined hypersphere of the received signal. Another important improvement to the standard QRD approach is QRD- $m$ , where the  $m$  best paths are considered while traversing the search tree [16]. In the work by Radosavljevic *et al.* [17], a technique that is referred to in this paper as the QR-QL Parallel Searching Algorithm (QRLPSA) was proposed. This technique reduces the complexity of QRD with SD by simultaneously considering the equivalent QL Decomposition (QLD) search tree. The QRD search tree is based on an upper, right triangular structure; whereas the QLD search tree is based on a lower, left triangular structure. As such, the order in which symbols are

detected is reversed depending on the search tree structure used. By performing partial, parallel searches through both trees, only half of each individual tree need be traversed to obtain estimates for all symbols. The QRLPSA has been extended by Peer *et al.* [18], whose algorithm introduces two additional detection stages. The first additional stage involves merging the  $m$  partial candidate symbol vectors obtained from the QR and QL search trees respectively, and pruning these to only the  $K$  best candidate vectors. The second additional stage is to search through these  $K$  candidate vectors, using either the QR or QL search tree, and generate an ML-hypothesis candidate vector. A set of counter-hypotheses is generated and the log-likelihood ratio (LLR) between the ML-hypothesis and each of the counter-hypotheses is then computed, after which the suitability of the ML hypothesis is determined.

In this paper, USTLD is extended from the  $2 \times N_{\text{Rx}}$  model originally proposed by Xu *et al.* [2] to a more general  $N_{\text{Tx}} \times N_{\text{Rx}}$  HR-USTLD model. Increasing the number of transmit antennas allows for higher data rates to be achieved. In other works on USTLD [19, 21], a search-based LCDA based on performing an orthogonal projection has been proposed. However, the manner in which this LCDA is presented is only valid for two transmit antennas. For this reason, this paper further proposes a new LCDA for HR-USTLD, based on the QRLPSA [17] and its extension [18]. It is shown that the proposed LCDA is capable of achieving ML performance at significantly reduced complexity. It is also noted that the SD approach is not applicable to USTLD and HR-USTLD due to the manner in which mappers are designed to achieve labelling diversity, and that the use of LLRs is not feasible for uncoded systems such as USTLD and HR-USTLD.

### Structure and Notation

The remainder of this paper is structured as follows: In Section 2.3, the system model for HR-USTLD is given. Section 2.3.1 describes the transmission model and Section 2.3.2 describes various detection schemes which may be applied - including ML detection, existing LCDAs and the proposed LCDA for this paper. Section 2.4 provides analytical expressions to evaluate the proposed system. Section 2.4.1 derives the analytical average bit error probability (ABEP), and Section 2.4.2 gives analytical expressions to evaluate and compare the algorithmic complexity of the detection algorithms given in Section 2.3.2. Section 2.5 provides and discusses the results obtained through Monte Carlo simulations, and finally, Section 2.6 concludes this paper.

The notation used in this paper is to denote vectors in boldface, matrices in italicised boldface and scalars in italics. Occasionally, two levels of subscripts are used when referring to elements of a matrix or vector during a particular time slot. In these cases, the inner subscript refers to the position of the element within the matrix and the outer subscript refers to the time slot considered. For example,  $V_{3_2}$  is read as the third element of vector  $\mathbf{V}$  during the second time slot. When referring to elements within a matrix, the a comma separates the column and row within the subscript. For example,  $W_{2,5}$  is read as the element in the second row and fifth column of matrix  $\mathbf{W}$ . The operators  $\mathcal{E}\{\cdot\}$ ,  $\|\cdot\|$ ,  $\lfloor \cdot \rfloor$ ,  $\lceil \cdot \rceil$ ,  $(\cdot)^{\text{H}}$  and  $(\cdot)^{\text{T}}$  denote the statistical expectation, Frobenius vector norm, floor, ceiling, Hermitian and matrix transpose, respectively. Sets of variables are denoted in braces,

and a superscript outside the braces indicates the size of the set. Angular brackets are used to indicate symbol pairs. The operator  $|\cdot|$  represents either the magnitude of a complex number or the cardinality of a set, depending on the argument used.

### Contributions

The original contributions of this article are as follows:

1. The achievable data rates of USTLD systems are increased by employing a HR-USTLD transmission model with any arbitrary  $N_{\text{Tx}}$  transmit antennas. A tight, closed-form union bound expression for the ABEP of HR-USTLD systems is presented.
2. A comprehensive study of the application of existing QRD-based LCDAs to HR-USTLD systems is conducted. Each of these LCDAs was originally proposed for systems that do not achieve labelling diversity, hence they have been adapted for USTLD systems. It is noted that the only previous LCDA for USTLD systems [19, 21] cannot be applied to HR-USTLD systems as it fails when used with more than two transmit antennas.
3. A new LCDA designed specifically for HR-USTLD systems is proposed, which achieves significantly higher detection accuracy when compared to the existing LCDAs studied.
4. New insights on the manner in which labelling diversity affects the BER performance of systems are presented. These were not reported in the original work on USTLD systems [2].
5. Expressions are derived to quantitatively evaluate the computational complexity for all detection algorithms presented in this paper.

## 2.3 System Model

### 2.3.1 Transmission Model

This paper considers an  $N_{\text{Tx}} \times N_{\text{Rx}}$  HR-USTLD system, where the number of transmit antennas is constrained such that  $N_{\text{Tx}} \leq N_{\text{Rx}}$ . A stream of  $N_{\text{Tx}} \log_2 M$  information bits is transmitted over two time slots. These bits are grouped into  $N_{\text{Tx}}$  labels denoted by vector  $\mathbf{B} = [B_1 \ \dots \ B_{N_{\text{Tx}}}]^T$ , where the term ‘label’ is for the  $\log_2 M$  consecutive bits from the information bitstream. To achieve labelling diversity, in each time slot, transmitted symbols are selected from constellations with different mappings. The constellation mapper used in the  $t$ -th time slot, where  $t \in [1 : 2]$ , is denoted  $\Omega_t$ .

$N_{\text{Tx}} \times 1$  transmit symbol vector  $\mathbf{x}_t = [x_{1t} \ \dots \ x_{N_{\text{Tx}}t}]^T$  is generated such that  $x_{i_1} = \Omega_1(B_i)$  and  $x_{i_2} = \Omega_2(B_i)$ , where  $i \in [1 : N_{\text{Tx}}]$ . The set of  $M$  possible symbol pairs is denoted  $\xi$ , such that its  $j$ -th entry  $\xi^{(j)}$  is given by  $\xi^{(j)} = \langle \Omega_1(j-1), \Omega_2(j-1) \rangle$ , where  $j \in [1 : M]$ . After transmission, the  $N_{\text{Rx}} \times 1$  received signal vector,  $\mathbf{y}_t$ , transmitted in the  $t$ -th time slot, is given by

$$\mathbf{y}_t = \sqrt{\frac{\gamma}{N_{\text{Tx}}}} \mathbf{H}_t \mathbf{x}_t + \mathbf{n}_t; \langle x_{i_1}, x_{i_2} \rangle \in \xi, i \in [1 : N_{\text{Tx}}]. \quad (2.1)$$

In (2.1),  $\gamma$  represents the total average signal-to-noise ratio (SNR) of the transmission, assumed to be equally distributed among the  $N_{\text{Tx}}$  transmit antennas. The variable  $\mathbf{H}_t$  is the  $N_{\text{Rx}} \times N_{\text{Tx}}$  matrix of channel coefficients. These channels are assumed to follow a Rayleigh amplitude distribution of zero mean and unit variance, the probability density function of which is  $f_{\text{Rayleigh}}(\alpha) = \alpha e^{-0.5\alpha^2}$ ,

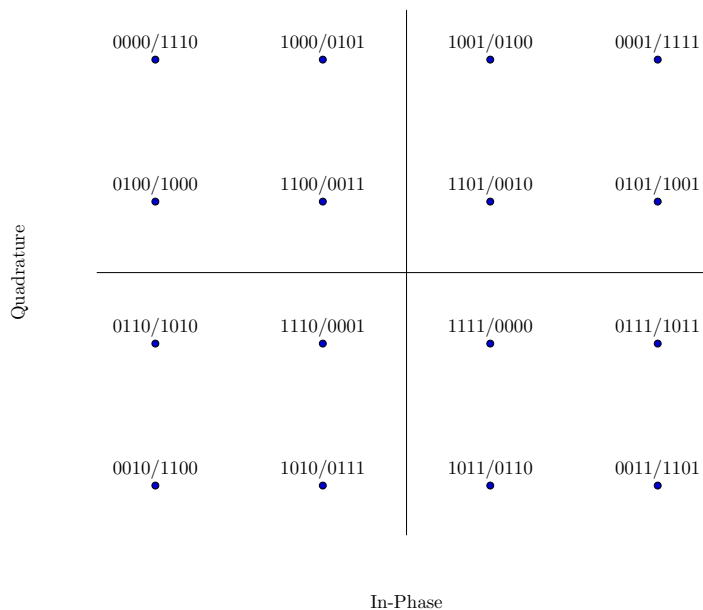


FIGURE 2.1: 16QAM Binary Constellation Mapping, Key:  $\Omega_1/\Omega_2$

where  $\alpha$  is the fading amplitude [1]. Furthermore, channels are assumed to be frequency flat and fast-fading.  $N_{\text{Rx}} \times 1$  vector  $\mathbf{n}_t$  represents additive white Gaussian noise (AWGN) which follows a complex normal distribution with zero mean and variance  $\sigma_n^2 = \frac{N_0}{2}$  per dimension, where  $N_0$  is the single-sided power spectral density of the noise. Both the fading channels and AWGN have uniform phase distribution.

As suggested in the original work on USTLD systems [2],  $\Omega_1$  is chosen to be a Gray-coded mapping. Mapper  $\Omega_2$  then requires a different mapping to be selected. In this paper, for the case of 16QAM, the mapper proposed by Samra *et al.* [9], found to be optimal by previous works on labelling diversity systems [2, 9], is used. These constellation mappings are illustrated in Figure 2.1. In [9], the optimal mapper design technique used is only feasible for up to 16-ary constellation sizes. Therefore, the heuristic-based 64QAM mapper design proposed by Seddik *et al.* [20] is used. This heuristic design was found to be superior to the 64QAM mapper design presented by Xu *et al.* [2] in other works on USTLD systems [3]. For the case of MPSK constellations, the secondary mapper is constructed by swapping alternate symbols with their diagonally opposite counterparts, as suggested by Xu *et al.* [2]. All constellations are power normalised such that  $\mathcal{E}\{|x_{i_t}|^2\} = 1$ , where  $i \in [1 : N_{\text{Tx}}]$  and  $t \in [1 : 2]$ .

The proposed HR-USTLD model achieves a data rate of  $0.5N_{\text{Tx}} \log_2 M$  bits/sec/Hz.

### 2.3.2 Detection Model

In this work, different detection algorithms are implemented and compared in terms of accuracy and complexity.

Detection is performed by first dividing (2.1) by the SNR factor to produce

$$\mathbf{z}_t = \sqrt{\frac{N_{\text{Tx}}}{\gamma}} \mathbf{y}_t = \mathbf{H}_t \mathbf{x}_t + \hat{\mathbf{n}}_t, \quad (2.2)$$

where the equivalent noise term  $\hat{\mathbf{n}}_t$  is defined as  $\hat{\mathbf{n}}_t = \sqrt{\frac{N_{\text{Tx}}}{\gamma}} \mathbf{n}_t$ . All detection techniques investigated assume that perfect channel state information is available at the receiver. After detecting the transmitted symbol pairs, decoding is done to recover the associated labels and hence, the transmitted information.

#### 2.3.2.1 Maximum Likelihood Detection

Maximum Likelihood Detection (ML detection or MLD) is the benchmark detection technique investigated in this paper. To perform MLD on the proposed HR-USTLD system, it is required that received symbol vectors from both time slots are considered simultaneously. Unlike conventional MIMO detection, MLD for labelling diversity is concerned with joint detection using corresponding

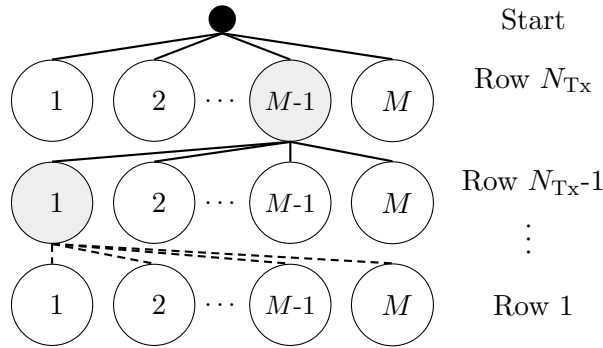


FIGURE 2.2: Illustration of a QRD Search Tree

symbols from both mappers. As such, the output of the ML detector is two  $N_{\text{Tx}} \times 1$  symbol vectors,  $\tilde{\mathbf{x}}_1$  and  $\tilde{\mathbf{x}}_2$ . The detected data is represented by the label vector,  $\tilde{\mathbf{B}}$ , which corresponds to the labels associated with the pair  $\langle \tilde{\mathbf{x}}_1, \tilde{\mathbf{x}}_2 \rangle$ . The MLD search based on (2.2) is described by

$$\langle \tilde{\mathbf{x}}_1, \tilde{\mathbf{x}}_2 \rangle = \arg \min_{\substack{\langle \hat{x}_{j_1}, \hat{x}_{j_2} \rangle \in \xi \\ j \in [1:N_{\text{Tx}}]}} \mathcal{A}(\hat{\mathbf{x}}_1, \hat{\mathbf{x}}_2), \quad (2.3)$$

where the MLD detection metric  $\mathcal{A}$  is defined as

$$\mathcal{A}(\hat{\mathbf{x}}_1, \hat{\mathbf{x}}_2) = \|\mathbf{z}_1 - \mathbf{H}_1 \hat{\mathbf{x}}_1\|^2 + \|\mathbf{z}_2 - \mathbf{H}_2 \hat{\mathbf{x}}_2\|^2. \quad (2.4)$$

MLD incurs high-complexity, but ensures the most accurate results, as there are  $M^{N_{\text{Tx}}}$  candidate symbol pairs that need to be considered.

### 2.3.2.2 Standard QR Decomposition and QRD-m

QR Decomposition (QRD) and QL Decomposition (QLD) are two techniques for decomposing an arbitrary complex-valued matrix,  $\mathbf{A}$ , into an equivalent matrix product. The QRD of  $\mathbf{A}$  is defined as  $\mathbf{A} = \mathbf{Q}_{\text{QR}} \mathbf{R}$ , and similarly the QLD of  $\mathbf{A}$  is  $\mathbf{A} = \mathbf{Q}_{\text{QL}} \mathbf{L}$ .  $\mathbf{Q}_{\text{QR}}$  and  $\mathbf{Q}_{\text{QL}}$  are unitary, complex orthogonal matrices such that  $(\mathbf{Q}_{\text{QR}})^{\text{H}} \mathbf{Q}_{\text{QR}} = (\mathbf{Q}_{\text{QL}})^{\text{H}} \mathbf{Q}_{\text{QL}} = \mathbf{I}$ ; where  $\mathbf{I}$  is the identity matrix.  $\mathbf{R}$  is an upper, right triangular matrix and  $\mathbf{L}$  is a lower, left triangular matrix.

To apply these techniques to detection in MIMO systems, the channel coefficient matrix,  $\mathbf{H}$ , is first decomposed. Thereafter (2.2) is left-multiplied by the Hermitian of the unitary matrix to produce (2.5) for QRD, and (2.6) for QLD.

$$\boldsymbol{\alpha}_t = \left( \mathbf{Q}_{\text{QR}_t} \right)^{\text{H}} \mathbf{z}_t = \mathbf{R}_t \mathbf{x}_t + \left( \mathbf{Q}_{\text{QR}_t} \right)^{\text{H}} \hat{\mathbf{n}}_t \quad (2.5)$$

$$\boldsymbol{\beta}_t = \left( \mathbf{Q}_{\text{QL}_t} \right)^{\text{H}} \mathbf{z}_t = \mathbf{L}_t \mathbf{x}_t + \left( \mathbf{Q}_{\text{QL}_t} \right)^{\text{H}} \hat{\mathbf{n}}_t \quad (2.6)$$

Due to the triangular structure of matrices  $\mathbf{R}$  and  $\mathbf{L}$ , detection may be performed on a row-by-row

basis starting with the row with the most zero elements (i.e. the  $N_{\text{Tx}}$ -th row of  $\mathbf{R}$  and the 1st row of  $\mathbf{L}$ ). Back-substitution is then used, so that in each row there are only  $M$  candidate symbol pairs that must be tested. This allows the detection to be formulated as a tree search, through  $N_{\text{Tx}}$  layers, with  $M$  candidate nodes per layer. Each node represents a candidate label and its associated symbol pair generated from  $\Omega_1$  and  $\Omega_2$ . The simplest case of QRD and QLD is when the system of equations defined by (2.5) and (2.6) is perfectly determined. This is the case if the decomposed matrix,  $\mathbf{H}$ , was a square matrix (i.e.  $N_{\text{Tx}} = N_{\text{Rx}}$ ). Figure 2.2 illustrates the QRD search tree for a perfectly determined system. Searching begins at the  $N_{\text{Tx}}$ -th row of matrix  $\mathbf{R}$  and ends at its first row. Without loss of generality, it is assumed that Node  $M - 1$  is detected from Row  $N_{\text{Tx}}$  and Node 1 is detected from Row  $N_{\text{Tx}} - 1$  to illustrate expansion of nodes during the search.

If  $\mathbf{H}$  is not a square matrix, QRD and QLD may still be performed. When  $\mathbf{H}$  has fewer rows than columns (i.e.  $N_{\text{Tx}} < N_{\text{Rx}}$ ), the system of equations it represents is overdetermined. After decomposition, the triangular matrix of an overdetermined system has rank  $N_{\text{Tx}}$  and  $N_{\text{Rx}} - N_{\text{Tx}}$  zero rows. The case of  $\mathbf{H}$  having more rows than columns (i.e.  $N_{\text{Tx}} > N_{\text{Rx}}$ ), does not arise due to the constraints placed on the system.

If all zero rows of any overdetermined system are discarded, the  $q$ -th rows of (2.5) and (2.6), during the  $t$ -th time slot, are given by the scalar equations:

$$\alpha_{qt} = \sum_{i=q}^{N_{\text{Tx}}} r_{q,i_t} x_{i_t} \quad (2.7)$$

$$\beta_{qt} = \sum_{i=1}^q l_{q,i_t} x_{i_t} \quad (2.8)$$

The row-by-row detection adapted from (2.3) and based on (2.7) for the  $q$ -th row of a QRD search is then given by:

$$\langle \tilde{x}_{q_1}, \tilde{x}_{q_2} \rangle = \arg \min_{\langle \hat{x}_1, \hat{x}_2 \rangle \in \xi} \sum_{t=1}^2 |\alpha_{qt} - r_{q,q_t} \hat{x}_t - S_{1t}|^2, \quad (2.9)$$

and likewise, for the  $q$ -th row of a QLD search, the row-by-row detection based on (2.8) is:

$$\langle \tilde{x}_{q_1}, \tilde{x}_{q_2} \rangle = \arg \min_{\langle \hat{x}_1, \hat{x}_2 \rangle \in \xi} \sum_{t=1}^2 |\beta_{qt} - S_{2t} - l_{q,q_t} \hat{x}_t|^2, \quad (2.10)$$

where the summation terms are defined as:

$$S_{1t} = \sum_{i=q+1}^{N_{\text{Tx}}} r_{q,i_t} \tilde{x}_{i_t} \quad (2.11)$$

$$S_{2t} = \sum_{i=1}^{q-1} l_{q,i_t} \tilde{x}_{i_t} \quad (2.12)$$

It may be intuitively observed that both QRD and QLD are equivalent techniques. Radosavljevic *et al.* [17] has previously shown that performing QRD on a column-reversed channel matrix  $\mathbf{H}^{\text{ev}} = \begin{bmatrix} \mathbf{h}_{N_{\text{Tx}}} & \cdots & \mathbf{h}_1 \end{bmatrix}$  produces a decomposition equivalent to the QLD of the original channel matrix  $\mathbf{H}$ , where  $\mathbf{h}_i$  represents the  $i$ -th column of the un-reversed channel matrix  $\mathbf{H}$ .

A drawback of standard QRD detection is that it is susceptible to error propagation through the search tree due to the use of back-substitution. Referring to Figure 2.2, suppose an error occurs in Row  $N_{\text{Tx}}$  and correct detection should have yielded Node 1. This incorrect detection then increases the likelihood of a detection error in all rows from Row  $N_{\text{Tx}} - 1$  to Row 1. An approach to combat this is to change the detection order to maximise the probability of correct detection in upper rows of the search tree [22]. A simple method of achieving this is by pre-processing and reordering the columns of  $\mathbf{H}$ . Columns are arranged such that the sum of column-norms from both time slots are in ascending order, and the rows of  $\mathbf{x}$  are also reordered accordingly. For example, assuming a  $5 \times N_{\text{Rx}}$  HR-USTLD system described according to (2.2) by

$$\mathbf{z}_t = \begin{bmatrix} \mathbf{h}_1 & \mathbf{h}_2 & \mathbf{h}_3 & \mathbf{h}_4 & \mathbf{h}_5 \end{bmatrix}_t \begin{bmatrix} x_1 \\ x_2 \\ x_3 \\ x_4 \\ x_5 \end{bmatrix}_t + \mathbf{n}_t. \quad (2.13)$$

Ordering is done according to the sum of column-norms across time slots  $t = 1$  and  $t = 2$ . Without loss of generality, assume that it is found that  $\sum_{t=1}^2 \|\mathbf{h}_3\|_t^2 < \sum_{t=1}^2 \|\mathbf{h}_1\|_t^2 < \sum_{t=1}^2 \|\mathbf{h}_5\|_t^2 < \sum_{t=1}^2 \|\mathbf{h}_4\|_t^2 < \sum_{t=1}^2 \|\mathbf{h}_2\|_t^2$ . This means that the probability of correctly detecting  $x_2$  is highest, and the probability of erroneously detecting  $x_3$  is highest. Re-ordering (2.13) accordingly for QRD produces

$$\mathbf{z}_t = \begin{bmatrix} \mathbf{h}_3 & \mathbf{h}_1 & \mathbf{h}_5 & \mathbf{h}_4 & \mathbf{h}_2 \end{bmatrix}_t \begin{bmatrix} x_3 \\ x_1 \\ x_5 \\ x_4 \\ x_2 \end{bmatrix}_t + \mathbf{n}_t. \quad (2.14)$$

Due to the upper, right triangular structure of  $\mathbf{R}$  after decomposition, it is evident that detection is now done in order of descending  $\sum \|\mathbf{h}\|^2$ . Similarly, the appropriate re-ordering for QLD is

$$\mathbf{z}_t = \begin{bmatrix} \mathbf{h}_2 & \mathbf{h}_4 & \mathbf{h}_5 & \mathbf{h}_1 & \mathbf{h}_3 \end{bmatrix}_t \begin{bmatrix} x_2 \\ x_4 \\ x_5 \\ x_1 \\ x_3 \end{bmatrix}_t + \mathbf{n}_t. \quad (2.15)$$

Another improvement to standard QRD, presented by Kim *et al.* [16], is QRD- $m$  detection. In QRD- $m$ , the best  $m$  nodes are expanded at each level of the search tree, where  $m \in [1 : M]$ . The case of  $m = 1$  is identical to the standard QRD approach. In QRD- $m$ , the cumulative metrics are considered at each search layer. QRD- $m$  is illustrated with  $m = 2$  on a perfectly determined system in Figure 2.3.

### 2.3.2.3 QR-QL Parallel Searching

The QR-QL Parallel Searching Algorithm (QRLPSA) [17] takes advantage of the symmetry of matrices  $\mathbf{R}$  and  $\mathbf{L}$  to reduce the number of layers to be searched through when performing detection. If the channel matrix of an HR-USTLD system is decomposed using the QRD approach, the order in which labels are detected starts from label  $B_{N_{\text{Tx}}}$  and ends at label  $B_1$ . If the QLD approach is used, this order is reversed. It may be observed from (2.9) and (2.10) that the latter layers of either search tree have more terms to be computed when performing detection.

QRLPSA exploits the similar structure of the search trees obtained via QRD and QLD. By evaluating only the first  $\lfloor \frac{N_{\text{Tx}}}{2} \rfloor$  layers of each search tree in parallel, the QLD search tree is able to detect labels  $B_1$  to  $B_{\lfloor \frac{N_{\text{Tx}}}{2} \rfloor}$  and the QRD search tree is able to detect labels  $B_{N_{\text{Tx}} - \lfloor \frac{N_{\text{Tx}}}{2} \rfloor + 1}$  to  $B_{N_{\text{Tx}}}$ .

In general, for the case of even  $N_{\text{Tx}}$ , the floor operator is redundant and thus by parallel searching through the first  $\frac{N_{\text{Tx}}}{2}$  layers of both search trees, an estimate for  $\mathbf{B}$  can be obtained. In the case of odd  $N_{\text{Tx}}$ , the  $\lfloor \frac{N_{\text{Tx}}}{2} \rfloor$ -th layer remains after parallel searching. This requires that either the QRD or QLD search tree be expanded by one extra layer. The original work by Radosavljevic *et al.* [17] also uses multiple search paths, as in QRD- $m$ . It further makes use of re-ordering the matrix  $\mathbf{H}$  such that the outermost columns have the highest summed column-norms. To illustrate this, consider the example system given in Section 2.3.2.2 and equations (2.13)-(2.15). Re-ordering (2.13) to perform

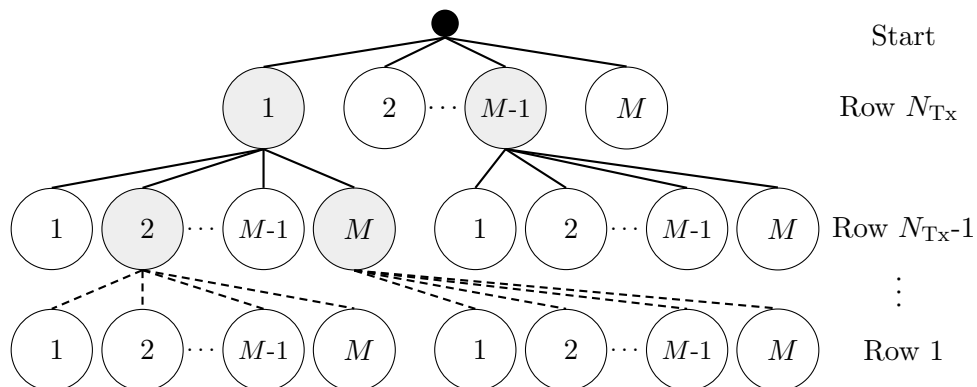


FIGURE 2.3: Illustration of a QRD- $m$  Search Tree

parallel searching produces

$$\mathbf{z}_t = \begin{bmatrix} \mathbf{h}_2 & \mathbf{h}_5 & \mathbf{h}_3 & \mathbf{h}_1 & \mathbf{h}_4 \end{bmatrix}_t \begin{bmatrix} x_2 \\ x_5 \\ x_3 \\ x_1 \\ x_4 \end{bmatrix}_t + \hat{\mathbf{n}}_t. \quad (2.16)$$

In this way, the QLD search tree is marginally more accurate than the QRD search tree, which suggests that the remaining layer after parallel searching be obtained by expanding one more layer of the QLD search tree.

### 2.3.2.4 Extended QR-QL Parallel Searching Algorithm

An extension to the QRLPSA was proposed by Peer *et al.* [18], where two further stages are introduced to the detection process. Peer *et al.* [18] developed their algorithm for a coded system - as such, only the aspects applicable to uncoded systems such as HR-USTLD are investigated further in this paper.

The three stage structure of the uncoded aspects of Extended QRLPSA is illustrated in Figure 2.4. The first stage is to perform parallel searching as in the QRLPSA, which produces  $m$  partial candidate label vectors from the QRD and QLD search trees respectively, denoted  $\{\tilde{\mathbf{B}}\}_{\text{QR}}^m$  and  $\{\tilde{\mathbf{B}}\}_{\text{QL}}^m$ . The second stage is to merge these partial candidate symbol pair vectors to form a set of  $m^2$  candidate symbol pair vectors, denoted  $\xi_{\text{merged}}$ , for which the corresponding set of labels are  $\{\tilde{\mathbf{B}}\}^{m^2}$  such that

$$\xi_{\text{merged}} = \left\langle \Omega_1 \left( \{\tilde{\mathbf{B}}\}^{m^2} \right), \Omega_2 \left( \{\tilde{\mathbf{B}}\}^{m^2} \right) \right\rangle. \quad (2.17)$$

The detection metrics of the partial candidate vectors are summed to produce a detection metric for the merged candidate vectors. This set is then reduced to a set of  $K$  candidate labels,  $\{\tilde{\mathbf{B}}\}^K \subset \{\tilde{\mathbf{B}}\}^{m^2}$ , where  $K \in [1 : m^2]$ .  $\{\tilde{\mathbf{B}}\}^K$  is then populated with the  $K$  candidate label vectors from  $\{\tilde{\mathbf{B}}\}^{m^2}$  with the lowest merged detection metrics, and defines candidate symbol vector pairs

$$\xi_{\text{reduced}} = \left\langle \Omega_1 \left( \{\tilde{\mathbf{B}}\}^K \right), \Omega_2 \left( \{\tilde{\mathbf{B}}\}^K \right) \right\rangle. \quad (2.18)$$



FIGURE 2.4: Block Diagram of Extended QRLPSA

In the final stage, a QLD tree search through only  $\xi_{\text{reduced}}$  is performed, yielding the final estimate of the transmitted labels. The detection metric for the  $q$ -th layer of this search is given by (2.19), where  $q \in [1 : N_{\text{Tx}}]$ . This metric has been obtained by modifying (2.10). Thereafter, Peer *et al.* [18] make use of techniques applicable to coded systems to determine the suitability of this estimate, however, these techniques are not applicable for HR-USTLD.

$$\langle \tilde{x}_{q_1}, \tilde{x}_{q_2} \rangle = \arg \min_{\langle \hat{x}_1, \hat{x}_2 \rangle \in \xi_{\text{reduced}}} \sum_{t=1}^2 \left| \beta_{q_t} - \sum_{i=1}^{q-1} l_{q,i_t} \tilde{x}_{i_t} - l_{q,q_t} \hat{x}_t \right|^2 \quad (2.19)$$

### 2.3.2.5 Proposed LCDA: Multiple Stage Reduced Set Detection for USTLD

As shown by the results in Section 2.5, the Extended QRLPSA [18] does not improve detection accuracy compared to QRLPSA [17] when applied to HR-USTLD. It is also shown that both these algorithms offer poor detection accuracy compared to MLD, with up to 7dB loss in the high SNR region of the systems investigated (see Figures 2.8 and 2.9).

There is generally a trade-off between accuracy and complexity in LCDAs. The QRD-based LCDAs presented reduce complexity by transforming the exhaustive ML search to a layer-by-layer tree search, which reduces the search space of candidate symbol vector pairs considered. However, adopting a layer-by-layer approach reduces the amount of information used to perform detection at each stage of the tree search, which results in these LCDAs being unable to fully capture the diversity of the system. By considering more received signals during detection, such as when computing ML metric  $\mathcal{A}$  in (2.4), more information about the channel is present to increase detection accuracy. Moreover, QRD-based LCDAs are susceptible to error propagation through the search tree, which leads to severe consequences if there is a detection error in earlier layers of the search tree.

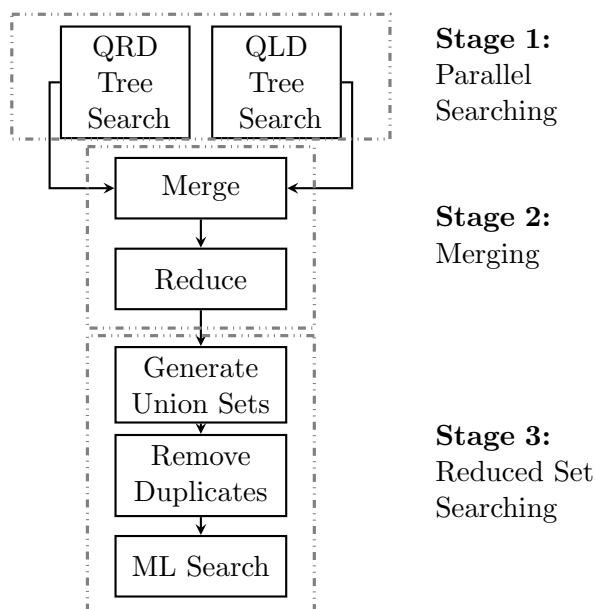


FIGURE 2.5: Block Diagram of MSRSD-USTLD

In order to improve the accuracy of Extended QRLPSA, this paper proposes a new scheme called Multiple Stage Reduced Set Detection for USTLD (MSRSD-USTLD). The proposed scheme follows the same three-stage structure as Extended QRLPSA (shown in Figure 2.4), but increases accuracy by considering a greater search space than Extended QRLPSA during the final stage of detection. In addition, the final reduced set search for MSRSD-USTLD is based on the ML metric,  $\mathcal{A}$ , instead of the QLD tree search used in Extended QRLPSA. This further increases accuracy, but also causes an increase in complexity. A more detailed block diagram of MSRSD-USTLD is given in Figure 2.5.

The first two stages of MSRSD-USTLD are logically the same as for the Extended QRLPSA. Parallel searching is performed during Stage 1 to obtain partial candidate label vectors  $\{\tilde{\mathbf{B}}\}_{\text{QR}}^m$  and  $\{\tilde{\mathbf{B}}\}_{\text{QL}}^m$ , which are merged and reduced during Stage 2 to produce  $\{\tilde{\mathbf{B}}\}^{m^2}$ ,  $\xi_{\text{merged}}$  (2.17),  $\{\tilde{\mathbf{B}}\}^K$  and  $\xi_{\text{reduced}}$  (2.18), as described in Section 2.3.2.4. However, MSRSD-USTLD differs from Extended QRLPSA in that instead of summing the metrics from  $\{\tilde{\mathbf{B}}\}_{\text{QR}}^m$  and  $\{\tilde{\mathbf{B}}\}_{\text{QL}}^m$ , the detection metric for the merged candidate label vectors are obtained by evaluating ML metric  $\mathcal{A}$ , given in (2.4), for each candidate symbol vector pair in  $\xi_{\text{merged}}$ . The  $K$  candidate label vectors with the lowest merged detection metrics are again used for constructing  $\{\tilde{\mathbf{B}}\}^K$  and  $\xi_{\text{reduced}}$ .

In Stage 3 of MSRSD-USTLD,  $N_{\text{Tx}}$  reduced sets of candidate symbol vector pairs,  $\xi_j^*$ ,  $j \in [1 : N_{\text{Tx}}]$  are defined as the ‘union sets’. The final estimate of the transmitted information is obtained by performing an ML search through the union sets as described by

$$\langle \tilde{\mathbf{x}}_1, \tilde{\mathbf{x}}_2 \rangle = \arg \min_{\substack{\langle \hat{x}_{j_1}, \hat{x}_{j_2} \rangle \in \xi_j^* \\ j \in [1 : N_{\text{Tx}}]}} \mathcal{A}(\tilde{\mathbf{x}}_1, \tilde{\mathbf{x}}_2). \quad (2.20)$$

To generate the union sets, it is first necessary to perform pre-processing and generate a lookup table of  $M$  reduced constellation sets,  $\xi_i^\lambda$ .  $\xi_i^\lambda$  represents the  $\lambda$  most likely symbol vector pairs to be detected for transmitted information label  $i$ , where  $1 < \lambda \leq M$ . The metric chosen to determine which symbol pairs should be selected to build the reduced constellation sets is the product ED, as it is shown by Samra *et al.* [9] and Xu *et al.* [2] that USTLD mappers are designed to maximise the minimum product ED between labels across both constellation mappers. The product ED between the labels  $a$  and  $b$  is defined by:

$$\prod d(a, b) = d_1(a, b) d_2(a, b), \quad (2.21)$$

where

$$d_t(a, b) = |\Omega_t(a) - \Omega_t(b)|^2; \quad t \in [1 : 2] \quad (2.22)$$

is the squared ED between the symbols represented by labels  $a$  and  $b$  as a result of each mapper  $\Omega_1$  and  $\Omega_2$ . To construct  $\xi_i^\lambda$  for label  $i$ ,  $i \in [0 : M - 1]$ , the algorithm given in Table 2.1 is implemented.

Given the existence of the reduced constellation sets, the union set is constructed based on the output set of candidate label vectors from Stage 2 of MSRSD-USTLD,  $\{\tilde{\mathbf{B}}\}^K = \{\tilde{\mathbf{B}}^{(1)}, \tilde{\mathbf{B}}^{(2)}, \dots, \tilde{\mathbf{B}}^{(K)}\}$ . Each

TABLE 2.1: Algorithm for generating lookup table entries of  $\xi_i^\lambda, i \in [1 : M]$ 


---

<b>Step 1:</b>	Compute the product distances $\prod d(i, \hat{i}), \hat{i} \in [0 : M - 1]$ and store these as the set $\{\prod d\}^M$ .
<b>Step 2:</b>	Sort $\{\prod d\}^M$ in ascending order.
<b>Step 3:</b>	Construct $\{\hat{i}\}^\lambda$ by storing the first $\lambda$ candidate labels, $\hat{i}$ , from the sorted list $\{\prod d\}^M$ . The first label should always correspond to the case of $\prod d(i, \hat{i}) = 0$ , which occurs when $i = \hat{i}$ .
<b>Step 4:</b>	Construct the reduced constellation set $\xi_i^\lambda$ by mapping the candidate label set $\{\hat{i}\}^\lambda$ using the USTLD mappers, as described by:

---

$$\xi_i^\lambda = \left\langle \Omega_1(\{\hat{i}\}^\lambda), \Omega_2(\{\hat{i}\}^\lambda) \right\rangle. \quad (2.23)$$


---

candidate label vector is described by  $\tilde{\mathbf{B}}^{(j)} = [\tilde{B}_1^{(j)} \ \dots \ \tilde{B}_{N_{\text{Tx}}}^{(j)}]^\text{T}; j \in [1 : K]$ . Thus, the union set for transmitted label  $B_k, k \in [1 : N_{\text{Tx}}]$  is defined as:

$$\xi_k^* = \xi_{B_k^{(1)}}^\lambda \cup \xi_{B_k^{(2)}}^\lambda \cup \dots \cup \xi_{B_k^{(K)}}^\lambda = \bigcup_{j \in [1:K]} \xi_{B_k^{(j)}}^\lambda. \quad (2.24)$$

The union set may be optimised by removing any duplicate entries in the set. As such, the cardinality of each union set is in the range  $\lambda \leq |\xi_j^*| \leq K\lambda$ .

It is noted that the search described in (2.20) has worst-case ML search space  $K\lambda^{N_{\text{Tx}}}$ , which incurs much higher complexity than the LCDAs discussed in Section 2.3.2.1 to Section 2.3.2.4. However, by selecting a suitably small value for  $K$  and an appropriate  $\lambda$ , it is possible to ensure that  $K\lambda^{N_{\text{Tx}}} \ll M^{N_{\text{Tx}}}$ , thereby allowing significant complexity reduction compared to MLD. In this way, MSRSU-USTLD defines three adjustable parameters  $m, K$  and  $\lambda$ , the values for which present a trade-off between detection accuracy and complexity. By comparison, the QRD-m [16] and QRLPSA [17] have only one degree of freedom ( $m$ ) and the Extended QRLPSA [18] has two ( $m$  and  $K$ ).

A final optimisation to reduce the complexity of MSRSU-USTLD is to retain the  $m^2$  ML metrics computed in Stage 2 of detection and re-use them in Stage 3 if any of the same candidate symbol vector pairs arise. Since  $\left\langle \Omega_1(\{\tilde{\mathbf{B}}\}^K), \Omega_2(\{\tilde{\mathbf{B}}\}^K) \right\rangle \subset \xi_{\text{merged}}$  and  $\left\langle \Omega_1(\{\tilde{B}_j\}^K), \Omega_2(\{\tilde{B}_j\}^K) \right\rangle \subset \xi_j^*; j \in [1 : N_{\text{Tx}}]$ , the maximum number of ML metrics computed during the third detection stage is reduced to  $K(\lambda - 1)^{N_{\text{Tx}}}$ .

## 2.4 Performance Analysis

### 2.4.1 Average Bit Error Probability for High-Rate USTLD

An approach to analysing the average bit error probability (ABEP) for a  $2 \times N_{\text{Rx}}$  MIMO system in both fast-fading and quasi-static Rayleigh fading conditions is given by Xu *et al* [2]. This paper follows the same approach and extends it to the more general case of an  $N_{\text{Tx}} \times N_{\text{Rx}}$  HR-USTLD system. An important assumption made at the start of the analysis by Xu *et al.* [2] is that at high SNR, only one of the transmitted symbol pairs is incorrectly detected. This assumption is reasonable, as the the system is expected to have high link reliability at high SNRs. Therefore, the same assumption is also used when analysing the performance of HR-USTLD in this paper. Given this assumption, the bound of the ABEP for HR-USTLD is defined as [2]:

$$P_e(\gamma) \leq \frac{1}{M \log_2 M} \sum_{i=0}^{M-1} \sum_{\substack{j=0 \\ j \neq i}}^{M-1} \delta(i, j) P(\mathbf{X} \rightarrow \tilde{\mathbf{X}}), \quad (2.25)$$

where  $\delta(i, j)$  is the number of bit errors between the labels  $i$  and  $j$  and  $P(\mathbf{X} \rightarrow \tilde{\mathbf{X}})$  is the pairwise error probability (PEP) of an erroneous detection of matrix  $\mathbf{X} = \begin{bmatrix} \mathbf{x}_1 & \mathbf{x}_2 \end{bmatrix}$  to estimated matrix  $\tilde{\mathbf{X}} = \begin{bmatrix} \tilde{\mathbf{x}}_1 & \tilde{\mathbf{x}}_2 \end{bmatrix}$ .

For the sake of notation, and without loss of generality, it is assumed that the incorrectly detected symbol pair is  $\langle \tilde{x}_{a_1}, \tilde{x}_{a_2} \rangle$ ,  $a \in [1 : N_{\text{Tx}}]$ . The corresponding transmitted symbol pair is denoted  $\langle x_{a_1}, x_{a_2} \rangle$ . Hence, the PEP  $P(\mathbf{X} \rightarrow \tilde{\mathbf{X}})$  may be equivalently written as  $P(\langle x_{a_1}, x_{a_2} \rangle \rightarrow \langle \tilde{x}_{a_1}, \tilde{x}_{a_2} \rangle)$ .

Given the assumption that only one symbol pair is incorrect, Xu *et al.* [2] have shown that the conditional PEP may be expressed as:

$$\begin{aligned} P(\mathbf{X} \rightarrow \tilde{\mathbf{X}} | \mathbf{H}_1, \mathbf{H}_2) &= P(\langle x_{a_1}, x_{a_2} \rangle \rightarrow \langle \tilde{x}_{a_1}, \tilde{x}_{a_2} \rangle | \mathbf{H}_1, \mathbf{H}_2) \\ &= P\left(\sum_{k=1}^2 \|\mathbf{y}_t - \sqrt{\frac{\gamma}{N_{\text{Tx}}}} \mathbf{H}_t \tilde{\mathbf{x}}_t\|^2 < \sum_{k=1}^2 \|\mathbf{n}_t\|^2\right) \\ &= \mathcal{Q}\left(\sqrt{\phi_1 + \phi_2}\right), \end{aligned} \quad (2.26)$$

where  $\mathcal{Q}(x) = \frac{1}{\pi} \int_0^{0.5\pi} \exp\left(0.5(x \csc y)^2\right) dy$  is the Gaussian Q-function [23]. In (2.26),  $\phi_1$  and  $\phi_2$  are central chi-squared random variables which each have  $2N_{\text{Rx}}$  degrees of freedom [2]. The underlying Gaussian random variables that form  $\phi_1$  have zero mean and variance  $\frac{\gamma}{4N_{\text{Tx}}} |x_{a_1} - \tilde{x}_{a_1}|^2$ . Similarly, the Gaussian random variables that form  $\phi_2$  have zero mean and variance  $\frac{\gamma}{4N_{\text{Tx}}} |x_{a_2} - \tilde{x}_{a_2}|^2$ . The derivations for the variance of these random variables can be found in the work by Xu *et al* [2].

As shown by Xu *et al.* [2], the unconditional PEP is found by integrating the conditional PEP, given by (2.26), over the probability density functions of  $\phi_1$  and  $\phi_2$  and applying a trapezoidal

approximation. This produces the result:

$$P(\mathbf{X} \rightarrow \tilde{\mathbf{X}}) \approx \frac{1}{4n} \prod_{t=1}^2 \mathcal{M}_t\left(\frac{1}{2}\right) + \frac{1}{2n} \sum_{m=1}^{n-1} \prod_{t=1}^2 \mathcal{M}_t\left(\frac{1}{2} \csc^2\left(\frac{m\pi}{2n}\right)\right), \quad (2.27)$$

where  $\mathcal{M}_1(s)$  and  $\mathcal{M}_2(s)$  are the respective moment generating functions (MGFs) of  $\phi_1$  and  $\phi_2$  under the assumption of  $N_{\text{Rx}}$  independent and identically distributed (i.i.d.) Rayleigh fading channels, and  $n$  is an arbitrarily large integer value that allows the summation to converge to the same result as the underlying integral. Xu *et al.* [2] have shown that the MGF is defined in terms of the variance of the Gaussian random variables that underlie  $\phi_1$  and  $\phi_2$ . These were derived by Xu *et al.* for the specific case of  $N_{\text{Tx}} = 2$ . Abstracting for the more general case of  $N_{\text{Tx}}$  transmit antennas, and expressing the MGF in terms of the squared ED between labels, given in (2.22), yields [1, 2]:

$$\mathcal{M}_t(s) = \left(1 + \frac{\gamma}{2N_{\text{Tx}}} d_t s\right)^{-N_{\text{Rx}}}; \quad t \in [1 : 2]. \quad (2.28)$$

Thus, the overall ABEP for an  $N_{\text{Tx}} \times N_{\text{Rx}}$  HR-USTLD system in i.i.d. Rayleigh fading channels is obtained by substituting (2.27) in (2.25). The resulting expression is:

$$P_e(\gamma) \leq \frac{1}{2nM \log_2 M} \sum_{i=0}^{M-1} \sum_{\substack{j=0 \\ j \neq i}}^{M-1} \delta(i, j) \left[ \frac{1}{2} \prod_{t=1}^2 \mathcal{M}_t\left(\frac{1}{2}\right) + \sum_{m=1}^{n-1} \prod_{t=1}^2 \mathcal{M}_t\left(\frac{1}{2} \csc^2\left(\frac{m\pi}{2n}\right)\right) \right]. \quad (2.29)$$

#### 2.4.2 Analytical Evaluation of Algorithmic Complexity

When reviewing literature, it is found that the authors of the existing LCDAs discussed in Section 2.3.2 analyse complexity using different metrics [16–18]. In Table I of the paper by Kim *et al.* [16], QRD-m is compared to MLD in terms of complex additions, subtractions and multiplications, as well as real multiplications. Radosaljevic *et al.* [17] implement the QRLPSA on a field programmable gate array and evaluate its performance in terms of the number of arithmetic units used and the search latencies experienced in the hardware implementation. Finally, Peer *et al.* [18] analyse the complexity of the Extended QRLPSA in terms of the number of expanded nodes during the detection search. To fairly analyse and compare the LCDAs investigated in this work, a unified means of evaluating complexity is considered: the effective number of real mathematical operations performed during the detection process, which is denoted by the symbol  $\Psi$ . Real operations were also used by Pillay and Xu [4] in their complexity analysis of USTLD systems with media-based modulation. Complex addition, or subtraction, is considered to have 2 effective real operations and complex multiplication is considered to have 6 effective real operations. Vector norms are said to consist of  $4|\mathbf{V}| - 1$  operations, where  $|\mathbf{V}|$  is the length of the vector.

According to Peer *et al.* [18], the complexity of decomposing matrix  $\mathbf{H}$  by either QRD or QLD is negligible compared to the complexity of searching, and is thus neglected.

TABLE 2.2: Complexity Comparison of LCDAs in terms of Number of Candidate Label Vectors

LCDA	No. of Candidate Label Vectors (Nodes)
MLD	$M^{N_{\text{Tx}}}$
QRD	$MN_{\text{Tx}}$
QRD-m [16]	$M + mM(N_{\text{Tx}} - 1)$
QRLPSA [17]	$2M + mM(N_{\text{Tx}} - 2)$
Extended QRLPSA [18]	$2M + mM(N_{\text{Tx}} - 2) + K \left\lfloor \frac{N_{\text{Tx}}}{2} \right\rfloor$
MSRSD-USTLD	$2M + mM(N_{\text{Tx}} - 2) + m^2 + K(\lambda - 1)^{N_{\text{Tx}}}$

TABLE 2.3: Complexity Comparison of LCDAs in terms of Effective Real Operations

LCDA	Number of Effective Real Operations ( $\Psi$ )
MLD	$M^{N_{\text{Tx}}}(16N_{\text{Tx}}N_{\text{Rx}} + 8N_{\text{Rx}} - 1)$
QRD	$16N_{\text{Rx}}^2 - 4N_{\text{Rx}} + M(8N_{\text{Tx}}^2 + 15N_{\text{Tx}})$
QRD-m [16]	$16N_{\text{Rx}}^2 - 4N_{\text{Rx}} + M(23 + m(8N_{\text{Tx}}^2 + 15N_{\text{Tx}} - 23))$
QRLPSA [17]	$\begin{cases} 32N_{\text{Rx}}^2 - 8N_{\text{Rx}} + M(46 + m(4N_{\text{Tx}}^2 + 15N_{\text{Tx}} - 46)); & \text{even } N_{\text{Tx}} \\ 32N_{\text{Rx}}^2 - 8N_{\text{Rx}} + M(46 + m(4N_{\text{Tx}}^2 + 15N_{\text{Tx}} - 42)); & \text{odd } N_{\text{Tx}} \end{cases}$
Extended QRLPSA [18]	$\begin{cases} \Psi_{\text{QRLPSA, even } N_{\text{Tx}}} + m^2 + K(6N_{\text{Tx}}^2 + \frac{15}{2}N_{\text{Tx}}); & \text{even } N_{\text{Tx}} \\ \Psi_{\text{QRLPSA, odd } N_{\text{Tx}}} + m^2 + K(6N_{\text{Tx}}^2 + \frac{23}{2}N_{\text{Tx}} + \frac{11}{2}); & \text{odd } N_{\text{Tx}} \end{cases}$
MSRSD-USTLD	$\begin{aligned} & \Psi_{\text{QRLPSA}} + (m^2 + K(\lambda - 1)^{N_{\text{Tx}}})(16N_{\text{Tx}}N_{\text{Rx}} + 8N_{\text{Rx}} - 1) \\ & \approx (m^2 + K(\lambda - 1)^{N_{\text{Tx}}})(16N_{\text{Tx}}N_{\text{Rx}} + 8N_{\text{Rx}} - 1) \end{aligned}$

The pre-processing and ordering of  $\mathbf{H}$  incurs a complexity of  $8N_{\text{Tx}}N_{\text{Rx}} - N_{\text{Tx}}$  operations.

A summary of the complexity of each detection scheme is given in terms of the number of expanded nodes during the detection search in Table 2.2. Table 2.3 presents a similar summary in terms of the number of effective real operations,  $\Psi$ . Derivations for the expressions in Table 2.3 are provided in the Appendix. Note that for MSRSD-USTLD, the complexity cannot be exactly determined (see Appendix, Section 2.7.4). Thus, the expression given in the last row of Table 2.3 is for the upper bound of the complexity of MSRSD-USTLD.

## 2.5 Results and Discussion

Monte Carlo simulations were used to produce all results presented in this section. In the first set of results, the analytical expression for the ABEP (2.29), which was derived in Section 2.4.1, is verified. As shown in Figure 2.6, simulation results based on ML detection converge to the theoretical ABEP in the high SNR region. Results are presented for various antenna array sizes, modulation orders and for both QAM and PSK modulation.

The next set of results compares the performance of HR-USTLD and similar schemes of equal data rate. The results presented in Figure 2.7 and Table 2.4 compare the theoretical performance of six systems which achieve a data rate of 6 bits/sec/Hz: i) a conventional  $3 \times 4$  4QAM MIMO system, ii) a conventional  $1 \times 4$  64QAM single-input, multiple-output (SIMO) system, iii) a  $2 \times 4$  64QAM Alamouti space-time block coded system [8], iv) a  $2 \times 4$  64QAM USTLD system [2], v) a  $3 \times 4$  64QAM USTLD system with 3 labelling diversity mappers [10] and vi) a  $3 \times 4$  16QAM HR-USTLD system. It is highlighted that the ‘conventional’ SIMO and MIMO systems considered utilise a single time slot to transmit information [5], and that the USTLD system with 3 labelling diversity mappers utilises 3 time slots to transmit information [10]. The mappers used for the 3 mapper USTLD system are constructed by following the design rules presented in Section 4 of the work by Ayanda *et al* [10]. The results in Figure 2.7 show that by using a lower order modulation and more transmit antennas, the  $3 \times 4$  16QAM HR-USTLD system outperforms the existing  $2 \times 4$  64QAM USTLD

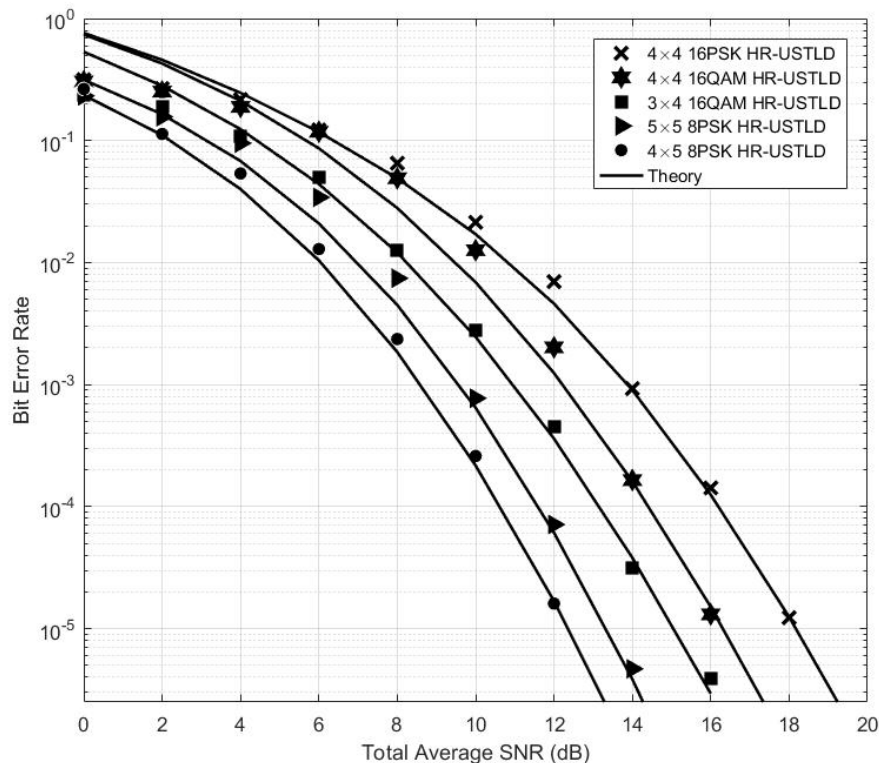


FIGURE 2.6: Analytical ABEP converging to simulated results using ML Detection

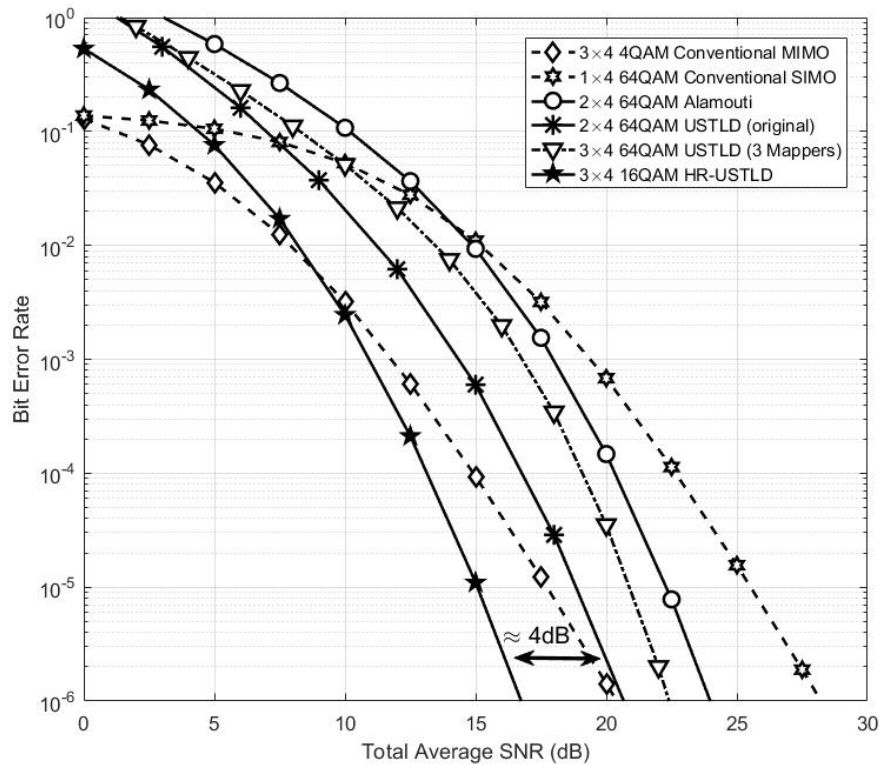


FIGURE 2.7: Bit Error Rate Comparison of Uncoded Systems with Equal Data Rate

TABLE 2.4: Diversity Order Comparison of Systems in Figure 2.7

Transmission Scheme	Diversity Order ( $\Gamma$ )
Conventional MIMO [5]	$N_{Rx}$
Conventional SIMO [5]	$N_{Rx}$
Alamouti [8]	$2N_{Rx}$
USTLD (original) [2]	$2N_{Rx}$
USTLD (3 Mappers) [10]	$3N_{Rx}$
HR-USTLD	$2N_{Rx}$

system by approximately 4dB in the high SNR region. The gradient of the curves also confirm that HR-USTLD achieves similar diversity to the original USTLD model. This may be quantified in terms of the diversity order,  $\Gamma$ , which is defined as [24]:

$$\Gamma = - \lim_{\gamma \rightarrow \infty} \frac{\log P_e(\gamma)}{\log \gamma}. \quad (2.30)$$

By using (2.30) to determine the diversity order of each of the systems presented in Figure 2.7, the results given in Table 2.4 are obtained. The values for  $\Gamma_{\text{Alamouti}}$  and  $\Gamma_{\text{USTLD (3 Mappers)}}$  match those that have been reported in literature [8, 10]. The values obtained for  $\Gamma_{\text{USTLD (original)}}$ ,  $\Gamma_{\text{USTLD (3 Mappers)}}$  and  $\Gamma_{\text{HR-USTLD}}$  indicate that the diversity order of USTLD systems is a product of the number of time slots over which the same information is transmitted and the number of receive antennas.

Stated differently, the diversity order represents the total number of independent copies of the same information codeword that are available at the receiver when performing detection. It is interesting to note that the number of labelling diversity mappers in the system does not directly influence the diversity order. This is shown most clearly by the result that  $\Gamma_{\text{Alamouti}} = \Gamma_{\text{USTLD (original)}} = 2N_{\text{Rx}}$ . Qualitative analysis of the results presented in other works that apply labelling diversity to systems that utilise only one transmission time slot, such as those studied by Naidoo [25], also indicate that diversity order is unaffected by labelling diversity.

This leads to an interesting deduction which was not reported in the original work on USTLD systems [2] – the inclusion of labelling diversity in system does not change the diversity order of the system. Rather, the BER performance improvement as a result of labelling diversity is qualitatively observed by a lateral shift of the high-SNR region of BER vs Total Average SNR curve (as shown in Figure 2.7). These lateral shifts of the BER vs Total Average SNR curve are generally typical of a coding gain [5], however labelling diversity does not introduce coding to the system.

A further observation that is drawn from the results in Figure 2.7 highlights the importance of mapper design USTLD systems. In their work, Ayanda *et al.* [10] compared their 3 mapper USTLD with a 2 mapper USTLD system based on the secondary mapper design by Xu *et al.* [2] for a 64QAM USTLD system. It was since shown by Quazi and Patel [3] that the secondary mapper design technique by Seddik *et al.* [20] is better than that proposed by Xu *et al.* for 64QAM modulation. The results in Figure 2.7 show that the  $3 \times 4$  64QAM USTLD system with 3 mappers [10] performs worse than the original  $2 \times 4$  64QAM 2 mapper USTLD system [2] (utilising the secondary mapper design proposed by Seddik *et al.*) by approximately 2dB. This emphasises that mapper design has a drastic influence on the performance of USTLD systems.

The final set of results in this paper investigates the performance of QRD-based LCDAs on HR-USTLD. Algorithms are compared in terms of accuracy and complexity to the benchmark case of MLD. Accuracy is observed graphically by the closeness of the BER curves to the ML case, and complexity is compared by using the equations presented in Tables 2.2 and 2.3. Since the number of effective real operations gives a more realistic indication of performance, the discussion focusses on this metric. It is also useful to define the percentage reduction in effective real operations for an LCDA, which is given by:

$$\% \text{ Reduction of } \Psi_{\text{LCDA}} = 1 - \frac{\Psi_{\text{LCDA}}}{\Psi_{\text{MLD}}}. \quad (2.31)$$

From the results presented in Figure 2.8 and 2.9, as well as Tables 2.5 and 2.6, it is clear that existing QRD-based LCDAs are unsuitable for HR-USTLD systems. Despite reducing the number of effective real operations by over 99%, these schemes fail to capture the system diversity and do not achieve detection accuracy comparable to MLD. By contrast, the proposed MSRS-D-USTLD algorithm achieves near-ML accuracy. The results indicate that there is a significant complexity cost associated with this increase in accuracy, as expected, when comparing MSRS-D-USTLD to existing QRD-based LCDAs. However, MSRS-D-USTLD provides considerable complexity reduction when

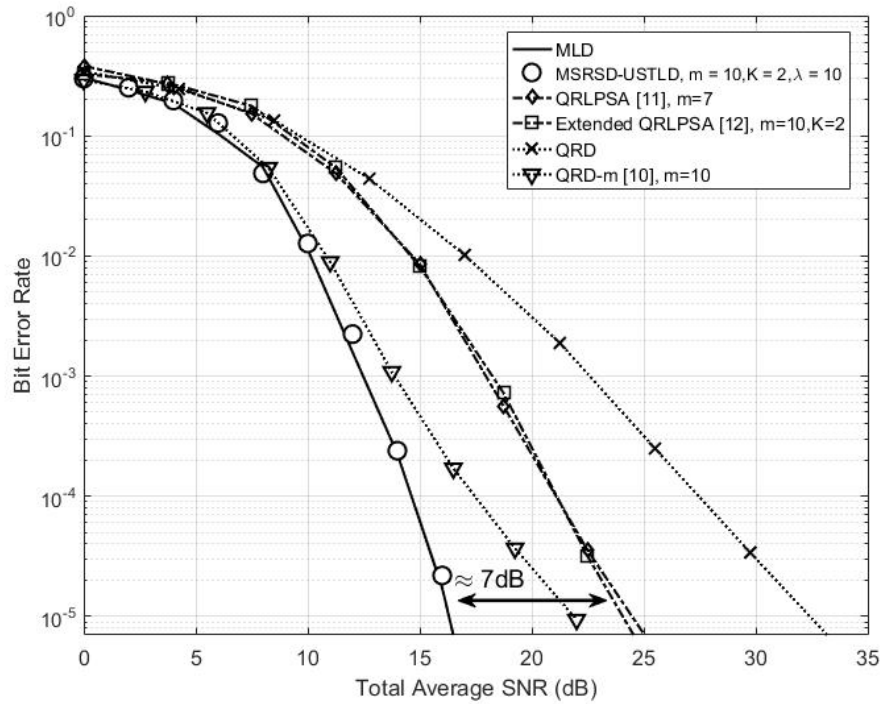

 FIGURE 2.8: Comparison of LCDA Accuracy for  $4 \times 4$  16QAM HR-USTLD

TABLE 2.5: Comparison of LCDA Complexity for HR-USTLD System in Figure 2.8

Candidate Label Vectors		
LCDA	No. of Candidate Label Vectors	
QRD	64	
QRD-m, $m = 10$	496	
QRLPSA, $m = 7$	256	
Extended QRLPSA, $m = 10, K = 85$	522	
MSRSU-USTLD, $m = 10, K = 2, \lambda = 10$	13 574	
MLD	65 536	
Effective Real Operations		
LCDA	$\Psi_{\text{LCDA}}$	% Reduction in $\Psi$
QRD	3 372	99.98%
QRD-m, $m = 10$	27 132	99.86%
QRLPSA, $m = 7$	10 076	99.95%
Extended QRLPSA, $m = 10, K = 85$	24 630	99.87%
MSRSU-USTLD, $m = 10, K = 2, \lambda = 10$	3 808 534	79.75%
MLD	18 808 832	0%

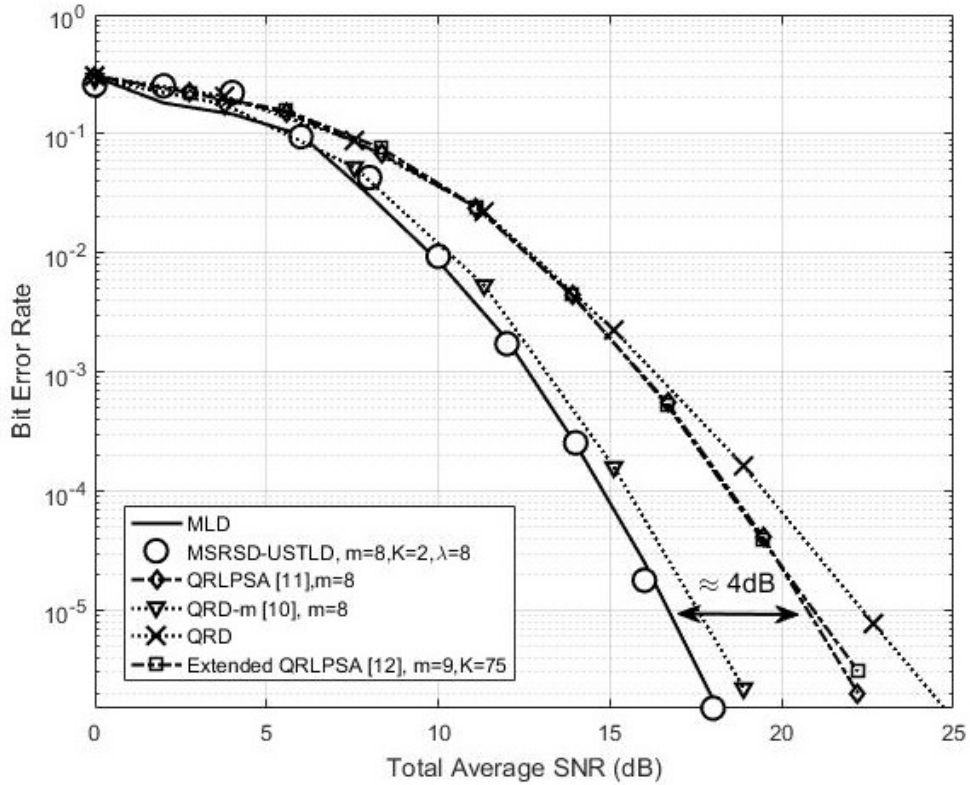

 FIGURE 2.9: Comparison of LCDA Accuracy for  $4 \times 5$  16PSK HR-USTLD

TABLE 2.6: Comparison of LCDA Complexity for HR-USTLD System in Figure 2.9

Candidate Label Vectors		
LCDA	No. of Candidate Label Vectors	
QRD	64	
QRD-m, $m = 8$	400	
QRLPSA, $m = 8$	288	
Extended QRLPSA, $m = 9, K = 75$	470	
MSRSD-USTLD, $m = 8, K = 2, \lambda = 8$	5 154	
MLD	65 536	
Effective Real Operations		
LCDA	$\Psi_{\text{LCDA}}$	% Reduction
QRD	3544	99.98%
QRD-m, $m = 8$	22 024	99.91%
QRLPSA, $m = 8$	11 636	99.95%
Extended QRLPSA, $m = 9, K = 75$	22 415	99.90%
MSRSD-USTLD, $m = 8, K = 2, \lambda = 8$	1 758 530	92.53%
MLD	23 527 424	0%

compared to the benchmark case of MLD. For high modulation orders, the achievable complexity reduction of MSRSD-USTLD may be approximated as  $1 - \left(\frac{\lambda-1}{M}\right)^{N_{\text{Tx}}}$ . For reasonable values such as  $\lambda = 35$  and a  $4 \times N_{\text{Rx}}$  64-ary QAM or PSK system, this results in complexity reduction of approximately  $1 - \left(\frac{34}{64}\right)^4 = 92.03\%$ .

## 2.6 Conclusion

In this paper, USTLD was extended to a more general case of any  $N_{\text{Tx}}$  transmit antennas. The motivation behind such an extension is that increasing  $N_{\text{Tx}}$  allows for higher data rates to be achieved at lower modulation orders; which results in better system error performance. Results confirm this and show a 4dB performance improvement between HR-USTLD and existing USTLD systems for a 6 bits/sec/Hz data rate. In addition to defining the HR-USTLD system model, this paper derives an analytical expression for the upper bound of the ABEP which is verified against simulated results.

To combat the exponential increase in computational complexity associated with systems with multiple transmit antennas, a new LCDA designed specifically for the HR-USTLD systems is presented (MSRSD-USTLD). It is shown that MSRSD-USTLD is capable of achieving near-ML detection accuracy. From the systems investigated, the worst-case complexity of MSRSD-USTLD is shown to still achieve 79.75% complexity reduction when compared to MLD in a  $4 \times 4$  16QAM HR-USTLD system and 92.53% reduction in a  $4 \times 5$  16PSK HR-USTLD system. It is noted that although the MSRSD-USTLD algorithm proposed has been developed using QRD-based LCDAs in its initial stages, this is not a strict constraint. As such, future works may investigate the application of other existing LCDAs in the initial stages of MSRSD-USTLD.

## 2.7 Appendix: Derivations of Complexity in Terms of Effective Real Operations

In the work of Pillay and Xu [4], it is suggested that algorithmic complexity be measured in terms of real operations. This paper considers the same metric when determining the complexity of the detection schemes considered. When working with complex numbers, a single complex multiplication consists of 4 real multiplications and 2 real additions, equalling 6 effective real operations. Complex addition consists of 2 real additions, and similarly for complex subtractions. The derivation of complexity in terms of this metric for the detection schemes given in Section 2.3.2 follows.

### 2.7.1 MLD Derivation

MLD for HR-USTLD is done by evaluating the decision metric given in (2.4) for each of the  $M^{N_{\text{Tx}}}$  possible vector pairs  $\langle \hat{\mathbf{x}}_1, \hat{\mathbf{x}}_2 \rangle$ , where  $\langle \hat{x}_{i_1}, \hat{x}_{i_2} \rangle \in \xi, i \in [1 : N_{\text{Tx}}]$ . For a given vector  $\hat{\mathbf{x}}_t, t \in [1 : 2]$ , the following derives the complexity of calculating vector norm  $\|\mathbf{z}_t - \mathbf{H}_t \hat{\mathbf{x}}_t\|^2$ :

1. Matrix product  $\mathbf{H}_t \hat{\mathbf{x}}_t$ :  $N_{\text{Tx}} N_{\text{Rx}}$  complex multiplications,  $N_{\text{Rx}} N_{\text{Tx}} - N_{\text{Rx}}$  complex additions.
2. Vector subtraction  $\mathbf{z}_t - \mathbf{H}_t \hat{\mathbf{x}}_t$ :  $N_{\text{Rx}}$  complex subtractions.
3. Vector norm  $\|\mathbf{z}_t - \mathbf{H}_t \hat{\mathbf{x}}_t\|^2$ :  $4N_{\text{Rx}} - 1$  real operations.

This gives a total of  $8N_{\text{Tx}} N_{\text{Rx}} + 4N_{\text{Rx}} - 1$  effective real operations. It then follows that the complexity of MLD is given by

$$\begin{aligned} \Psi_{\text{MLD}} &= M^{N_{\text{Tx}}} (2(8N_{\text{Tx}} N_{\text{Rx}} + 4N_{\text{Rx}} - 1) + 1) \\ &= M^{N_{\text{Tx}}} (16N_{\text{Tx}} N_{\text{Rx}} + 8N_{\text{Rx}} - 1). \end{aligned} \quad (2.32)$$

### 2.7.2 QRD, QRD-m and QRLPSA Derivations

For QRD, QRD-m and QRLPSA, the derivations presented are for perfectly determined systems. This approach is identical when considering overdetermined systems if zero rows are discarded. Pre-processing by re-ordering  $\mathbf{H}$  is not considered part of the algorithm, and the complexity of performing the actual decompositions (i.e. converting  $\mathbf{H}$  to matrix product  $\mathbf{QR}$  or matrix product  $\mathbf{QL}$ ) is neglected, as per Peer *et al* [18].

When considering any QRD-based detection schemes, the first step of detection after decomposing matrix  $\mathbf{H}$  is to perform left-multiplication as shown in (2.5). This matrix multiplication consists of  $2N_{\text{Rx}}^2$  complex multiplications and  $2N_{\text{Rx}}(N_{\text{Rx}} - 1)$  complex additions, giving a total complexity of  $16N_{\text{Rx}}^2 - 4N_{\text{Rx}}$  effective real operations. The left-multiplication for a QLD-based system, which

is necessary for the QRLPSA, is described by (2.6) and incurs the same complexity as for QRD. Searching through the  $q$ -th layer of the QRD search tree during time slot  $t$ , as described by (2.9), the complexity may be calculated as:

1. Summation  $S_{1t}$ :  $q - 1$  complex multiplications,  $q - 2$  complex additions.
2. Scalar subtraction  $\alpha_{qt} - r_{q,qt}\hat{x}_t - S_{1t}$ : 1 complex multiplication, 2 complex subtractions.
3. ED  $|\alpha_{qt} - r_{q,qt}\hat{x}_t - S_{1t}|^2$ : 3 real operations

Thus the complexity of searching through the  $q$ -th layer of the QRD search tree has  $8q + 3$  effective real operations. Summing this result across both time slots yields:

$$\Psi_{\text{layer}}(q) = 2(8q + 3) + 1 = 16q + 7. \quad (2.33)$$

The complexity for searching through the QRD tree is found by summing the result of (2.33) through all  $N_{\text{Tx}}$  layers of the QRD search tree and testing  $M$  candidate symbol pairs per layer. Using the identity given by Weisstein [26],  $\sum_{k=1}^A k = \frac{A}{2}(A + 1)$ , the result is:

$$\begin{aligned} \Psi_{\text{QRD}} &= 16N_{\text{Rx}}^2 - 4N_{\text{Rx}} + M \sum_{q=1}^{N_{\text{Tx}}} \Psi_{\text{layer}}(q) \\ &= 16N_{\text{Rx}}^2 - 4N_{\text{Rx}} + M (8N_{\text{Tx}}^2 + 15N_{\text{Tx}}), \end{aligned} \quad (2.34)$$

where the first two terms are as a result of the left-multiplication as explained previously. The same result is obtained for a QLD search tree.

For QRD- $m$ , (2.34) is adjusted to cater for the  $m$  search paths considered from the second search layer onwards, yielding:

$$\begin{aligned} \Psi_{\text{QRD-}m} &= 16N_{\text{Rx}}^2 - 4N_{\text{Rx}} + M\Psi_{\text{layer}}(1) + mM \sum_{q=2}^{N_{\text{Tx}}} \Psi_{\text{layer}}(q) \\ &= 16N_{\text{Rx}}^2 - 4N_{\text{Rx}} + 23M + mM (8N_{\text{Tx}}^2 + 15N_{\text{Tx}} - 23). \end{aligned} \quad (2.35)$$

For parallel searching, it is sufficient to consider only the complexity of the QRD search tree and double the result to take the QLD search tree into account. While traversing the search tree, the best  $m$  paths of the search tree are considered and  $M$  nodes are expanded at each layer, for each path. Only  $\left\lfloor \frac{N_{\text{Tx}}}{2} \right\rfloor$  layers of the QRD and QLD search trees may be evaluated in parallel, and for odd  $N_{\text{Tx}}$ , the  $\left\lceil \frac{N_{\text{Tx}}}{2} \right\rceil$ -th layer is evaluated after parallel searching.

Thus, the complexity of QRLPSA may be expressed as:

$$\begin{aligned} \Psi_{\text{QRLPSA}} = & \left( \left\lceil \frac{N_{\text{Tx}}}{2} \right\rceil - \left\lfloor \frac{N_{\text{Tx}}}{2} \right\rfloor \right) \Psi_{\text{layer}} \left( \left\lceil \frac{N_{\text{Tx}}}{2} \right\rceil \right) \\ & + 2 \left( 16N_{\text{Rx}}^2 - 4N_{\text{Rx}} + M\Psi_{\text{layer}}(1) + mM \sum_{q=2}^{\left\lfloor \frac{N_{\text{Tx}}}{2} \right\rfloor} \Psi_{\text{layer}}(q) \right). \end{aligned} \quad (2.36)$$

Solving for the cases of even and odd  $N_{\text{Tx}}$  respectively yields:

$$\Psi_{\text{QRLPSA, even } N_{\text{Tx}}} = 32N_{\text{Rx}}^2 - 8N_{\text{Rx}} + 46M + mM(4N_{\text{Tx}}^2 + 15N_{\text{Tx}} - 46) \quad (2.37)$$

$$\Psi_{\text{QRLPSA, odd } N_{\text{Tx}}} = 32N_{\text{Rx}}^2 - 8N_{\text{Rx}} + 46M + mM(4N_{\text{Tx}}^2 + 15N_{\text{Tx}} - 42) \quad (2.38)$$

### 2.7.3 Extended QRLPSA Derivation

For the Extended QRLPSA, the first stage is to perform parallel searching and thus incurs the complexity described by (2.36)-(2.38). During the second stage, there are only  $m^2$  real additions as a result of summing the metrics of the partial candidate label vectors during merging. Sorting and reducing to the set of  $K$  merged vectors incurs minimal complexity and is neglected. Finally, the complexity of the third stage is found by evaluating (2.33) for the latter  $\left\lceil \frac{N_{\text{Tx}}}{2} \right\rceil$  layers of the QRD search tree and expanding  $K$  nodes per layer. Thus the complexity of Extended QRLPSA is:

$$\begin{aligned} \Psi_{\text{Extended QRLPSA}} = & \Psi_{\text{QRLPSA}} + m^2 + K \sum_{q=\left\lceil \frac{N_{\text{Tx}}}{2} \right\rceil}^{N_{\text{Tx}}} \Psi_{\text{layer}}(q) \\ = & \Psi_{\text{QRLPSA}} + m^2 + K \left( \sum_{p=1}^{N_{\text{Tx}}} \Psi_{\text{layer}}(p) - \sum_{q=1}^{\left\lfloor \frac{N_{\text{Tx}}}{2} \right\rfloor} \Psi_{\text{layer}}(q) \right). \end{aligned} \quad (2.39)$$

For even  $N_{\text{Tx}}$ , the summation term reduces to  $K(6N_{\text{Tx}}^2 + \frac{15}{2}N_{\text{Tx}})$ . Similarly, for odd  $N_{\text{Tx}}$ , the summation reduces to  $K(6N_{\text{Tx}}^2 + \frac{23}{2}N_{\text{Tx}} + \frac{11}{2})$ .

### 2.7.4 MSRSD-USTLD Derivation

Similarly to Extended QRLPSA, the first stage of MSRSD-USTLD is to perform parallel searching, the complexity of which is given in (2.36)-(2.38). Stages 2 and 3 both evaluate the MLD detection metric  $\mathcal{A}$ , which has been defined in (2.4), through  $\xi_{\text{merged}}$  and  $\xi_{\text{reduced}}$  respectively. Complexity for each of these stages may be found by using the result from (2.32) for the complexity of the ML metric and multiplying by the cardinality of the respective search set. For Stage 2,  $|\xi_{\text{merged}}| = m^2$

and thus the complexity is:

$$\Psi_{\text{MSRSD-USTLD, Stage 2}} = m^2 (16N_{\text{Tx}}N_{\text{Rx}} + 8N_{\text{Rx}} - 1). \quad (2.40)$$

For Stage 3, due to the optimisations outlined in Section 2.3.2.5, the size of the search space  $|\xi_{\text{reduced}}|$  cannot be exactly determined. The maximum size of the reduced set search space is given by  $|\xi_{\text{reduced}}|_{\text{max}} = K(\lambda - 1)^{N_{\text{Tx}}}$ . Thus, the resulting upper bound on the Stage 3 complexity is:

$$\Psi_{\text{MSRSD-USTLD, Stage 3}} \leq K(\lambda - 1)^{N_{\text{Tx}}} (16N_{\text{Tx}}N_{\text{Rx}} + 8N_{\text{Rx}} - 1). \quad (2.41)$$

Finally, the complexity of MSRSD-USTLD is given by:

$$\Psi_{\text{MSRSD-USTLD}} \leq \Psi_{\text{QRLPSA}} + \Psi_{\text{MSRSD-USTLD, Stage 2}} + \Psi_{\text{MSRSD-USTLD, Stage 3}}. \quad (2.42)$$

Substituting (2.36), (2.40) and (2.41) into (2.42) produces the expression given in Table 2.3.

## References

- [1] Simon MK, Alouini M-S. *Digital Communication over Fading Channels, A Unified Approach to Performance Analysis*. New York (USA): John Wiley & Sons Inc.; 2000.
- [2] Xu H, Govindasamy K, Pillay N. Uncoded Space-Time Labeling Diversity. *IEEE Commun. Lett.* 2016; 20(8):1511–1514.
- [3] Quazi T, Patel SS. USTLD Mapper Design for APSK Constellation over Satellite Channels. *Trans. Emerging Telecomm. Tech.* 2018: under review.
- [4] Pillay N, Xu H. Uncoded Space-Time Labeling Diversity – Application of Media-based Modulation with RF Mirrors. *IEEE Commun. Lett.* 2018;22(2):272–275.
- [5] Goldsmith A. *Wireless Communications*. Cambridge (USA): Cambridge University Press; 2005.
- [6] Cormen TH, Leiserson CE, Rivest RL, Stein C. *Introduction to Algorithms*. Cambridge (USA): The MIT Press; 2009.
- [7] Fincke U, Pohst M. Improved Methods for Calculating Vectors of Short Length in a Lattice. *Math. of Computation.* 1985; 44(170):463–471.
- [8] Alamouti SM. A Simple Transmit Diversity Technique for Wireless Communications. *IEEE J. on Sel. Areas in Commun.* 1998; 16(8):1451–1458.
- [9] Samra H, Ding Z, Hahn P. Symbol Mapping Diversity Design for Multiple Packet Transmissions. *IEEE Trans. Commun.* 2005;53(5):810–817.
- [10] Ayanda D, Xu H, Pillay N. Uncoded M-ary quadrature amplitude modulation space-time labeling diversity with three transmit antennas. *Int. J. Commun. Syst.* 2018:e3818. DOI: 10.1002/dac.3818.
- [11] Xu R, Lau FCM. Performance analysis for MIMO systems using zero forcing detector over fading channels. *IEE Proc. Commun.* 2006;153(1):74–80.
- [12] Prasad S, Sur SN. Lattice Reduction Aided Detection Techniques for MIMO Systems. *Int. Research Jour. of Eng. and Tech.* 2016; 3(3):1496–1502.
- [13] Jiang Y, Varanasi MK, Li J. Performance analysis of ZF and MMSE equalizers for MIMO systems: An in-depth study of the high SNR regime. *IEEE Trans. Inf. Theory.* 2011;57(4):2008–2026.
- [14] Neinavaie M, Derakhtian M. ML Performance Achieving Algorithm with the Zero-Forcing Complexity at High SNR Regime. *IEEE Trans. Wireless Commun.* 2016;15(7):4651–4659.
- [15] Vikalo H, Hassibi B. On the sphere-decoding algorithm II. Generalizations, second-order statistics, and applications to communications. *IEEE Trans. Signal Process.* 2005; 53(8):2819–2834.

- [16] Kim, KJ, Yue J, Iltis RA, Gibson JD. A QRD-D/Kalman Filter-Based Detection and Channel Estimation Algorithm for MIMO-OFDM Systems. *IEEE Trans. Wireless Commun.* 2005;4(2):710–721.
- [17] Radosavljevic P, Kim KJ, Shen H, Cavallaro JR. Parallel Searching-Based Sphere Detector for MIMO Downlink OFDM Systems. *IEEE Trans. Signal Process.* 2012;60(6):3240–3252.
- [18] Peer N, Murin Y, Dabora R. Improved QRD-QLD Algorithm for Low Complexity MIMO Decoding. *IEEE Commun. Lett.* 2014;18(10):1703–1706.
- [19] Govindasamy K. *Space-Time Labelling Diversity and Space-Time Block Coded Spatial Modulation with Labelling Diversity*. Masters Thesis, University of Kwa-Zulu Natal, 2015.
- [20] Seddik KG, Ibrahim AS, Liu KJR. Trans-Modulation in Wireless Relay Networks. *IEEE Commun. Lett.* 2008;12(3):170–172.
- [21] Govindasamy K, Xu H, Pillay N. Space-time block coded spatial modulation with labeling diversity. *Int. J. Commun. Syst.* 2017;31(1):e3395. DOI: 10.1002/dac.3395.
- [22] Dai Y, Sun S, Lei Z. A Comparative Study of QRD-M Detection and Sphere Decoding for MIMO-OFDM Systems. In: Proc. IEEE Int. Symp. Pers., Indoor and Mobile Radio Commun. Syst., Berlin (Germany); 2005:186–190.
- [23] Craig JW. A new, simple, and exact result for calculating the probability of error for two-dimensional signal constellations. In: IEEE Military Commun. Conf. (MILCOM), McLean, VA (USA); 1991:571–575.
- [24] Zhang H, Dai H, Zhou Q, Hughes BL. On the Diversity Order of Spatial Multiplexing Systems With Transmit Antenna Selection: A Geometrical Approach. *IEEE Trans. Inf. Theory.* 2006; 52(12): 5297–5311.
- [25] Naidoo NR. *Enhanced performance and efficiency schemes for Generalised Spatial Modulation*. Doctoral Thesis, University of Kwa-Zulu Natal, 2017.
- [26] Weisstein EW. Triangular Number (A Wolfram Web Resource). [Online Resource] <http://mathworld.wolfram.com/TriangularNumber.html>. Accessed May 25, 2017.

## Chapter 3

### Journal Article 2

# Error performance of Uncoded Space-Time Labelling Diversity in spatially correlated Nakagami-q channels

Sulaiman Saleem Patel, Tahmid Quazi, Hongjun Xu

Published: *International Journal of Communication Systems*

2018, vol. 31, no. 12, e-locator e3720, DOI: 10.1002/dac.3720

This article has been modified from its published version, which is in US English, to UK English for consistency with the rest of this thesis. Other minor typesetting changes were also done.

### 3.1 Abstract

Greater spectral efficiency has recently been achieved for Uncoded Space Time Labelling Diversity (USTLD) systems by increasing the number of antennas in the transmit antenna array. However, due to constrained physical space in hardware, the use of more antennas can lead to degradation in error performance due to correlation. Thus, this paper studies the effects of spatial correlation on the error performance of USTLD systems. The union bound approach, along with the Kronecker correlation model, is used to derive an analytical expression for the average bit error probability (ABEP) in the presence of Nakagami- $q$  fading. This expression is validated by the results of Monte Carlo simulations, which shows a tight fit in the high signal-to-noise ratio (SNR) region. The degradation in error performance due to transmit and receive antenna correlation is investigated independently. Results indicate that transmit antenna correlation in the USTLD systems investigated ( $3 \times 3$  8PSK,  $2 \times 4$  16PSK,  $2 \times 4$  16QAM and  $2 \times 4$  64QAM) causes a greater degradation in error performance than receive antenna correlation. It is also shown that  $2 \times 4$  USTLD systems are more susceptible to correlation than comparable space-time block coded systems for 8PSK, 16PSK, 16QAM and 64QAM.

## 3.2 Introduction

The idea of labelling diversity was initially proposed by Huang and Ritcey [1, 2] for bit-interleaved coded systems with iterative decoding (BICSS-ID), which was later expanded on by Krasicki [3, 4]. The use of convolutional coding in BICSS-ID incurs high detection complexity, resulting in higher latencies and increased power consumption. This motivated for the subsequent application of labelling diversity to uncoded systems, such as: decode-and-forward relay systems [5], multi-packet data transmissions with automatic repeat requests [6, 7], space-time block coded (STBC) systems [8], STBC systems with spatial modulation [9] and space time channel modulated STBC systems using radio frequency mirrors [10].

The focus of this paper is on the Uncoded Space Time Labelling Diversity (USTLD) systems proposed by Xu *et al* [8]. USTLD systems achieve improved error performance compared to conventional multiple-input, multiple-output (MIMO) systems as a result of two diversity mechanisms: labelling diversity and antenna diversity. Labelling diversity is achieved by transmitting the same binary data over two time slots using symbols from two different constellation mappings. The binary mappers are designed such that adjacent symbols in each constellation map are spaced further apart in subsequent maps. This allows detection to be based on symbol pairs instead of individual symbols. In doing so, error performance is improved in a similar manner to conventional error correction codes [11], despite USTLD being an uncoded system.

Antenna diversity is achieved by adopting a MIMO structure, which creates more signal paths between transmitter and receiver, each of which experiences independent fading. Ideally, these signal paths are independent and identically distributed (i.i.d.). The use of multiple signal paths leads to lower error rates when compared to a single path [11, 12]. The original MIMO structure of USTLD [8] describes a system with two transmit antennas and any arbitrary  $N_{\text{Rx}}$  receive antennas. This  $2 \times N_{\text{Rx}}$  structure, along with the use of two time slots to transmit the same binary information, closely resembles the orthogonal STBC system proposed by Alamouti [13]. Xu *et al.* show that labelling diversity allows USTLD systems to achieve better error performance than Alamouti STBC systems.

The  $2 \times N_{\text{Rx}}$  USTLD model was recently extended to consider any arbitrary  $N_{\text{Tx}}$  transmit antennas by Patel *et al* [14]. It is noted that  $N_{\text{Tx}} \times N_{\text{Rx}}$  USTLD systems are comparable to existing quasi-orthogonal STBC (Q-STBC) systems with more than two transmit antennas [15–17]. The use of  $N_{\text{Tx}} > 2$  transmit antennas allows Q-STBC systems to achieve more transmit antenna diversity, improving error performance. However, Q-STBC systems use more than two time slots to transmit the same binary information. As a result, Q-STBC systems experience higher latencies, decreased spectral efficiency and increased processing overheads.  $N_{\text{Tx}} \times N_{\text{Rx}}$  USTLD systems are not as affected by these challenges as they use *only two* time slots.

Conventional ideal analysis of MIMO systems, such as USTLD, assumes that signal paths are i.i.d., and hence, the channels are uncorrelated. However, in a real system, channels may experience

spatial or temporal correlation. Temporal correlation arises when the system experiences deep fading [12, 18]. Spatial correlation results from the physical proximity of antennas and may be expressed as a function of the spacing between antennas and the wavelength of the transmission carrier [19–21]. Due to the inverse proportionality between wavelength and frequency, there is a greater likelihood of antenna correlation occurring at higher frequencies (such as the millimetre wave frequency spectrum that has been studied for next-generation MIMO systems [22]). To this end, the study of USTLD in spatially correlated channels provides insight into the degradation in error performance that may be expected when USTLD is applied to real systems, such as mobile ad-hoc networks or satellite telecommunication. Temporal correlation is not studied in detail, as the error performance of USTLD does not degrade in the presence of quasi-static fading across both transmission time slots [8].

The simplest case of correlated channel analysis is to consider a system with dual-correlated receive antennas (i.e. two correlated receive antennas). In Fang *et al.* [23], it is shown that identical, dual-correlated channels may be modelled as equivalent non-identical, uncorrelated channels by applying an orthogonal transform. This technique was adapted in a study of USTLD systems in dual-correlated channels [24], which presents results for a  $2 \times 2$  system assuming no transmit antenna correlation. The same work [24] also shows that, for dual-correlated systems, the error performance of USTLD deteriorates more rapidly as channel correlation increases when compared to conventional MIMO systems.

This paper extends the aforementioned study [24] to the more general case of  $N_{\text{Tx}} \times N_{\text{Rx}}$  USTLD systems in the presence of antenna correlation, at either the transmit or receive sides, or both. To achieve this, the methods of analysis given in Hedayet *et al.* [18] are adopted in this paper. By using the Kronecker model [25], Hedayet *et al.* showed that the identical correlated channels of space-time coded MIMO systems may be modelled as eigenvalue-weighted, uncorrelated channels for statistical analysis [18]. This technique has previously been employed in the study of various other correlated MIMO systems such as: space-time trellis coded systems [18], super-orthogonal space-time trellis coded systems [18], generalised STBC systems [18], STBC spatial modulation systems [26], decode-and-forward based cooperative STBC spatial modulation systems [27], linear dispersion coded systems [18] and diagonal-algebraic space-time coded systems [18]. It is noted that other correlation models have been proposed in literature, such as the non-separable correlation model [29–32]. These studies indicate that the non-separable model provides a better fit to measured data than the Kronecker model when analysing channel capacity. However, the works of Tulino *et al.* [30], Lin *et al.* [33] and Moustakas *et al.* [34] show that the non-separable model reduces to the Kronecker model for systems that achieve antenna diversity, and hence they are equivalent for USTLD systems.

Previous studies of USTLD [8, 14, 24] have all been conducted under the assumption of Rayleigh fading channels. The Rayleigh fading model describes transmission paths where there is no strong line-of-sight path between the transmitter and receiver [11, 12]. A more general model that better indicates the worst-case performance of a MIMO system is the Nakagami- $q$  fading model [28, 35],

which encompasses Rayleigh fading as a specific case. Literature shows that Nakagami- $q$  provides a good fit for modelling signal propagation in satellite links subjected to strong ionospheric scintillation [12, 36]. To this end, a further contribution of this paper is that the error performance of USTLD is derived for Nakagami- $q$ .

In terms of notation, this paper represents vectors and matrices in boldface and scalars in italics.  $(\cdot)^T$ ,  $(\cdot)^H$ ,  $\|\cdot\|$  and  $\mathcal{E}\{\cdot\}$  represent the transpose, Hermitian operator, vector Frobenius norm and statistical expectation, respectively.  $J_0(z)$  and  $I_0(z)$  are the respective unmodified and modified zeroth-order Bessel functions of the first kind, related by  $J_0(z) = I_0(-jz)$ , as indicated by Weisstein [37].  $a \sim \mathcal{N}(\bar{x}, \sigma^2)$  means that the random variable  $a$  follows a normal distribution with mean  $\bar{x}$  and variance  $\sigma^2$ . The superscripts  $(\cdot)^I$  and  $(\cdot)^Q$  represent the in-phase and quadrature components of complex signals respectively. The operator  $\mathcal{V}\{\mathbf{A}\}$  returns the eigenvalues of matrix  $\mathbf{A}$ .

### 3.3 System Model

#### 3.3.1 Transmission Model

The system considers an  $N_{\text{Tx}} \times N_{\text{Rx}}$  USTLD system as defined by Patel *et al.* [14], where  $N_{\text{Tx}} \leq N_{\text{Rx}}$ . For a  $2^m$ -ary constellation, every  $m$  bits from the data stream defines a codeword, or ‘label’,  $L$ . Thus, a bitstream of  $mN_{\text{Tx}}$  information bits produces a label vector with  $N_{\text{Tx}}$  entries,  $\mathbf{L} = [L_1 \ \cdots \ L_{N_{\text{Tx}}}]^T$ .  $\mathbf{L}$  is used to produce symbols that are transmitted across two time slots. To achieve labelling diversity, the transmitted symbols in each time slot are selected from different binary mappers  $\Omega_1$  and  $\Omega_2$ . The vector of symbols transmitted in time slot  $k$ , where  $k \in [1 : 2]$ , is thus  $[\Omega_k(\mathbf{L})] = [\Omega_k(L_1) \ \cdots \ \Omega_k(L_{N_{\text{Tx}}})]^T$ . This work focuses on quadrature amplitude modulated (QAM) and phase shift keyed (PSK) constellations, due to the existence of binary mappers which achieve labelling diversity for these modulation schemes [6, 8]. The sub-optimal binary mappers proposed by Xu *et al.* [8] are used for 64QAM and all PSK constellations. For 16QAM, the mapping structure of Samra *et al.* [6] (illustrated in Figure 3.1) is used, as it is found to be optimal [6, 8]. All constellations are power-normalised such that  $\mathcal{E}\{|\Omega_1(l)|^2\} = \mathcal{E}\{|\Omega_2(l)|^2\} = 1$  for all possible labels  $l \in [0 : 2^m - 1]$ .

The received signal vector,  $\mathbf{r}$ , during time slot  $k$  is thus given by

$$\mathbf{r}_k = \sqrt{\frac{\gamma}{N_{\text{Tx}}}} \mathbf{H}_k [\Omega_k(\mathbf{L})] + \mathbf{n}_k, \quad k \in [1 : 2], \quad (3.1)$$

where  $\gamma$  represents the total average signal-to-noise ratio (SNR) of the transmission, assumed to be equally distributed among the  $N_{\text{Tx}}$  transmit antennas.  $\mathbf{n}_k = [n_{1k} \ \cdots \ n_{N_{\text{Rx}}k}]^T$  represents additive

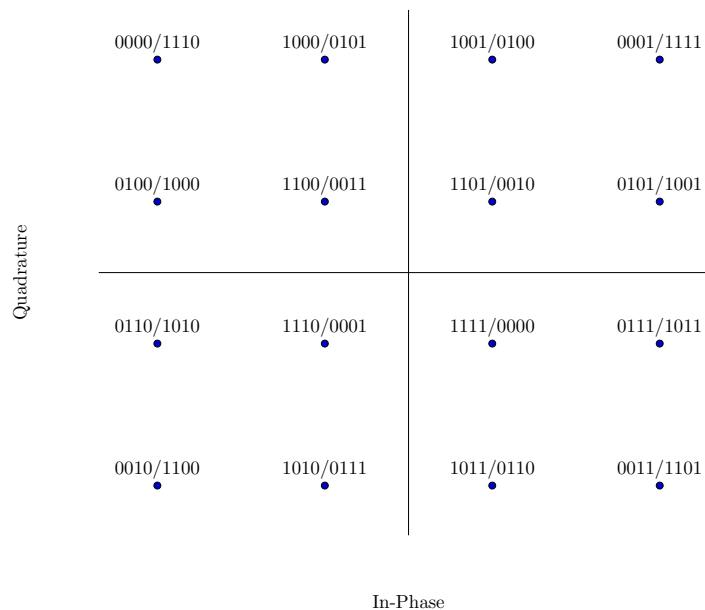


FIGURE 3.1: 16QAM Binary Constellation Mapping. Key:  $\Omega_1/\Omega_2$

white Gaussian noise (AWGN) during time slot  $k$  which follows a complex normal distribution with zero mean and unit variance.  $\mathbf{H}_k = [\mathbf{h}_k^{(1)} \ \dots \ \mathbf{h}_k^{(N_{\text{Tx}})}]$  represents the correlated fading channels during time slot  $k$ , which are assumed to be frequency-flat and may either be fast or quasi-static fading over the duration of the two time slots. Each vector  $\mathbf{h}_k^{(a)}$ ,  $a \in [1 : N_{\text{Tx}}]$ , is a column with  $N_{\text{Rx}}$  entries. It is assumed that the fading follows a Nakagami- $q$  amplitude distribution. The entry of  $\mathbf{H}_k$  in column  $a$  and row  $b$  is denoted  $h_{b_k}^{(a)} = \left(h_{b_k}^{(a)}\right)^{\text{I}} + \text{j} \left(h_{b_k}^{(a)}\right)^{\text{Q}}$ ,  $a \in [1 : N_{\text{Rx}}]$ ,  $b \in [1 : N_{\text{Tx}}]$ ,  $k = [1 : 2]$ . The fading parameter  $q$  is the ratio of the standard deviations of the quadrature to in-phase components of each entry in  $\mathbf{H}_k$ , as stated by Amol and Kaur [28], and lies in the range  $0 \leq q \leq 1$ . Romero-Jerez and Lopez-Martinez [35] further indicate that  $q$  may also be viewed as an indication of the correlation between  $\left(h_{b_k}^{(a)}\right)^{\text{I}}$  and  $\left(h_{b_k}^{(a)}\right)^{\text{Q}}$ . Each component of the elements in  $\mathbf{H}_k$  may be modelled as Gaussian-distributed random variables (RVs) such that  $\left(h_{b_k}^{(a)}\right)^{\text{I}} \sim \mathcal{N}\left(0, \frac{1}{1+q^2}\right)$  and  $\left(h_{b_k}^{(a)}\right)^{\text{Q}} \sim \mathcal{N}\left(0, \frac{q^2}{1+q^2}\right)$  for all  $a \in [1 : N_{\text{Rx}}]$ ,  $b \in [1 : N_{\text{Tx}}]$ ,  $k = [1 : 2]$  [38]. The probability density function (PDF) for the Nakagami- $q$  fading amplitude,  $x$ , which has zero mean and unit variance is [12]

$$f_x(x) = \frac{x(1+q^2)}{q} \exp\left(-\frac{x^2(1+q^2)^2}{4q^2}\right) I_0\left(\frac{x^2(1-q^4)}{4q^2}\right). \quad (3.2)$$

It may be observed that the bounds of  $q$  correspond to the respective cases of single-sided Gaussian (SSG) ( $q = 0$ ) and Rayleigh ( $q = 1$ ) amplitude distributions [12]. Additionally, in (3.1),  $\mathbf{n}_k$  and  $\mathbf{H}_k$  are assumed to have uniform phase distribution.

### 3.3.2 Correlation Model

In this paper, the Kronecker correlation model [25] is adopted to relate the correlated channel matrix in the  $k$ -th time slot ( $\mathbf{H}_k$ ) to an uncorrelated channel matrix in the same time slot ( $\check{\mathbf{H}}_k$ ), as given in (3.3).

$$\mathbf{H}_k = \mathbf{C}_{\text{Rx}}^{\frac{1}{2}} \check{\mathbf{H}}_k \left(\mathbf{C}_{\text{Tx}}^{\frac{1}{2}}\right)^{\text{T}}, \quad k \in [1 : 2], \quad (3.3)$$

where  $\mathbf{C}_{\text{Tx}}$  and  $\mathbf{C}_{\text{Rx}}$  represent the respective antenna correlation matrices at the transmitter and receiver. The  $N_{\text{Rx}} \times N_{\text{Rx}}$  receive antenna correlation matrix is described by [20]

$$\mathbf{C}_{\text{Rx}} = \begin{bmatrix} 1 & \rho_{\text{Rx}}^{(1,2)} & \dots & \rho_{\text{Rx}}^{(1,N_{\text{Rx}})} \\ \rho_{\text{Rx}}^{(2,1)} & 1 & \dots & \rho_{\text{Rx}}^{(2,N_{\text{Rx}})} \\ \vdots & \vdots & \ddots & \vdots \\ \rho_{\text{Rx}}^{(N_{\text{Rx}},1)} & \dots & \rho_{\text{Rx}}^{(N_{\text{Rx}},N_{\text{Rx}}-1)} & 1 \end{bmatrix}, \quad (3.4)$$

where  $\rho_{\text{Rx}}^{(i,j)}$  denotes the correlation coefficient between the  $i$ -th and  $j$ -th receive antennas.  $N_{\text{Tx}} \times N_{\text{Tx}}$  matrix  $\mathbf{C}_{\text{Tx}}$  is similarly defined in terms of the correlation coefficients between the  $i$ -th and  $j$ -th

transmit antennas,  $\rho_{\text{Tx}}^{(i,j)}$ . Both  $\mathbf{C}_{\text{Tx}}$  and  $\mathbf{C}_{\text{Rx}}$  are symmetrical matrices such that  $\rho_{\text{Tx}}^{(i,j)} = \rho_{\text{Tx}}^{(j,i)}$ ;  $i \neq j, i, j \in [1 : N_{\text{Tx}}]$  and  $\rho_{\text{Rx}}^{(i,j)} = \rho_{\text{Rx}}^{(j,i)}$ ;  $i \neq j, i, j \in [1 : N_{\text{Rx}}]$ . It is noted that instances of complex correlation coefficients exist in literature, in which case  $\rho_{\text{Tx}}^{(i,j)} = \rho_{\text{Tx}}^{\bar{(i,j)}}$ ;  $i \neq j, i, j \in [1 : N_{\text{Tx}}]$  and  $\rho_{\text{Rx}}^{(i,j)} = \rho_{\text{Rx}}^{\bar{(j,i)}}$ ;  $i \neq j, i, j \in [1 : N_{\text{Rx}}]$ , where  $\bar{(\cdot)}$  denotes the complex conjugate. However, in the context of only spatial correlation, only the magnitude of the correlation coefficient is of interest. Hence, this work only considers real values of  $\rho_{\text{Tx}}$  and  $\rho_{\text{Rx}}$ .

It is shown in [19]- [21] that the correlation coefficient between the  $i$ -th and  $j$ -th antennas in a linear array is given by

$$\rho^{(i,j)} = J_0 \left( \frac{2\pi}{\lambda} \mu^{(i,j)} \right). \quad (3.5)$$

Based on (3.5), for receive antennas with uniformly distributed angle of arrival, the correlation coefficient  $\rho_{\text{Rx}}^{(i,j)}$  is expressed in terms of receive antenna spacing  $\mu_{\text{Rx}}^{(i,j)}$ . Similarly, for transmit antennas with uniformly distributed angle of transmission,  $\rho_{\text{Tx}}^{(i,j)}$  is expressed in terms of  $\mu_{\text{Tx}}^{(i,j)}$ .

If antennas are not arranged linearly, alternate models to represent the correlation between antennas must be used. Examples of such cases are when antennas are very closely spaced, which results in a constant correlation between all antennas [39, 40]. If they are arranged non-linearly, such that they are all equispaced in some sense, correlation between antennas may be described by the exponential correlation model [39, 41, 42].

### 3.3.3 Detection

Maximum-likelihood detection (MLD), assuming perfect channel state information, is used to estimate the transmitted information label vector  $\tilde{\mathbf{L}}$  according to (3.6).

$$\tilde{\mathbf{L}} = \arg \min_{\hat{\mathbf{L}} \in \xi} \sum_{k=1}^2 \left\| \mathbf{r}_k - \sqrt{\frac{\gamma}{N_{\text{Tx}}}} \mathbf{H}_k[\Omega_k(\hat{\mathbf{L}})] \right\|^2, \quad (3.6)$$

where  $\xi$  is the set of all  $2^{mN_{\text{Tx}}}$  possible transmitted label vectors and  $\hat{\mathbf{L}}$  is a candidate label vector from  $\xi$ .

### 3.4 Error Performance Analysis

The union bound of the average bit error probability (ABEP) for an  $N_{\text{Tx}} \times N_{\text{Rx}}$  USTLD system has previously been derived under the assumption that only one received label is detected erroneously in the high SNR region [8, 14]. While the results presented in previous works on USTLD systems [8, 14] validate this assumption, it cannot be used when the methods of correlation analysis developed by Hedayat *et al.* [18] are applied. For this reason, this paper first derives the ABEP under uncorrelated conditions for a Nakagami- $q$  fading channel using the same assumption as previous works [8, 14]. Thereafter, the analysis is extended to the correlated case without this assumption. The expressions derived are valid for both fast fading and quasi-static fading.

#### 3.4.1 Uncorrelated Nakagami- $q$ Error Performance

When evaluating the uncorrelated ABEP of  $N_{\text{Tx}} \times N_{\text{Rx}}$  USTLD systems, the assumption that only one received label is detected erroneously in the high SNR region may be used [8, 14].

From Patel *et al.* [14], the union bound of the ABEP is given by

$$P_b(\gamma) \leq \sum_{L=0}^{2^m-1} P(L) \sum_{\substack{\tilde{L}=0 \\ \tilde{L} \neq L}}^{2^m-1} \frac{\delta(L, \tilde{L})}{m} P(L \rightarrow \tilde{L}). \quad (3.7)$$

In (3.7),  $P(L) = 2^{-m}$  is the uniformly-distributed probability of label  $L$  being transmitted.  $\delta(L, \tilde{L})$  and  $P(L \rightarrow \tilde{L})$  are, respectively, the number of bit errors and the pairwise error probability (PEP) between  $L$  and estimated label  $\tilde{L}$ .

Given the assumption that only one symbol pair is incorrect, the conditional PEP (3.8) may be expressed in terms of the Gaussian Q-function [43],  $\mathcal{Q}(x) = \frac{1}{\pi} \int_0^{\frac{\pi}{2}} \exp\left(-\frac{x}{2 \sin^2(y)}\right) dy$ , and four chi-squared RVs,  $\phi_1, \phi_2, \phi_3$  and  $\phi_4$  as

$$P(\mathbf{L} \rightarrow \tilde{\mathbf{L}} | \mathbf{H}_1, \mathbf{H}_2) = P\left(\sum_{k=1}^2 \left\| \mathbf{r}_k - \sqrt{\frac{\gamma}{N_{\text{Tx}}}} \mathbf{H}_k[\Omega_k(\tilde{\mathbf{L}})] \right\|^2 < \sum_{k=1}^2 \|\mathbf{n}_k\|^2\right) \quad (3.8)$$

$$= \mathcal{Q}\left(\sqrt{\phi_1 + \phi_2 + \phi_3 + \phi_4}\right). \quad (3.9)$$

Following the procedure given in the Appendix of Xu *et al.* [8], it may be shown that in a Nakagami- $q$  distribution, the chi-squared RVs are formed from Gaussian-distributed RVs with zero mean and different variances related by the fading parameter  $q$  [35]. Each of the chi-squared RVs have  $N_{\text{Rx}}$  degrees of freedom and may be defined by

$$\phi_l = \sum_{p=1}^{N_{\text{Rx}}} \alpha_{pl}^2, \quad l \in [1 : 4]. \quad (3.10)$$

The Gaussian RVs  $\alpha_{pl}$  follow normal distributions (as derived in the Appendix, Section 3.7) such that

$$\alpha_{p_1} \sim \mathcal{N} \left( 0, \frac{\gamma |d_1(L, \tilde{L})|^2}{2N_{\text{Tx}}(1+q^2)} \right), \quad (3.11)$$

$$\alpha_{p_2} \sim \mathcal{N} \left( 0, \frac{\gamma q^2 |d_1(L, \tilde{L})|^2}{2N_{\text{Tx}}(1+q^2)} \right), \quad (3.12)$$

$$\alpha_{p_3} \sim \mathcal{N} \left( 0, \frac{\gamma |d_2(L, \tilde{L})|^2}{2N_{\text{Tx}}(1+q^2)} \right), \quad (3.13)$$

$$\alpha_{p_4} \sim \mathcal{N} \left( 0, \frac{\gamma q^2 |d_2(L, \tilde{L})|^2}{2N_{\text{Tx}}(1+q^2)} \right), \quad (3.14)$$

where  $d_k(L, \tilde{L})$ ,  $k \in [1 : 2]$  is the difference between the symbols obtained by mapping  $L$  and  $\tilde{L}$  using mapper  $\Omega_k$ , as shown in (3.15).

$$d_k(L, \tilde{L}) = \Omega_k(L) - \Omega_k(\tilde{L}), \quad k \in [1 : 2]. \quad (3.15)$$

As in Xu *et al.* [8], the final unconditional PEP is obtained by integrating (3.9) over the PDF of the underlying chi-squared RVs. Applying the trapezoidal approximation to this integral, as done in previous works [8, 14] produces the result

$$\begin{aligned} P(L \rightarrow \tilde{L}) &\approx \frac{1}{4n} \prod_{k=1}^2 \left[ \mathcal{M}_k \left( \frac{1}{2}, |d_k(L, \tilde{L})|^2 \right) \right]^{N_{\text{Rx}}} \\ &+ \frac{1}{2n} \sum_{m=1}^{n-1} \prod_{k=1}^2 \left[ \mathcal{M}_k \left( \frac{1}{2 \sin^2 \left( \frac{m\pi}{2n} \right)}, |d_k(L, \tilde{L})|^2 \right) \right]^{N_{\text{Rx}}}. \end{aligned} \quad (3.16)$$

In (3.16),  $n$  is an arbitrarily large integer that allows the trapezoidal approximation to converge to the integral result.  $\mathcal{M}_k(s, x)$  denotes the moment generating function (MGF) of the received signal amplitude during the  $k$ -th time slot ( $k \in [1 : 2]$ ), as a function of dummy variables  $s$  and  $x$ . For a

Nakagami- $q$  distribution, the MGF is given by [12]

$$\mathcal{M}_k(s, x) = \left[ 1 + \frac{s\gamma x}{N_{\text{Tx}}} + \left( \frac{sq\gamma x}{N_{\text{Tx}}(1+q^2)} \right)^2 \right]^{-\frac{1}{2}}. \quad (3.17)$$

### 3.4.2 Correlated Nakagami- $q$ Error Performance

To apply the method of correlated channel analysis used given in Hedayet *et al.* [18], the union bound of the USTLD system considered is obtained by considering all possible combinations of transmitted and detected label vectors. The union bound is then modified from (3.7) to reflect that it is now dependent on the transmitted label vector  $\mathbf{L}$  and the estimated label vector  $\tilde{\mathbf{L}}$ . The bound is given by

$$P_b(\gamma) \leq \sum_{\mathbf{L} \in \boldsymbol{\xi}} P(\mathbf{L}) \sum_{\substack{\tilde{\mathbf{L}} \in \boldsymbol{\xi} \\ \mathbf{L} \neq \tilde{\mathbf{L}}}} \frac{\delta(\mathbf{L}, \tilde{\mathbf{L}})}{mN_{\text{Tx}}} P(\mathbf{L} \rightarrow \tilde{\mathbf{L}}). \quad (3.18)$$

Note that  $\boldsymbol{\xi}$  is the set of all possible transmitted label vectors, as defined in Section 3.3.3. As in Section 3.4.1,  $\delta(\mathbf{L}, \tilde{\mathbf{L}})$  is the total number of bit errors between  $\mathbf{L}$  and  $\tilde{\mathbf{L}}$ .

In (3.18), the probability that label vector  $\mathbf{L}$  was transmitted,  $P(\mathbf{L})$ , is uniformly distributed, resulting in

$$P(\mathbf{L}) = 2^{-mN_{\text{Tx}}} \quad (3.19)$$

The PEP,  $P(\mathbf{L} \rightarrow \tilde{\mathbf{L}})$ , is defined in terms of label vectors, as opposed to scalar labels used in Section 3.4.1. The vector of distances between the symbols defined by label vectors  $\mathbf{L}$  and  $\tilde{\mathbf{L}}$  on mapper  $\Omega_k$  is given in terms of (3.15) as

$$\mathbf{d}_k = \begin{bmatrix} d_k(L_1, \tilde{L}_1) \\ \vdots \\ d_k(L_{N_{\text{Tx}}}, \tilde{L}_{N_{\text{Tx}}}) \end{bmatrix}, \quad k \in [1 : 2]. \quad (3.20)$$

The non-zero eigenvalue of  $\mathbf{d} \cdot \mathbf{d}^{\text{H}}$  is analogous to the squared Euclidean distance  $|d|^2$  of the scalar case.

As shown in (3.3), the Kronecker correlation model shows that the correlated channel matrix during the  $k$ -th time slot,  $\mathbf{H}_k$ ,  $k \in [1 : 2]$ , may be expressed in terms of an artificial, uncorrelated channel matrix  $\check{\mathbf{H}}_k$ . By adopting this model and applying the analysis techniques of Hedayet *et al.* [18], the ABEP in *correlated* channels is found by using the result found for *uncorrelated* channels and weighting the MGFs (3.17) in the PEP expression by the  $N_{\text{Rx}}$  eigenvalues of the receive antenna correlation matrix (3.21). The squared Euclidean distances are replaced by the non-zero eigenvalue of the squared-distance weighted transmit antenna correlation matrix in each time slot (3.22). It is

noted that in (3.22),  $\mathbf{d}_k \cdot \mathbf{d}_k^H \cdot \mathbf{C}_{\text{Tx}}$  has rank one and thus there is only one non-zero eigenvalue for each value of  $k, k \in [1 : 2]$ , as shown by Hedayet *et al.* [18]. This would not be the case under the assumption that only one label is detected incorrectly in the high SNR region, as used in Section 3.4.1, and hence this assumption is inappropriate for the correlated channel analysis of USTLD systems.

$$\begin{bmatrix} \nu_1 \\ \vdots \\ \nu_{N_{\text{Rx}}} \end{bmatrix} = \mathcal{V}\{\mathbf{C}_{\text{Rx}}\}. \quad (3.21)$$

$$\eta_k = \mathcal{V}\{\mathbf{d}_k \cdot \mathbf{d}_k^H \cdot \mathbf{C}_{\text{Tx}}\}, \quad \eta_k \neq 0, k \in [1 : 2]. \quad (3.22)$$

The final result for the PEP of an  $N_{\text{Tx}} \times N_{\text{Rx}}$  USTLD system in correlated Nakagami- $q$  channels is thus

$$\begin{aligned} P(\mathbf{L} \rightarrow \tilde{\mathbf{L}}) &\approx \frac{1}{4n} \prod_{k=1}^2 \prod_{j=1}^{N_{\text{Rx}}} \mathcal{M}_k \left( \frac{1}{2}, \nu_j \eta_k \right) \\ &+ \frac{1}{2n} \sum_{m=1}^{n-1} \prod_{k=1}^2 \prod_{j=1}^{N_{\text{Rx}}} \mathcal{M}_k \left( \frac{1}{2 \sin^2 \left( \frac{m\pi}{2n} \right)}, \nu_j \eta_k \right). \end{aligned} \quad (3.23)$$

The result for correlated PEP (3.23) is of a similar form to that of the uncorrelated PEP (3.16). The difference between these two expressions is that the second argument of MGF  $\mathcal{M}_k$  is the squared Euclidean distance  $\left| d_k(L, \tilde{L}) \right|^2$  for the uncorrelated PEP, whereas it is the eigenvalue product  $\nu_j \eta_k$  for the correlated PEP.

It may be noted that uncorrelated USTLD systems may also be analysed using this approach. In the case of no transmit antenna correlation, the matrix  $\mathbf{C}_{\text{Tx}}$  is an  $N_{\text{Tx}} \times N_{\text{Tx}}$  identity matrix. Similarly, for no receive antenna correlation,  $\mathbf{C}_{\text{Rx}}$  is an  $N_{\text{Rx}} \times N_{\text{Rx}}$  identity matrix.

### 3.5 Results and Discussion

In this section, results are presented to investigate the effects of spatial correlation on  $N_{\text{Tx}} \times N_{\text{Rx}}$  USTLD systems in Nakagami- $q$  fading. The first set of results, given in Figures 3.2 to 3.4, verifies that the theoretical bound of the ABEP for correlated  $N_{\text{Tx}} \times N_{\text{Rx}}$  USTLD systems in the presence of Nakagami- $q$  fading (derived in Section 3.4) converges to simulated results. Thereafter, the change in error performance as a result of fading parameter  $q$  is demonstrated in Figure 3.5. USTLD systems are then studied under transmit and receive correlation independently to determine which causes greater degradation of error performance, and the results are given in Figure 3.6. Finally, a comparison between USTLD and conventional MIMO STBC Alamouti [13] systems is presented in Figure 3.7, wherein the susceptibility of each system to antenna correlation is determined. For all results produced, antennas are equidistantly spaced and arranged linearly at both the transmitter and the receiver (that is,  $\mu_{\text{Tx}}^{(i,i+1)} = \mu_{\text{Tx}}^{(1,2)} = \mu_{\text{Tx}}$ ,  $i \in [1 : N_{\text{Tx}} - 1]$  and  $\mu_{\text{Rx}}^{(j,j+1)} = \mu_{\text{Rx}}^{(1,2)} = \mu_{\text{Rx}}$ ,  $j \in [1 : N_{\text{Rx}} - 1]$ ) and the correlation between them is determined by (3.5).

In Figures 3.2 and 3.3, simulations are shown for 16QAM and 16PSK USTLD systems under the conditions of: 1) both transmit and receive antenna correlation, 2) only transmit antenna correlation, 3) only receive antenna correlation and 4) uncorrelated transmit and receive antennas. To show that the ABEP is valid for other modulation orders and antenna array sizes, results are also shown for  $2 \times 4$  64QAM,  $3 \times 3$  8PSK and  $3 \times 5$  8PSK USTLD systems with both transmit and receive antenna

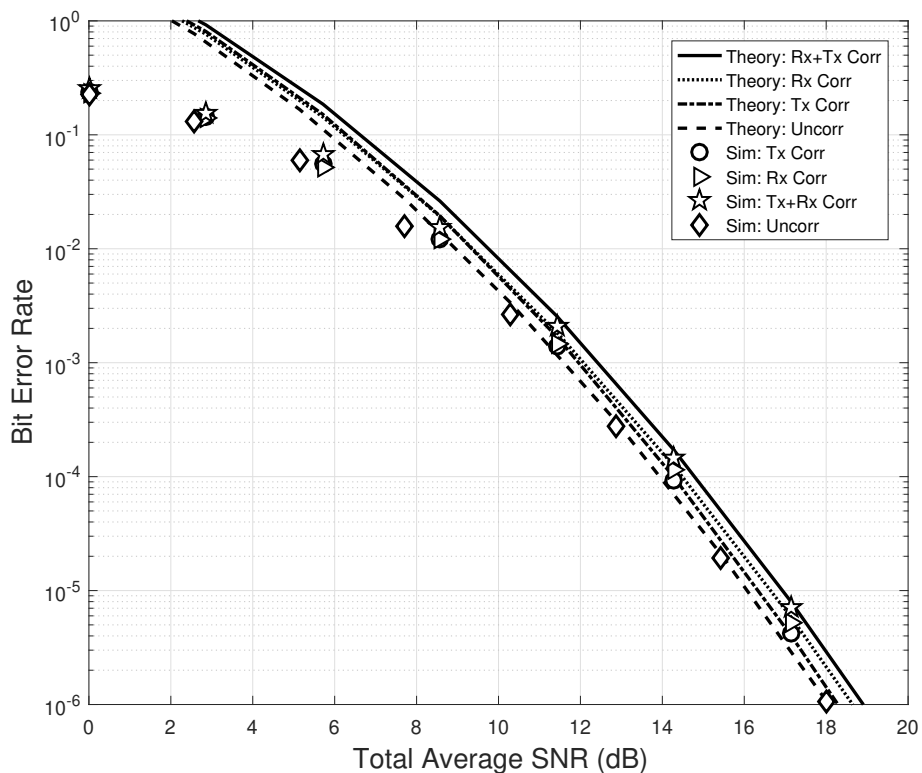


FIGURE 3.2: Comparison of Theoretical and Simulated Results:  $2 \times 3$  16QAM USTLD

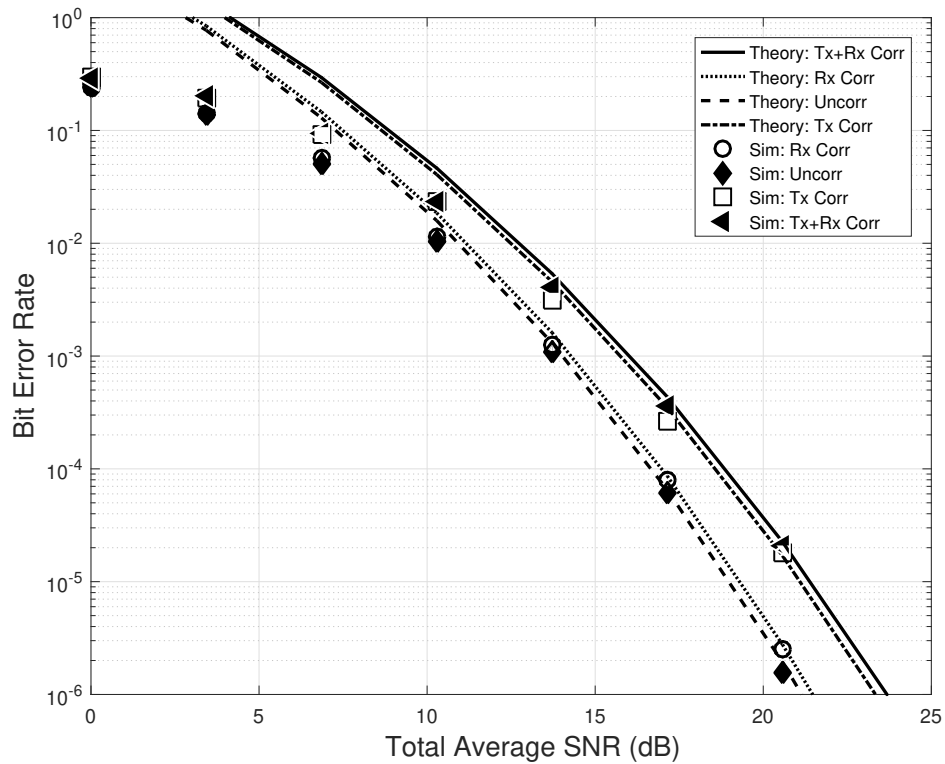


FIGURE 3.3: Comparison of Theoretical and Simulated Results:  $2 \times 3$  16PSK USTLD

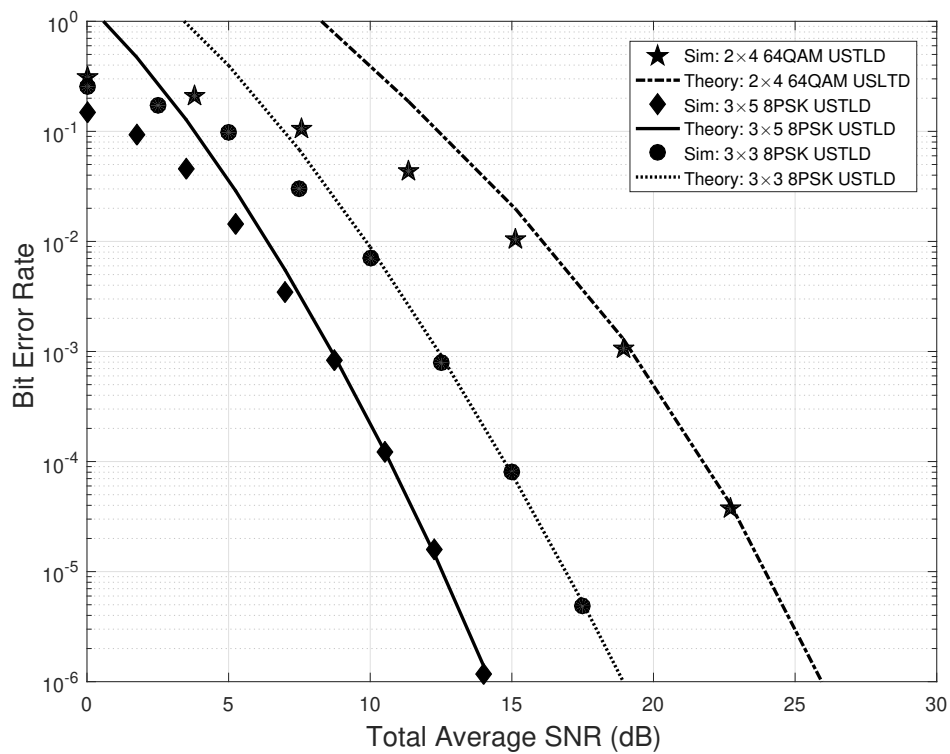


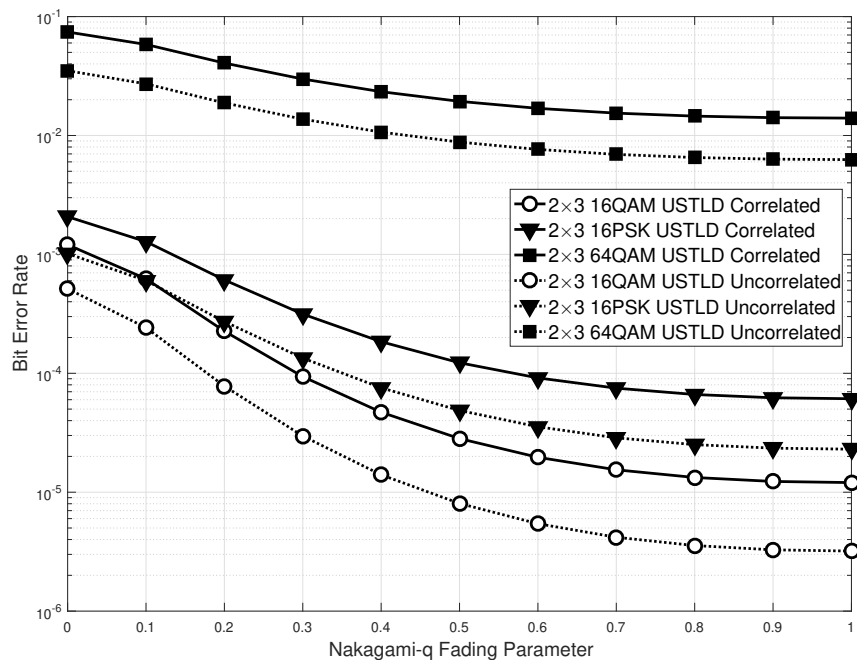
FIGURE 3.4: Comparison of Theoretical and Simulated Results: Different USTLD Systems with Transmit and Receive Antenna Correlation

Modulation	$\mu_{\text{Tx}}$	$\mu_{\text{Rx}}$	$q$
16PSK	$0.15\lambda$	$0.70\lambda$	0.4
16QAM	$0.24\lambda$	$0.30\lambda$	0.8
8PSK	$0.25\lambda$	$0.75\lambda$	0.9
64QAM	$0.24\lambda$	$0.5\lambda$	0.3

TABLE 3.1: Simulation Parameters for Figures 3.2 to 3.4

correlation (Figure 3.4). The results show that the bound of the ABEP converge to Monte Carlo simulation output in the high SNR region for all systems presented. The transmit antenna spacing ( $\mu_{\text{Tx}}$ ), receive antenna spacing ( $\mu_{\text{Rx}}$ ) and fading parameter ( $q$ ) used for each system are presented in Table 3.1.

Figure 3.5 shows the change in error performance of both correlated and uncorrelated USTLD systems across the range of the Nakagami- $q$  fading parameter. The correlated results were produced using arbitrary transmit and receive correlation parameters  $\mu_{\text{Tx}} = 0.21\lambda$  and  $\mu_{\text{Rx}} = 0.30\lambda$ . The results indicate that the error performance of USTLD in the presence of SSG fading ( $q = 0$ ) is significantly worse than in Rayleigh fading ( $q = 1$ ). In particular, 16QAM USTLD in SSG fading is two orders of magnitude worse than in Rayleigh fading. Similarly, 16PSK USTLD degrades by an order of magnitude. It is also observed that the performance is approximately constant in the range  $0.6 \leq q \leq 1$ . Finally, it is noted the results for correlated and uncorrelated systems follow the same trend. This may be attributed to the in-phase and quadrature components of the fading having different variances, as specified in Section 2.1. For smaller values of  $q$ , the power of the

FIGURE 3.5: Effect of Fading Parameter  $q$  at 20dB.

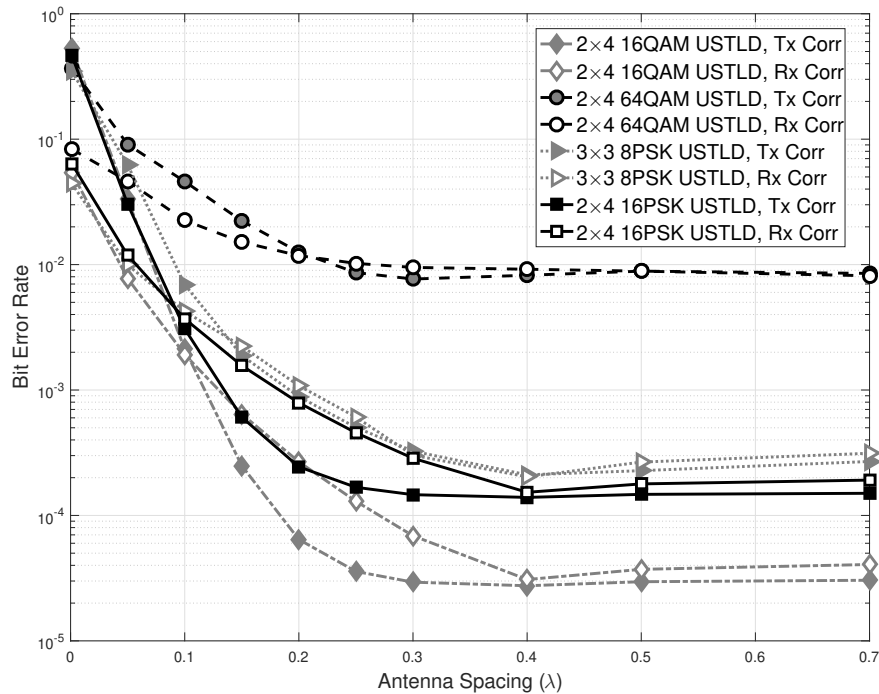


FIGURE 3.6: Comparing the Effects of Transmit and Receive Antenna Correlation at 15dB ( $q = 0.2$ )

quadrature component is almost negligible. Hence, the power of the in-phase component dominates the total power of the fading coefficient. As  $q$  increases above 0.6, the powers of the in-phase and quadrature components become comparable, hence further increases in  $q$  have a smaller effect on error performance.

The next set of results investigates the degradation in error performance of USTLD systems due to antenna correlation, by considering transmit and receive antenna correlation independently. The results are presented in Figure 3.6 for  $3 \times 3$  8PSK,  $2 \times 4$  16PSK,  $2 \times 4$  16QAM and  $2 \times 4$  64QAM USTLD systems at an SNR of  $\gamma = 15$ dB with arbitrary Nakagami- $q$  fading parameter  $q = 0.2$ .

Intuitively, as the spacing between antennas increase, the correlation between them decreases. This may be confirmed numerically by (3.5). As such, the gradient of the curves in Figure 3.6 indicates the rate at which error performance improves as antenna correlation decreases. By observing the gradient of the curves in the range  $0 < \mu \leq 0.4\lambda$ , it is found that transmit antenna correlation causes a more severe degradation in error performance than receive antenna correlation in USTLD systems. This concurs with the results shown in Figures 3.2 and 3.3, where it is observed that there is a larger dB gap between the uncorrelated and transmit antenna correlated systems than between the uncorrelated and receive antenna correlated systems. The reason for transmit antenna correlation having a more dominant effect on performance may be explained mathematically. From (3.22), it is observed that the transmit antenna correlation matrix  $\mathbf{C}_{\text{Tx}}$  is weighted by the distance vector product  $\mathbf{d} \cdot \mathbf{d}^{\text{H}}$  before being decomposed into its eigenvalues. By contrast,  $\mathbf{C}_{\text{Rx}}$  undergoes eigenvalue

decomposition directly, as shown in (3.21). Thus, the eigenvalue product which governs the PEP of correlated USTLD systems (shown in (3.23)) is more affected by the transmit antenna correlation matrix. A secondary observation is that all curves have a very flat gradient in the region  $\mu > 0.4\lambda$ . This indicates that spacing antennas further than  $0.4\lambda$  apart does not significantly improve the robustness of USTLD systems to antenna correlation. Hence,  $0.4\lambda$  is a theoretical optimal spacing for a linear array of antennas used for USTLD systems, which balances correlation and small form factor.

These results provide a guideline for implementing USTLD systems: to reduce degradation in error performance due to spatial correlation, it is more important to avoid correlation between transmit antennas than receive antennas. This may be achieved by ensuring that transmit antennas are spaced further than  $0.4\lambda$  apart.

The final set of results investigates the susceptibility of USTLD systems to spatial correlation when compared to existing MIMO systems. To provide a fair comparison in terms of both spectral efficiency and antenna array sizes, the USTLD systems are compared to traditional Alamouti STBC systems [13]. Thus, the systems investigated in Figure 3.7, and the curves associated with it, are constrained to only  $N_{\text{Tx}} = 2$  transmit antennas. The results compare  $2 \times 4$  systems with both

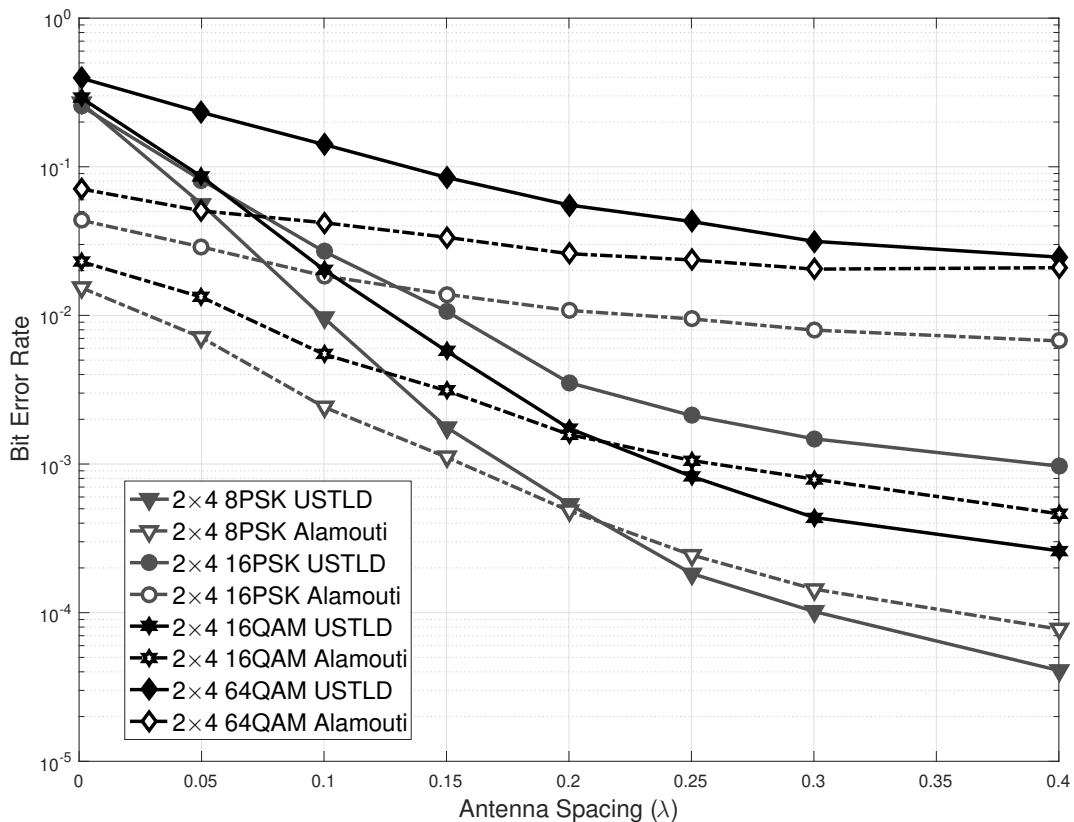


FIGURE 3.7: Comparing the Performance of USTLD and Alamouti-Coded Systems at 13dB ( $q = 0.7$ )

transmit and receive antenna correlation at SNR  $\gamma = 13\text{dB}$  and with Nakagami- $q$  fading parameter  $q = 0.7$ . The spacing between all antennas at both the transmitter and the receiver are assumed equal (i.e.  $\mu_{\text{Tx}}^{(i,i+1)} = \mu_{\text{Rx}}^{(j,j+1)} = \mu$ ,  $i \in [1 : N_{\text{Tx}} - 1]$ ,  $j \in [1 : N_{\text{Rx}} - 1]$ ). From the findings of Figure 3.6, it is only necessary to consider antenna spacings in the range  $0 < \mu \leq 0.4\lambda$ , as greater spacings have negligible impact on performance.

The results in Figure 3.7 show that the error performance of USTLD systems at high antenna correlation worse than that of Alamouti STBC systems. This may be observed in the regions  $0 < \mu \leq 0.2\lambda$  for the 8PSK and 16QAM systems,  $0 < \mu \leq 0.13\lambda$  for 16PSK, and across the full range  $0 < \mu \leq 0.4\lambda$  for 64QAM. This indicates that at high antenna correlations, labelling diversity decreases the error performance of MIMO systems compared to existing systems. Furthermore, USTLD systems are found to be more susceptible to antenna correlation as all curves show steeper gradients than the comparable Alamouti systems. This is in agreement with the results of previous work [24], wherein dual-correlated USTLD systems are found to be more susceptible to antenna correlation than comparable conventional MIMO systems.

### 3.6 Conclusion

This paper presents an analysis of the performance of USTLD in the presence of spatial correlation. An expression for the union bound of the ABEP is derived for the case of the Nakagami- $q$  fading model in both correlated and uncorrelated channels. This expression is verified by the results of Monte Carlo simulations, which show convergence in the high SNR region. The results presented also show the effect of the Nakagami- $q$  fading parameter on error performance: as the fading parameter decreases, so does error performance. In particular, the 16-ary modulation schemes show performance degradation of two orders of magnitude.

It is further concluded that transmit antenna correlation has a greater impact on degrading the error performance of USTLD systems than receive antenna correlation. Results indicate that, for linear antenna arrangements, there is a threshold spacing of  $0.4\lambda$ , after which greater antenna spacings do not improve the robustness towards spatial correlation. This provides a valuable practical guideline for implementing USTLD systems. Future work may consider determining the optimal antenna spacings of USTLD systems with non-linear antenna configurations.

Finally, it is found that  $2 \times 4$  USTLD systems more susceptible to spatial correlation than comparable MIMO Alamouti STBC systems. It is found that labelling diversity decreases the error performance of MIMO systems at high antenna correlations when compared to the existing Alamouti STBC system. Another open problem for future work is to study the effects of correlation on the capacity of USTLD systems.

### 3.7 Appendix: Details of Uncorrelated Nakagami- $q$ Derivation

To show that the PEP may be expressed in terms of four chi-squared RVs, as stated in Section 3.4.1, the inequality for the conditional PEP (3.8) is first modified to produce (3.24). The notation used assumes without loss of generality that the label  $L_i, i \in [1 : N_{\text{Tx}}]$ , was detected erroneously. Thus,  $\mathbf{H}_k \left( [\Omega_k(\mathbf{L})] - [\Omega_k(\tilde{\mathbf{L}})] \right) = \mathbf{h}_k^{(i)} \left( \Omega_k(L_i) - \Omega_k(\tilde{L}_i) \right) = \mathbf{h}_k^{(i)} d_k$ , where the abridged notation  $d_k = d_k(L_i, \tilde{L}_i)$  and  $d_k(L, \tilde{L})$  is given in (3.15).

$$P(\mathbf{L} \rightarrow \tilde{\mathbf{L}} | \mathbf{H}_1, \mathbf{H}_2) = P\left( \sum_{k=1}^2 \left\| \sqrt{\frac{\gamma}{N_{\text{Tx}}}} \mathbf{h}_k^{(i)} d_k + \mathbf{n}_k \right\|^2 < \sum_{k=1}^2 \|\mathbf{n}_k\|^2 \right).$$

The summed terms on the lesser side of the inequality may be written in terms of in-phase and quadrature components as

$$\begin{aligned} & \sum_{k=1}^2 \left\| \sqrt{\frac{\gamma}{N_{\text{Tx}}}} \mathbf{h}_k^{(i)} d_k + \mathbf{n}_k \right\|^2 \\ &= \sum_{k=1}^2 \left\| \left( \sqrt{\frac{\gamma}{N_{\text{Tx}}}} \left( \mathbf{h}_k^{(i)} \right)^{\text{I}} d_k^{\text{I}} - \sqrt{\frac{\gamma}{N_{\text{Tx}}}} \left( \mathbf{h}_k^{(i)} \right)^{\text{Q}} d_k^{\text{Q}} + \mathbf{n}_k^{\text{I}} \right) \right. \\ & \quad \left. + \text{j} \left( \sqrt{\frac{\gamma}{N_{\text{Tx}}}} \left( \mathbf{h}_k^{(i)} \right)^{\text{I}} d_k^{\text{Q}} + \sqrt{\frac{\gamma}{N_{\text{Tx}}}} \left( \mathbf{h}_k^{(i)} \right)^{\text{Q}} d_k^{\text{I}} + \mathbf{n}_k^{\text{Q}} \right) \right\|^2 \\ &= \sum_{k=1}^2 \sum_{p=1}^{N_{\text{Rx}}} \left[ \left( \sqrt{\frac{\gamma}{N_{\text{Tx}}}} \left( h_{p_k}^{(i)} \right)^{\text{I}} d_k^{\text{I}} - \sqrt{\frac{\gamma}{N_{\text{Tx}}}} \left( h_{p_k}^{(i)} \right)^{\text{Q}} d_k^{\text{Q}} + n_{p_k}^{\text{I}} \right)^2 \right. \\ & \quad \left. + \left( \sqrt{\frac{\gamma}{N_{\text{Tx}}}} \left( h_{p_k}^{(i)} \right)^{\text{I}} d_k^{\text{Q}} + \sqrt{\frac{\gamma}{N_{\text{Tx}}}} \left( h_{p_k}^{(i)} \right)^{\text{Q}} d_k^{\text{I}} + n_{p_k}^{\text{Q}} \right)^2 \right] \\ &= \sum_{k=1}^2 \sum_{p=1}^{N_{\text{Rx}}} \left[ \left( \sqrt{\frac{\gamma}{N_{\text{Tx}}}} \left( h_{p_k}^{(i)} \right)^{\text{I}} d_k^{\text{I}} \right)^2 + \left( \sqrt{\frac{\gamma}{N_{\text{Tx}}}} \left( h_{p_k}^{(i)} \right)^{\text{Q}} d_k^{\text{Q}} \right)^2 + \left( \sqrt{\frac{\gamma}{N_{\text{Tx}}}} \left( h_{p_k}^{(i)} \right)^{\text{I}} d_k^{\text{Q}} \right)^2 \right. \\ & \quad \left. + \left( \sqrt{\frac{\gamma}{N_{\text{Tx}}}} \left( h_{p_k}^{(i)} \right)^{\text{Q}} d_k^{\text{I}} \right)^2 + (n_{p_k}^{\text{I}})^2 + (n_{p_k}^{\text{Q}})^2 + g_{p_k} \right] \\ &= \sum_{k=1}^2 \left\| \sqrt{\frac{\gamma}{N_{\text{Tx}}}} \mathbf{h}_k^{(i)} d_k \right\|^2 + \sum_{k=1}^2 \|\mathbf{n}_k\|^2 + g. \end{aligned} \tag{3.24}$$

In (3.24),  $g = \sum_{k=1}^2 \sum_{p=1}^{N_{\text{Rx}}} g_{p_k}$  and the Gaussian RVs  $g_{p_k}, k \in [1 : 2], p \in [1 : N_{\text{Rx}}]$ , are given by

$$\begin{aligned} g_{p_k} &= 2\sqrt{\frac{\gamma}{N_{\text{Tx}}}} \left( h_{p_k}^{(i)} \right)^{\text{I}} n_{p_k}^{\text{I}} d_k^{\text{I}} - 2\sqrt{\frac{\gamma}{N_{\text{Tx}}}} \left( h_{p_k}^{(i)} \right)^{\text{Q}} n_{p_k}^{\text{I}} d_k^{\text{Q}} \\ & \quad + 2\sqrt{\frac{\gamma}{N_{\text{Tx}}}} \left( h_{p_k}^{(i)} \right)^{\text{I}} n_{p_k}^{\text{Q}} d_k^{\text{Q}} + 2\sqrt{\frac{\gamma}{N_{\text{Tx}}}} \left( h_{p_k}^{(i)} \right)^{\text{Q}} n_{p_k}^{\text{Q}} d_k^{\text{I}} \end{aligned} \tag{3.25}$$

and have mean  $\mathcal{E}\{g_{p_k}\} = 0$  and variance

$$\begin{aligned}\mathcal{E}\{g_{p_k}^2\} &= 2 \left( \sqrt{\frac{\gamma}{N_{\text{Tx}}}} \left( h_{p_k}^{(i)} \right)^{\text{I}} d_k^{\text{I}} \right)^2 + 2 \left( \sqrt{\frac{\gamma}{N_{\text{Tx}}}} \left( h_{p_k}^{(i)} \right)^{\text{Q}} d_k^{\text{Q}} \right)^2 \\ &+ 2 \left( \sqrt{\frac{\gamma}{N_{\text{Tx}}}} \left( h_{p_k}^{(i)} \right)^{\text{I}} d_k^{\text{Q}} \right)^2 + 2 \left( \sqrt{\frac{\gamma}{N_{\text{Tx}}}} \left( h_{p_k}^{(i)} \right)^{\text{Q}} d_k^{\text{I}} \right)^2 \\ &= 2 \left| \sqrt{\frac{\gamma}{N_{\text{Tx}}}} h_k^{(i)} d_k \right|^2.\end{aligned}\quad (3.26)$$

Thus, the distribution of the Gaussian RV  $g$  is given by  $g \sim \mathcal{N}(0, \sigma_g^2)$ ,  $k \in [1 : 2]$ , and  $\sigma_g^2 = 2 \sum_{k=1}^2 \left\| \sqrt{\frac{\gamma}{N_{\text{Tx}}}} \mathbf{h}_k^{(i)} d_k \right\|^2$ . This produces the same result as Xu *et al.* [8], and so (3.24) may be expressed as

$$\begin{aligned}P(\mathbf{L} \rightarrow \tilde{\mathbf{L}} | \mathbf{H}_1, \mathbf{H}_2) &= P\left(\sum_{k=1}^2 \left\| \sqrt{\frac{\gamma}{N_{\text{Tx}}}} \mathbf{h}_k^{(i)} d_k \right\|^2 + g < 0\right) \\ &= Q\left(\frac{\sum_{k=1}^2 \left\| \sqrt{\frac{\gamma}{N_{\text{Tx}}}} \mathbf{h}_k^{(i)} d_k \right\|^2}{\sigma_g}\right) \\ &= Q\left(\frac{1}{\sqrt{2}} \sum_{k=1}^2 \left\| \sqrt{\frac{\gamma}{N_{\text{Tx}}}} \mathbf{h}_k^{(i)} d_k \right\|\right).\end{aligned}\quad (3.27)$$

Using the intermediate steps of (3.24), the argument of the Q-function in (3.27) is squared to produce (3.28).

$$\begin{aligned}&\frac{1}{2} \sum_{k=1}^2 \left\| \sqrt{\frac{\gamma}{N_{\text{Tx}}}} \mathbf{h}_k^{(i)} d_k \right\|^2 \\ &= \frac{\gamma}{2N_{\text{Tx}}} \sum_{k=1}^2 \sum_{p=1}^{N_{\text{Rx}}} \left[ \left( \left( h_{p_k}^{(i)} \right)^{\text{I}} d_k^{\text{I}} \right)^2 + \left( \left( h_{p_k}^{(i)} \right)^{\text{Q}} d_k^{\text{Q}} \right)^2 + \left( \left( h_{p_k}^{(i)} \right)^{\text{I}} d_k^{\text{Q}} \right)^2 + \left( \left( h_{p_k}^{(i)} \right)^{\text{Q}} d_k^{\text{I}} \right)^2 \right] \\ &= \frac{\gamma}{2N_{\text{Tx}}} \sum_{k=1}^2 \sum_{p=1}^{N_{\text{Rx}}} \left[ \left( \left( h_{p_k}^{(i)} \right)^{\text{I}} \right)^2 |d_k|^2 + \left( \left( h_{p_k}^{(i)} \right)^{\text{Q}} \right)^2 |d_k|^2 \right].\end{aligned}\quad (3.28)$$

Since both the in-phase and quadrature components of fading follow Gaussian distributions, the Q-function in (3.27) is expressed using the results of (3.28) as

$$Q\left(\frac{1}{2} \sum_{k=1}^2 \left\| \sqrt{\frac{\gamma}{N_{\text{Tx}}}} \mathbf{h}_k^{(i)} d_k \right\|\right) = Q\left(\sqrt{\sum_{p=1}^{N_{\text{Rx}}} (\alpha_{p_1}^2 + \alpha_{p_2}^2 + \alpha_{p_3}^2 + \alpha_{p_4}^2)}\right).$$

where the Gaussian RVs  $\alpha_{p_1}, \alpha_{p_2}, \alpha_{p_3}$  and  $\alpha_{p_4}, p \in [1 : N_{\text{Rx}}]$ , are defined by

$$\alpha_{p(2k-1)} = \frac{\sqrt{\gamma} |d_k|}{\sqrt{2N_{\text{Tx}}}} \left( h_{p_k}^{(i)} \right)^{\text{I}}, \quad k \in [1 : 2] \quad (3.29)$$

$$\alpha_{p(,2k)} = \frac{\sqrt{\gamma} |d_k|}{\sqrt{2N_{\text{Tx}}}} \left( h_{p_k}^{(i)} \right)^{\text{Q}}, \quad k \in [1 : 2], \quad (3.30)$$

and have the distributions given in (3.11)–(3.14).

## References

- [1] Huang Y, Ritcey JA. Improved 16-QAM constellation labelling for BI-STCM-ID with the Alamouti scheme. *IEEE Commun. Letters*. 2005; 9(2): 157–159.
- [2] Huang Y, Ritcey JA. Optimal constellation labelling for iteratively decoded bit-interleaved space-time coded modulation. *IEEE Trans. Inf. Theory*. 2005; 51(5): 1865–1871.
- [3] Krasicki M. Improved labelling diversity for iteratively-decoded multiantenna systems. In: Proc. 7th Int. Conf. on Wireless Commun. and Mobile Computing (IWCMC), Istanbul (Turkey); 2011: 359–364.
- [4] Krasicki M. Essence of 16-QAM labelling diversity. *IET Electronics Lett*. 2013; 49(8): 567–569.
- [5] Seddik KG, Ibrahim AS, Liu KJR. Trans-Modulation in Wireless Relay Networks. *IEEE Commun. Lett*. 2008; 12(3): 170–172.
- [6] Samra H, Ding Z, Hahn P. Symbol Mapping Diversity Design for Multiple Packet Transmissions. *IEEE Trans. Commun*. 2005; 53(5): 810–817.
- [7] Zhao Z, Zhou L, Zheng X, Park S-E. Enhanced Constellation Rearrangement for HARQ with Symbol Combining. In: IEEE Mobile WiMax Symp. (MWS), Napa Valley, CA(USA); 2009.
- [8] Xu H, Govindasamy K, Pillay N. Uncoded Space-Time Labeling Diversity. *IEEE Commun. Lett*. 2016; 20(8):1511–1514.
- [9] Govindasamy K, Xu H, Pillay N. Space-time block coded spatial modulation with labeling diversity. *Int. J. Commun. Syst*. 2017;e3395. <https://doi.org/10.1002/dac.3395>
- [10] Pillay N, Xu H. Uncoded Space-Time Labeling Diversity – Application of Media-based Modulation with RF Mirrors. *IEEE Commun. Lett*. 2017. <https://doi.org/10.1109/LCOMM.2017.2770145>
- [11] Goldsmith A. *Wireless Communications*. Cambridge (USA): Cambridge University Press; 2005.
- [12] Simon MK, Alouini M-S. *Digital Communication over Fading Channels: A Unified Approach to Performance Analysis*. New York (USA): John Wiley & Sons, Inc.; 2000.
- [13] Alamouti SM. A Simple Transmit Diversity Technique for Wireless Communications. *IEEE J. on Sel. Areas in Commun*. 1998; 16(8): 1451–1458.
- [14] Patel SS, Quazi T, Xu H. High-Rate Uncoded Space-Time Labelling Diversity with Low Complexity Detection. *Trans. Emerging Telecomm. Tech*. 2018; under review.
- [15] Tseng S-M, Liao C-Y. Distributed Orthogonal and Quasi-Orthogonal Space-Time Block Code with Embedded AAF/DAF Matrix Elements in Wireless Relay Networks with Four Relays. *Wireless Pers. Commun*. 2014; 75(2): 1187–1198.

- [16] Choi M, Lee H, Nam H. Exact and asymptotic PEP derivations for various quasi-orthogonal space-time block codes. *Electronics Lett.* 2013; 49(21): 1358–1360.
- [17] Ranju MAAA, Rafi RS. Analysis of Rate One Quasi-Orthogonal Space-Time Block Coding over Rayleigh Fading Channel. *Int. J. Commun., Network and Syst. Sci.* 2014; 7: 196–202.
- [18] Hedayet A, Shah H, Nosratinia A. Analysis of Space-Time Coding in Correlated Fading Channels. *IEEE Trans. on Wireless Commun.* 2005; 4(6): 2882–2891.
- [19] Stüber GL. *Principles of Mobile Communication*. New York (USA): Kluwer Academic Publishers; 2002.
- [20] Akoun PO, Xu H. Optimal error analysis of receive diversity schemes on arbitrarily correlated Rayleigh fading channels. *IET Commun.* 2016; 10(7): 854–861.
- [21] Ebrahimi-Tofighi N, Ardebilipour M, Shahabadi M. Receive and Transmit Array Antenna Spacing and Their Effect on the Performance of SIMO and MIMO Systems by using an RCS Channel Model. *Int. J. of Elec., Comp., Energetic, Electronic and Commun. Eng.* 2007; 1(12): 1732–1736.
- [22] Rappaport TS, Sun S, Mayzus R, Zhao H, Azar Y, Wang K, Wong GN, Schulz JK, Samimi W, Gutierrez F. Millimeter Wave Mobile Communications for 5G Cellular: It Will Work! *IEEE Access.* 2013; 1: 335–349.
- [23] Fang L, Bi G, Cot AC. New method of performance analysis for diversity reception with correlated Rayleigh-fading signals. *IEEE Trans. on Vehicular Tech.* 2000; 49(5): 1807–1812.
- [24] Patel SS, Quazi T, Xu H. Performance of Uncoded Space-Time Labelling Diversity in Dual-Correlated Rayleigh-Fading Channels. In: Proc. Southern Africa Telecomm. Networks and Applications Conf. (SATNAC), Freedom of the Seas Cruise Liner, Barcelona (Spain); 2017: 68–73.
- [25] Kermoal JP, Schumacher L, Pedersen KI, Mogensen PE, Frederiksen F. A stochastic MIMO radio channel model with experimental validation. *IEEE J. on Sel. Areas in Commun.* 2002; 20(6): 1211–1226.
- [26] Khumbani B, Mohandas VK, Singh RP, Kabra S, Kshetrimayum RS. Analysis of Space-Time Block Coded Spatial Modulation in Correlated Rayleigh and Rician Fading Channels. In: IEEE Conf. on DSP, Singapore (Singapore); 2015: 516–520.
- [27] Varshney N, Goel A, Jagannatham AK. Cooperative communication in spatially modulated MIMO systems. In: IEEE Wireless Commun. and Networking Conf. (WCNC), Doha (Qatar); 2016.
- [28] Amol R, Kaur K. Performance Analysis of Hoyt Fading Channel for M-ary and Monte Carlo Simulation. *Int. J. of Adv. Computronics and Management Studies.* 2016; 1(3): 13–19.

- [29] Weichselberger W, Herdin M, Ozcelik H and Bonek E. A stochastic MIMO channel model with joint correlation of both link ends. *IEEE Trans. on Wireless Commun.* 2006; 5(1): 90–100.
- [30] Tulino AM, Lozano A and Verdú S. Impact of antenna correlation on the capacity of multi-antenna channels. *IEEE Trans. Inf. Theory.* 2005; 51(7): 2491–2509.
- [31] Lin C, Veeravalli VV. Optimal linear dispersion codes for correlated MIMO channels. *IEEE Trans. Wireless Commun.* 2008; 7(2): 657–666.
- [32] Raghavan V, Sayeed AM and Veeravalli VV. Semiunitary Precoding for Spatially Correlated MIMO Channels. *IEEE Trans. Inf. Theory.* 2011; 57(3): 1284–1298.
- [33] Lin C, Raghavan V, Veeravalli VV. To Code or Not to Code Across Time: Space-Time Coding with Feedback. *IEEE J. on Sel. Areas in Commun.* 2008; 26(8): 1588–1598.
- [34] Moustakas A, Baranger H, Balents L, Sengupta A and Simon S. Communication through a diffusive medium: Coherence and capacity. *Science.* 2000; 287: 287–290.
- [35] Romero-Jerez JM, Lopez-Martinez FJ. A New Framework for the Performance Analysis of Wireless Communications Under Hoyt (Nakagami- $q$ ) Fading. *IEEE Trans. Inf. Theory.* 2017; 63(3): 1693–1702.
- [36] Chytil B. The distribution of amplitude scintillation and the conversion of scintillation indices. *J. of Atmospheric and Terrestrial Phys.* 1967; 29(9): 1175–1177.
- [37] Weisstein EW. Modified Bessel Function of the First Kind (A Wolfram Web Resource). [Online] Cited 2017-11-11. Available at: <http://mathworld.wolfram.com/ModifiedBesselFunctionoftheFirstKind.html>
- [38] Ropokis GA, Rontogiannis AA, Mathiopoulos PT. Quadratic Forms in Normal RVs: Theory and Applications to OSTBC over Hoyt Fading Channels. *IEEE Trans. Wireless Commun.* 2008; 7(12): 5009–5019.
- [39] Aalo VA. Performance of Maximal-Ratio Diversity Systems in a Correlated Nakagami-Fading Environment. *IEEE Trans. Commun.* 1995; 43(8): 2360–2369.
- [40] Vaughan RG, Anderson JB. Antenna diversity in mobile communications. *IEEE Trans. Veh. Technol.* 1987; 36(4): 149–172.
- [41] Albdran S, Alshammari A, Matin MA. Spectral and energy efficiency for massive MIMO systems using exponential correlation model. In: *IEEE 7th Annual Comp. and Commun. Workshop and Conf. (CCWC)*, Las Vegas, NV (USA); 2017.
- [42] Loyka, SL. Channel capacity of MIMO architecture using the exponential correlation matrix. *IEEE Commun. Lett.* 2001; 5(9): 369–371.

- [43] Craig JW. A new, simple, and exact result for calculating the probability of error for two-dimensional signal constellations. In: IEEE Military Commun. Conf. (MILCOM), McLean, VA (USA); 1991: 571–575.

## Chapter 4

### Journal Article 3

# A MIMO Satellite Broadcasting Technique with Space, Time, Polarisation and Labelling Diversity

Sulaiman Saleem Patel, Tahmid Quazi, Hongjun Xu

Prepared for Submission: *International Journal of Satellite Communications  
and Networking*

## 4.1 Abstract

MIMO satellite broadcasting has been identified as a key technology to address the digital divide between under-developed and developed nations. Recent advancements in MIMO satellite broadcasting systems have considered incorporating diversity techniques from their terrestrial counterparts. The focus of these works was on enhancing the Alamouti space-time block code, which has undergone successful real-world implementation, using labelling and polarisation diversity independently. This paper presents a satellite broadcasting system that incorporates space, time, polarisation and labelling diversity. The key challenge in incorporating labelling diversity into a system is the design of appropriate bit-to-symbol mappers. Existing mapper design techniques are limited and cannot readily be applied to modulation schemes appropriate for satellite broadcasting. To overcome these limitations, the paper devises a genetic algorithm approach to mapper design which is appropriate for any generic modulation scheme. The proposed system is studied under ideal (uncorrelated) conditions, as well as in the presence of inter-beam and inter-antenna interference (correlated conditions). Analytical expressions are presented to model both the correlated and uncorrelated systems, and are verified via Monte Carlo simulations. When compared to the best comparable scheme for MIMO satellite broadcasting (the space-time-polarisation block code) at a bit-error-rate (BER) of  $10^{-6}$ , results show that the proposed system improves performance by  $\approx 7$ dB for a  $2 \times 2$  16APSK system configuration, and by  $\approx 5$ dB for both  $2 \times 4$  32APSK and  $2 \times 2$  64APSK system configurations. Results also show that the proposed system is highly sensitive to correlation at the transmitting satellite. In particular, transmit-side correlation degrades link reliability by 4 orders of magnitude for the  $2 \times 3$  8APSK configuration studied at 25dB.

## 4.2 Introduction

### Motivation for Research

The International Telecommunications Union [1] estimate that less than 20% of the population in the world's least-developed countries (LDCs) are able to use the Internet. This is a stark contrast to developed countries, where the over 80% of the population are Internet users [1]. Addressing this digital divide between LDCs and the rest of the developed world is among the key goals of the United Nations Sustainable Development Agenda for 2030 [2, 3], and is expected to have numerous socio-economic benefits for these nations [4–6].

Satellite broadcasting has emerged as an attractive technology to enable Internet penetration to LDCs, particularly for rural communities with limited telecommunication infrastructure [7–9]. An example of the successful deployment of satellite systems for these purposes was the Space4edu project, an initiative that brought Internet-based education to rural schools in South Africa [10]. Studies have also been conducted into facilitating e-health services through the use of satellite broadcast systems [11, 12]. In addition, satellite broadcasting is also of interest for developed nations to extend the range and reliability of terrestrial wireless systems [13–16]. The growing interest in satellite broadcasting systems has prompted research into the adaptation of the latest multiple-input, multiple-output (MIMO) terrestrial technologies for their satellite counterparts [17, 18].

MIMO systems are characterised by multiple transmission and reception streams, typically achieved by utilizing multiple antennas at both the transmitter and receiver [19]. As documented by Arapoglou *et al.* [17, 18], adopting a MIMO structure for satellite broadcast systems is a non-trivial task due to limitations in the physical space available on smaller satellites. Schwartz *et al.* [20] have addressed this limitation by proposing to use two single-antenna satellites in conjunction to act as a single dual-antenna node in the system. Another technique that has been considered is the use of dual-polarised antennas [21, 22]. If the polarisation streams are perfectly orthogonal, a system using 1 dual-polarised transmit antenna and 1 dual-polarised receive antenna is equivalent to a  $2 \times 2$  single-polarised antenna system [21]. Preliminary studies on the feasibility of MIMO satellite broadcasting have been positive. As recently as 2016, Hofmann *et al.* [23] and Byman *et al.* [24] documented results of implementing real-world MIMO satellite broadcast systems using each of the aforementioned configurations.

Although diversity techniques for terrestrial MIMO systems have been extensively researched, their adaptation for MIMO satellite broadcasting is still relatively new. One of the first terrestrial schemes to be adapted was the well-known Alamouti [25] orthogonal space-time block code (OSTBC), which was studied by Arapoglou *et al.* [17] and Arti *et al.* [26]. More recently, other terrestrial systems that have directly improved upon the Alamouti OSTBC [27, 28] were also adapted for MIMO satellite broadcasting [29–31]. Among these was the orthogonal space-time-polarisation block code (OSTPBC) proposed by Wysocki and Wysocki [27], which enhanced the Alamouti OSTBC by incorporating polarisation diversity. This was extended to the context of satellite broadcast systems

by Vineetha *et al.* [30] and Aparna *et al.* [31]. Another notable enhancement to the terrestrial Alamouti scheme is the uncoded space-time labelling diversity (USTLD) system proposed by Xu *et al.* [28]. This was recently extended to satellite broadcast systems by Quazi and Patel [29]. Labelling diversity enables the USTLD system to improve upon the BER performance of the Alamouti OSTBC in a manner similar to a coding gain, without actually introducing coding to the system [32]. To achieve labelling diversity, multiple copies of the same information codeword are transmitted using symbols from constellations with different bit-to-symbol mappings. The design of the bit-to-symbol mappers for each constellation determines the extent to which labelling diversity is able to improve the BER performance [28, 29, 32]. Due to the difficulties posed by mapper design, the work by Quazi and Patel [29] could only apply labelling diversity to a limited subset of the constellations from the DVB-S2X satellite broadcasting standard [33]. To address this limitation, this paper presents a mapper design algorithm that produces labelling diversity mappers for constellations of any modulation scheme and order.

Furthermore, this paper proposes a system that incorporates both polarisation and labelling diversity to improve upon the existing OSTBC-based, OSTPBC-based and USTLD-based satellite broadcast systems. The proposed space-time-polarisation-labelling diversity (STPLD) system model is studied under the assumption of Nakagami- $q$  fading [34, 35]. This fading model considers the case where there is no line-of-sight path between transmitter and receiver, providing insight into the worst-case error performance of the system [29, 36]. Literature has shown that the Nakagami- $q$  model is appropriate for satellite links subject to strong ionospheric scintillation [37].

### Contributions

The original contributions of this research article are as follows:

1. The STPLD system model for a MIMO satellite broadcasting downlink is proposed.
2. Closed-form numerical expressions for the STPLD system are derived for uncorrelated and correlated conditions.
3. A modified genetic algorithm (GA) to design bit-to-symbol mappers that achieve labelling diversity for the STPLD system is presented. This algorithm is based on the latest work in labelling diversity mapper design [29, 38].
4. Using the modified GA, new labelling diversity mappers for Amplitude Phase Shift Keying (APSK) constellations from the latest DVB-S2X standard [33] are designed.
5. The proposed STPLD system is compared to similar MIMO satellite broadcasting systems (based on the Alamouti OSTBC [18, 26], OSTPBC [30, 31] and USTLD [29] schemes) in terms of error performance and robustness to correlation.

### Notation

This paper denotes scalar quantities in italics, vectors in lowercase boldface and matrices in uppercase

boldface.  $|\cdot|$  and  $(\cdot)!$  respectively represent the absolute value and factorial operators. The matrix operators  $\text{Tr}\{\cdot\}$ ,  $(\cdot)^T$ , and  $\|\cdot\|$  represent the trace, transpose and Frobenius norm respectively. A complex number  $z$  is represented in terms of its real and imaginary parts as  $z = \Re(z) + j\Im(z)$ , where  $j = \sqrt{-1}$ . The complex conjugate of  $z$  is denoted with an overbar as  $\bar{z}$ . The binomial coefficient is represented as  $\binom{n}{k} = \frac{n!}{k!(n-k)!}$ . Finally, the statistical expectation is denoted by the operator  $E\{\cdot\}$

### 4.3 System Model

In this section, an overview of space, time, polarisation and labelling diversity is first provided. This overview focuses on how each diversity mechanism is achieved in the proposed STPLD system. Thereafter, the transmission and detection models of the STPLD system is discussed. Finally, the correlation model that will be adopted to consider the effects of inter-beam and inter-antenna interference on the system error performance is presented.

#### 4.3.1 Space, Time, Polarisation and Labelling Diversity

The proposed space-time-polarisation-labelling diversity (STPLD) system considers a MIMO configuration with  $N_{\text{Tx}} = 2$  transmit antennas at the satellite and  $N_{\text{Rx}}$  receive antennas at the base station.  $N_{\text{Tx}}$  is constrained due to the potentially limited space available on smaller satellites [17, 18]. The use of multiple transmit and receive antennas allows the system to achieve spatial diversity.

All transmit and receive antennas are assumed to be orthogonally dual-polarised (ODP), and the polarisations used are denoted P1 and P2. There are 2 common configurations to ensure that antennas are ODP [17]. The first is to utilise linear polarisations (i.e. a horizontal/vertical polarisation pair) and the second is to utilise circular polarisations (i.e. a left/right hand circular polarisation pair). Arapoglou *et al.* [17] indicate that the latter of these configurations is more robust to the effects of Faraday rotation in satellite systems. It is thus recommended that STPLD systems are implemented with a left/right circular polarisation pair.

The use of ODP transmit antennas allows the satellite to transmit a total of 4 signals in any given time slot (one signal across each polarisation from each antenna). Similarly, the base station receives a total of  $2N_{\text{Rx}}$  signals in any given time slot. Thus, the  $2 \times N_{\text{Rx}}$  ODP antenna configuration adopted by the proposed STPLD can be modelled as a  $4 \times 2N_{\text{Rx}}$  singular-polarised antenna system, effectively quadrupling the number of signal paths. The effect of more signal paths in the system is that more diversity is achieved. This comes at the expense of increased inter-beam interference (IBI) [17], which degrades the error performance of the system.

Labelling diversity, also referred to in some literature as ‘mapping diversity’, was first proposed for bit-interleaved coded systems with iterative decoding [39, 40]. The use of interleaving and coding in these systems results in higher latencies and increased power consumption. This prompted more recent studies of labelling diversity in uncoded systems [28, 29, 32, 36]. Notably, Xu *et al.* [28] proposed a scheme that applied labelling diversity to directly enhance the Alamouti OSTBC, which was named uncoded space-time labelling diversity (USTLD). It is emphasised that there are

TABLE 4.1: Nomenclature for describing systems with Labelling Diversity

Term	Description
Symbol	A symbol represents the magnitude and phase used when modulating the transmission carrier in order to transmit information codewords. This is represented by a complex number.
Constellation	A constellation refers to the set of all possible symbols that may be used to encode information codewords. Constellations are commonly represented with a scatter plot of points on the complex plane, where each point represents a unique symbol.
Label	The label assigned to a symbol is the information codeword associated with that symbol. Although information codewords are binary, it is common to represent labels in decimal form for brevity.
Mapping Mapper	Mapping is the process of assigning labels to symbols using a predefined function. A mapper, $\Omega(\cdot)$ , is the mapping function which assigns labels to symbols within a constellation. The argument of $\Omega$ is the label to be assigned, and its output is the corresponding symbol.

subtleties in nomenclature used when describing systems with labelling diversity, which are provided in Table 4.1.

In labelling diversity systems, different mappers are used to encode the same information prior to transmission. The mappers are designed such that the symbol corresponding to a given label has different neighbors when mapped by each mapper. Thus, for a labelling diversity system utilizing  $x$  mappers, each label is represented as point in a  $2x$ -dimensional hyperspace. The objective of mapper design is to maximise the distance between points corresponding to each label in this hyperspace. The constellation represented by each mapper is then simply a plane within the  $2x$ -dimensional hyperspace, and a strict constraint of the labelling diversity technique is that the symbols on each constellation remain the same, regardless of the label assigned to them.

Similar to USTLD systems [28, 29, 32, 36], the proposed STPLD system uses 2 mappers,  $\Omega_1$  and  $\Omega_2$ . These are referred to as the ‘primary mapper’ and ‘secondary mapper’ respectively. For brevity, this work will refer to the constellation with labels assigned by the primary mapper as the ‘primary constellation’. Similarly, the ‘secondary constellation’ refers to the constellation with labels assigned by the secondary mapper. It is important to note that, in terms of the definitions in Table 4.1, the symbols in these constellations are identical.

Time diversity is achieved in the STPLD system by transmitting the same information codewords across 2 time slots. This makes the STPLD system more robust to burst errors [19].

### 4.3.2 Modulation Scheme

The choice of modulation scheme for the STPLD system defines the constellation of symbols used to encode information. The latest Digital Video Broadcasting standard for satellite transmissions, DVB-S2X [33], recommends the use of circular constellations for these systems.

TABLE 4.2: Description of APSK Constellations

Modulation Order	Structure	Definition in DVB-S2X standard [33]
8	4+2+4	Table 10a, page 25
16	8+8	Figure 7, page 28
32	4+8+4+16	Table 12d, page 30
64	4+12+20+28	Table 13e, page 33

A key motivation for circular constellations in satellite broadcasting systems is that they typically have a lower peak-to-average power ratio (PAPR) than their rectangular counterparts [41]. A high PAPR is undesirable, as high-gain power amplifiers at the transmitter exhibit non-linear characteristics when operating near their saturation region [42].

The STPLD system model considers the circular constellations recommended in the DVB-S2X standard [33]. Due to the variety of constellations in the standard, this paper focusses on the subset of constellations given in Table 4.2 when presenting results. For all constellations in Table 4.2, the “+”-separated notation indicates the number of points located on each ring in the constellation structure. For example, a 4+12+16 structure would have 3 rings and a total of 32 constellation points. 4 points are located on the innermost ring, 12 points are located on the middle ring and 16 points are located on the outermost ring. Table 4.2 also directs the reader to the constellation and codeword mapping definitions in the DVB-S2X standard. These suggested codeword mappings are used to define the primary mapper,  $\Omega_1$ , for the STPLD system. It should be noted that the constellations considered in this paper are a wider variety of APSK configurations than was considered in previous work [29].

### 4.3.3 Transmission and Detection Models of Proposed System

An illustration of the proposed STPLD system is given in Figure 4.1. At the satellite, two  $m$ -bit information codewords,  $\ell_1$  and  $\ell_2$ , are mapped to complex symbols from a  $M$ -ary APSK constellation and transmitted across 2 time slots, where  $M = 2^m$ . To achieve labelling diversity, a different mapping function to select symbols is employed in each time slot, i.e. mapper  $\Omega_k$  is employed in time slot  $k$ , where  $k \in [1 : 2]$ . The APSK constellations considered in this paper are those recommended in the latest DVB-S2X satellite broadcasting standard [33], as discussed in Section 4.3.2. The design of the labelling diversity mappers for these constellations is detailed in Section 4.5. The system is designed such that a copy of each symbol  $\Omega_k(\ell_j)$ ,  $j \in [1 : 2]$ , is transmitted from each antenna and over each polarisation during time slot  $k$ ,  $k \in [1 : 2]$ .

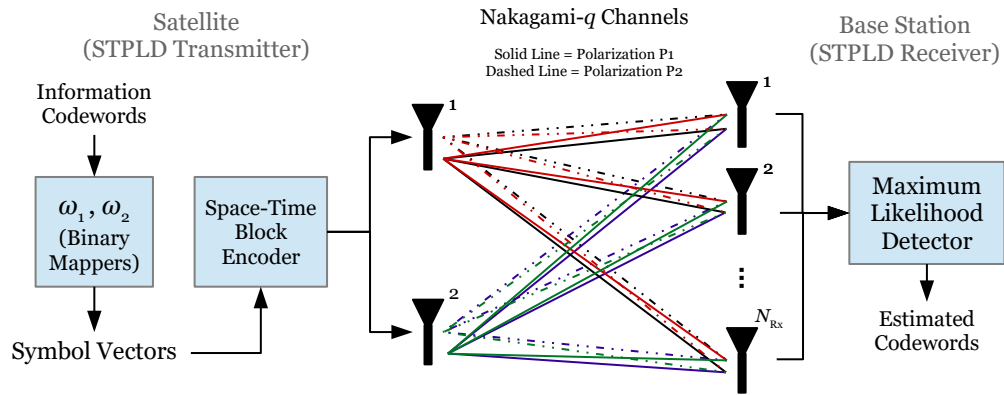


FIGURE 4.1: Illustration of the proposed STPLD system

At the base station, the  $2N_{Rx} \times 1$  received signal vector,  $\mathbf{y}$ , during time slot  $k$ , where  $k \in [1 : 2]$ , is given by:

$$\begin{aligned} \mathbf{y}_k &= \left[ y_{P1_k}^{(1)} \quad y_{P2_k}^{(1)} \quad y_{P1_k}^{(2)} \quad y_{P2_k}^{(2)} \quad \cdots \quad y_{P1_k}^{(N_{Rx})} \quad y_{P2_k}^{(N_{Rx})} \right]^T \\ &= \sqrt{\frac{E_{Tx}}{4E_\Omega E_n}} \begin{bmatrix} \mathbf{h}_{P1_k}^{(1)} & \mathbf{h}_{P2_k}^{(1)} & \mathbf{h}_{P1_k}^{(2)} & \mathbf{h}_{P2_k}^{(2)} \end{bmatrix} \begin{bmatrix} \Omega_k(\ell_1) \\ \Omega_k(\ell_2) \\ \Omega_k(\ell_2) \\ \Omega_k(\ell_1) \end{bmatrix} + \mathbf{n}_k, \end{aligned} \quad (4.1)$$

where  $y_{P1}^{(a)}$  represents the signal received by the  $a$ -th receive antenna with polarisation P1, where  $a \in [1 : N_{Rx}]$ , and similarly for  $y_{P2}^{(a)}$ .  $E_{Tx}$  is the total energy of the transmitted signal, which is split equally across each polarisation and each transmit antenna.  $E_\Omega = \frac{1}{M} \sum_{i=0}^{M-1} |\Omega_1(i)|^2 = \frac{1}{M} \sum_{i=0}^{M-1} |\Omega_2(i)|^2$  is a factor to ensure that transmitted symbols are power-normalised and  $E_n$  is the expected energy of additive white Gaussian noise (AWGN) at the receiver. These factors may be written more compactly by defining the total average signal-to-noise ratio (SNR) of the system,  $\gamma = \frac{E_{Tx}}{E_\Omega E_n}$ . This allows the entries of noise vector,  $\mathbf{n}$ , to be modeled as following a complex normal distribution with zero mean and unit variance. The  $2N_{Rx} \times 1$  vectors  $\mathbf{h}_{P1}^{(b)}$  and  $\mathbf{h}_{P2}^{(b)}$  represent the narrowband multipath fading experienced by the symbols transmitted from transmit antenna  $b$ ,  $b \in [1 : 2]$ , with the respective polarisations P1 and P2. It is assumed that the fading is fast, frequency-flat and that it follows a Nakagami- $q$  amplitude distribution with zero mean and unit variance. The Nakagami- $q$  fading model has been shown to be appropriate for modelling satellite links subject to strong ionospheric scintillation by Chytil [37]. Additionally, the Nakagami- $q$  model provides insight into the worst-case error performance of the STPLD system [36]. The fading parameter,  $q$ , lies in the continuous range  $0 \leq q \leq 1$  and is the energy ratio of the quadrature component of the fading to its in-phase component [34]. The boundary conditions of  $q$  correspond to the cases of single-sided Gaussian fading ( $q = 0$ ) and Rayleigh fading ( $q = 1$ ), as discussed by Simon and Alouini [35]. The phase distribution of both the noise and fading vectors entries in (4.1) is assumed uniform.

To estimate the transmitted codewords, the base station employs maximum likelihood detection

(MLD). Under the assumption that accurate channel state information is available at the receiver, the detected codewords,  $\tilde{\ell}_1$  and  $\tilde{\ell}_2$ , are given by:

$$\begin{aligned} \tilde{\ell}_1, \tilde{\ell}_2 = \arg \min_{l_1, l_2 \in [0:M-1]} & \left\| \mathbf{y}_1 - \sqrt{\frac{E_{Tx}}{4E_{\Omega}E_n}} \begin{bmatrix} \mathbf{h}_{P1_1}^{(1)} & \mathbf{h}_{P2_1}^{(1)} & \mathbf{h}_{P1_1}^{(2)} & \mathbf{h}_{P2_1}^{(2)} \end{bmatrix} \begin{bmatrix} \Omega_1(l_1) \\ \Omega_1(l_2) \\ \Omega_1(l_2) \\ \Omega_1(l_1) \end{bmatrix} \right\|^2 \\ & + \left\| \mathbf{y}_2 - \sqrt{\frac{E_{Tx}}{4E_{\Omega}E_n}} \begin{bmatrix} \mathbf{h}_{P1_2}^{(1)} & \mathbf{h}_{P2_2}^{(1)} & \mathbf{h}_{P1_2}^{(2)} & \mathbf{h}_{P2_2}^{(2)} \end{bmatrix} \begin{bmatrix} \Omega_2(l_1) \\ \Omega_2(l_2) \\ \Omega_2(l_2) \\ \Omega_2(l_1) \end{bmatrix} \right\|^2, \end{aligned} \quad (4.2)$$

where  $l_1$  and  $l_2$  are candidate codewords to be evaluated during the detection. Using the derivation by Patel *et al.* [32], the complexity of the MLD described by (4.2) is  $\mathcal{O}(4N_{Rx}M^2)$  effective real operations, where  $\mathcal{O}(\cdot)$  is the ‘order of’ operator commonly used in the upper-bound analysis of algorithmic complexity [43].

#### 4.3.4 Correlation Model

This paper adopts the separable Kronecker correlation model [44] to model the effect of inter-antenna and inter-beam interference on the STPLD system. The Kronecker model relates the correlated channel matrix in the  $k$ -th time slot,  $\begin{bmatrix} \mathbf{h}_{P1_k}^{(1)} & \mathbf{h}_{P2_k}^{(1)} & \mathbf{h}_{P1_k}^{(2)} & \mathbf{h}_{P2_k}^{(2)} \end{bmatrix}$ , to a virtual, uncorrelated channel matrix,  $\begin{bmatrix} \hat{\mathbf{h}}_{P1_k}^{(1)} & \hat{\mathbf{h}}_{P2_k}^{(1)} & \hat{\mathbf{h}}_{P1_k}^{(2)} & \hat{\mathbf{h}}_{P2_k}^{(2)} \end{bmatrix}$ , a transmitter-side correlation matrix ( $\mathbf{C}_{Tx}$ ) and a receiver-side correlation matrix ( $\mathbf{C}_{Rx}$ ) according to:

$$\begin{bmatrix} \mathbf{h}_{P1_k}^{(1)} & \mathbf{h}_{P2_k}^{(1)} & \mathbf{h}_{P1_k}^{(2)} & \mathbf{h}_{P2_k}^{(2)} \end{bmatrix} = \mathbf{C}_{Rx}^{\frac{1}{2}} \begin{bmatrix} \hat{\mathbf{h}}_{P1_k}^{(1)} & \hat{\mathbf{h}}_{P2_k}^{(1)} & \hat{\mathbf{h}}_{P1_k}^{(2)} & \hat{\mathbf{h}}_{P2_k}^{(2)} \end{bmatrix} \left( \mathbf{C}_{Tx}^{\frac{1}{2}} \right)^T, \quad k \in [1:2]. \quad (4.3)$$

As this paper considers the Nakagami- $q$  fading model, the amplitude of each entry of the virtual, uncorrelated channel matrix in (4.3) follows a Nakagami- $q$  distribution with zero mean and unit variance.

Each correlation matrix is defined in terms of the signal paths from each antenna, utilising each polarisation. As an example, the transmit-side correlation matrix is defined as:

$$\mathbf{C}_{Tx} = \begin{bmatrix} 1 & \rho_{Tx}^{(P1_1, P2_1)} & \rho_{Tx}^{(P1_1, P1_2)} & \rho_{Tx}^{(P1_1, P2_2)} \\ \rho_{Tx}^{(P2_1, P1_1)} & 1 & \rho_{Tx}^{(P2_1, P1_2)} & \rho_{Tx}^{(P2_1, P2_2)} \\ \rho_{Tx}^{(P1_2, P1_1)} & \rho_{Tx}^{(P1_2, P2_1)} & 1 & \rho_{Tx}^{(P1_2, P2_2)} \\ \rho_{Tx}^{(P2_2, P1_1)} & \rho_{Tx}^{(P2_2, P2_1)} & \rho_{Tx}^{(P2_2, P1_2)} & 1 \end{bmatrix}, \quad (4.4)$$

where  $\rho_{\text{Tx}}^{(X_i, Y_j)}$ ,  $X, Y \in \{P1, P2\}$ ,  $i, j \in [1 : 2]$ , represents the correlation coefficient between the signal sent across polarisation X from transmit antenna  $i$  and signal sent across polarisation Y from transmit antenna  $j$ . The correlation coefficients are complex-symmetrical such that  $\rho_{\text{Tx}}^{(X_i, Y_j)} = \bar{\rho}_{\text{Tx}}^{(Y_j, X_i)}$ . The entries of the correlation matrix model both IBI and inter-antenna interference (IAI) that may be present in the STPLD system. In (4.4), the correlation coefficient  $\rho_{\text{Tx}}^{(P1_1, P2_1)}$  is representative of the IBI between the P1-polarised and P2-polarised signals broadcast from transmit antenna 1. Similarly,  $\rho_{\text{Tx}}^{(P1_1, P1_2)}$  represents the IAI between the P1-polarised signals from transmit antennas 1 and 2.  $\rho_{\text{Tx}}^{(P1_1, P2_2)}$  is an example of an entry that models both IAI and IBI, as it represents the correlation between the P1-polarised signal transmitted from antenna 1 and the P2-polarised signal transmitted from antenna 2. Similar to (4.4), the  $2N_{\text{Rx}} \times 2N_{\text{Rx}}$  receive-side correlation matrix,  $\mathbf{C}_{\text{Rx}}$ , is defined in terms of correlation coefficients  $\rho_{\text{Rx}}^{(X_i, Y_j)}$ ,  $X, Y \in \{P1, P2\}$ ,  $i, j \in [1 : N_{\text{Rx}}]$ .

When constructing the antenna correlation matrix, 3 general cases may be considered: i) the case where there is only IBI, ii) the case where there is only IAI and iii) the case where there is both IBI and IAI. The following discussion show how the receive-side antenna correlation matrix is constructed for each of the above cases, assuming 3 dual-polarised receive antennas. The reasoning applied may be similarly extended for the transmit-side correlation matrix.

### Case 1: Only Inter-Beam Interference

Under the assumption that all antennas are manufactured identically, the IBI correlation coefficients for each antenna are the same. Denoting these as  $\rho^{\text{IBI}}$ , and assuming no IAI, the receive-side correlation matrix is given by:

$$\mathbf{C}_{\text{Rx, only IBI}} = \begin{bmatrix} 1 & \rho_{\text{Rx}}^{\text{IBI}} & 0 & 0 & 0 & 0 \\ \rho_{\text{Rx}}^{\text{IBI}} & 1 & 0 & 0 & 0 & 0 \\ 0 & 0 & 1 & \rho_{\text{Rx}}^{\text{IBI}} & 0 & 0 \\ 0 & 0 & \rho_{\text{Rx}}^{\text{IBI}} & 1 & 0 & 0 \\ 0 & 0 & 0 & 0 & 1 & \rho_{\text{Rx}}^{\text{IBI}} \\ 0 & 0 & 0 & 0 & \rho_{\text{Rx}}^{\text{IBI}} & 1 \end{bmatrix}. \quad (4.5)$$

$\mathbf{C}_{\text{Rx, only IBI}}$  is of a similar structure to the dual-correlation matrix presented by Reşat and Özyurt [46]. This is reasonable, as the signals received by each of the ODP antennas will be dual-correlated.

### Case 2: Only Inter-Antenna Interference

Under the assumption that only IAI is present in the system, correlation exists between the P1-polarised and P2-polarised beams from each antenna. Since IAI is independent of polarisation, the IAI experienced by the P1-polarised and P2-polarised beams are the same, and denoted as  $\rho^{\text{IAI}}$ . A common method to express the correlation matrix for systems with IAI is to use the exponential correlation model (ECM) [46–50]. Reşat and Özyurt [46] discuss that the ECM is more reasonable for modelling antenna correlation in real-world systems than the alternative constant and dual-correlation models. Using the ECM and assuming no IBI, the receive-side correlation matrix

becomes:

$$\mathbf{C}_{\text{Rx, only IAI}} = \begin{bmatrix} 1 & 0 & \rho_{\text{Rx}}^{\text{IAI}} & 0 & (\rho_{\text{Rx}}^{\text{IAI}})^2 & 0 \\ 0 & 1 & 0 & \rho_{\text{Rx}}^{\text{IAI}} & 0 & (\rho_{\text{Rx}}^{\text{IAI}})^2 \\ \rho_{\text{Rx}}^{\text{IAI}} & 0 & 1 & 0 & \rho_{\text{Rx}}^{\text{IAI}} & 0 \\ 0 & \rho_{\text{Rx}}^{\text{IAI}} & 0 & 1 & 0 & \rho_{\text{Rx}}^{\text{IAI}} \\ (\rho_{\text{Rx}}^{\text{IAI}})^2 & 0 & \rho_{\text{Rx}}^{\text{IAI}} & 0 & 1 & 0 \\ 0 & (\rho_{\text{Rx}}^{\text{IAI}})^2 & 0 & \rho_{\text{Rx}}^{\text{IAI}} & 0 & 1 \end{bmatrix}. \quad (4.6)$$

### Case 3: Both Inter-Antenna and Inter-Beam Interference

When modelling both IAI and IBI, the statistical definition of the correlation coefficient provided by Akoun and Xu [51], Equation (2), is used. Observing that IAI and IBI are independent, it can be shown that the correlation coefficient for a channel element that experiences both IAI and IBI is the product of the correlation coefficients arising from only IAI and only IBI. Thus, using (4.5) and (4.6), the receive-side correlation matrix becomes:

$$\begin{aligned} \mathbf{C}_{\text{Rx, IAI \& IBI}} &= \mathbf{C}_{\text{Rx, only IAI}} + \mathbf{C}_{\text{Rx, only IBI}} \\ &+ \begin{bmatrix} -1 & 0 & 0 & \rho_{\text{Rx}}^{\text{IBI}} \rho_{\text{Rx}}^{\text{IAI}} & 0 & \rho_{\text{Rx}}^{\text{IBI}} (\rho_{\text{Rx}}^{\text{IAI}})^2 \\ 0 & -1 & \rho_{\text{Rx}}^{\text{IBI}} \rho_{\text{Rx}}^{\text{IAI}} & 0 & \rho_{\text{Rx}}^{\text{IBI}} (\rho_{\text{Rx}}^{\text{IAI}})^2 & 0 \\ 0 & \rho_{\text{Rx}}^{\text{IBI}} \rho_{\text{Rx}}^{\text{IAI}} & -1 & 0 & 0 & \rho_{\text{Rx}}^{\text{IBI}} \rho_{\text{Rx}}^{\text{IAI}} \\ \rho_{\text{Rx}}^{\text{IBI}} \rho_{\text{Rx}}^{\text{IAI}} & 0 & 0 & -1 & \rho_{\text{Rx}}^{\text{IBI}} \rho_{\text{Rx}}^{\text{IAI}} & 0 \\ 0 & \rho_{\text{Rx}}^{\text{IBI}} (\rho_{\text{Rx}}^{\text{IAI}})^2 & 0 & \rho_{\text{Rx}}^{\text{IBI}} \rho_{\text{Rx}}^{\text{IAI}} & -1 & 0 \\ \rho_{\text{Rx}}^{\text{IBI}} (\rho_{\text{Rx}}^{\text{IAI}})^2 & 0 & \rho_{\text{Rx}}^{\text{IBI}} \rho_{\text{Rx}}^{\text{IAI}} & 0 & 0 & -1 \end{bmatrix} \\ &= \begin{bmatrix} 1 & \rho_{\text{Rx}}^{\text{IBI}} & \rho_{\text{Rx}}^{\text{IAI}} & \rho_{\text{Rx}}^{\text{IBI}} \rho_{\text{Rx}}^{\text{IAI}} & (\rho_{\text{Rx}}^{\text{IAI}})^2 & \rho_{\text{Rx}}^{\text{IBI}} (\rho_{\text{Rx}}^{\text{IAI}})^2 \\ \rho_{\text{Rx}}^{\text{IBI}} & 1 & \rho_{\text{Rx}}^{\text{IBI}} \rho_{\text{Rx}}^{\text{IAI}} & \rho_{\text{Rx}}^{\text{IAI}} & \rho_{\text{Rx}}^{\text{IBI}} (\rho_{\text{Rx}}^{\text{IAI}})^2 & (\rho_{\text{Rx}}^{\text{IAI}})^2 \\ \rho_{\text{Rx}}^{\text{IAI}} & \rho_{\text{Rx}}^{\text{IBI}} \rho_{\text{Rx}}^{\text{IAI}} & 1 & \rho_{\text{Rx}}^{\text{IBI}} & \rho_{\text{Rx}}^{\text{IAI}} & \rho_{\text{Rx}}^{\text{IBI}} \rho_{\text{Rx}}^{\text{IAI}} \\ \rho_{\text{Rx}}^{\text{IBI}} \rho_{\text{Rx}}^{\text{IAI}} & \rho_{\text{Rx}}^{\text{IAI}} & \rho_{\text{Rx}}^{\text{IBI}} & 1 & \rho_{\text{Rx}}^{\text{IBI}} \rho_{\text{Rx}}^{\text{IAI}} & \rho_{\text{Rx}}^{\text{IAI}} \\ (\rho_{\text{Rx}}^{\text{IAI}})^2 & \rho_{\text{Rx}}^{\text{IBI}} (\rho_{\text{Rx}}^{\text{IAI}})^2 & \rho_{\text{Rx}}^{\text{IAI}} & \rho_{\text{Rx}}^{\text{IBI}} \rho_{\text{Rx}}^{\text{IAI}} & 1 & \rho_{\text{Rx}}^{\text{IBI}} \\ \rho_{\text{Rx}}^{\text{IBI}} (\rho_{\text{Rx}}^{\text{IAI}})^2 & (\rho_{\text{Rx}}^{\text{IAI}})^2 & \rho_{\text{Rx}}^{\text{IBI}} \rho_{\text{Rx}}^{\text{IAI}} & \rho_{\text{Rx}}^{\text{IAI}} & \rho_{\text{Rx}}^{\text{IBI}} & 1 \end{bmatrix}. \end{aligned} \quad (4.7)$$

## 4.4 Analysis of Error Performance

### 4.4.1 Uncorrelated Error Performance

Due to the STPLD system achieving multiple forms of diversity, it is expected that the wireless link will be very reliable at high SNRs. It is thus reasonable to assume that in the high-SNR region, the ABEP of the STPLD system may be approximated by the probability of only a single codeword being detected erroneously. This is in agreement with the assumption used in other literature when analyzing space-time block coded systems with labelling diversity [28, 36]. Under this assumption, the following derivation considers the case (without loss of generality) wherein codeword  $\ell_2$  is detected correctly and codeword  $\ell_1$  is detected erroneously as  $l_1$ . The union bound of the ABEP for the uncorrelated STPLD system is thus given by:

$$\mathcal{P}_e \leq \frac{1}{M} \sum_{\ell_1=0}^{M-1} \sum_{l_1=0}^{M-1} \frac{\Delta(\ell_1, l_1)}{m} \mathcal{P}(\ell_1 \rightarrow l_1), \quad (4.8)$$

where  $\mathcal{P}(\ell_1 \rightarrow l_1)$  is the pairwise error probability (PEP) that transmitted codeword  $\ell_1$  is incorrectly detected as codeword  $l_1$ , and  $\Delta(\ell_1, l_1)$  is the number of bit errors between  $\ell_1$  and  $l_1$ .

Given the assumption that only  $\ell_1$  is detected incorrectly at the receiver, the PEP conditioned on perfect knowledge of all channels, across both polarisations and both time slots, is given by:

$$\begin{aligned} & \mathcal{P}(\ell_1 \rightarrow l_1 \mid \mathbf{h}_{P1_1}^{(1)}, \mathbf{h}_{P2_1}^{(1)}, \mathbf{h}_{P1_1}^{(2)}, \mathbf{h}_{P2_1}^{(2)}, \mathbf{h}_{P1_2}^{(1)}, \mathbf{h}_{P2_2}^{(1)}, \mathbf{h}_{P1_2}^{(2)}, \mathbf{h}_{P2_2}^{(2)}) \\ &= \mathcal{P} \left( \sum_{k=1}^2 \left\| \mathbf{y}_k - \sqrt{\frac{E_{Tx}}{4E_{\Omega}E_n}} \begin{bmatrix} \mathbf{h}_{P1_k}^{(1)} & \mathbf{h}_{P2_k}^{(1)} & \mathbf{h}_{P1_k}^{(2)} & \mathbf{h}_{P2_k}^{(2)} \end{bmatrix} \begin{bmatrix} \Omega_k(l_1) \\ \Omega_k(l_2) \\ \Omega_k(l_2) \\ \Omega_k(l_1) \end{bmatrix} \right\|^2 \right. \\ & \quad \left. < \sum_{k=1}^2 \left\| \mathbf{y}_k - \sqrt{\frac{E_{Tx}}{4E_{\Omega}E_n}} \begin{bmatrix} \mathbf{h}_{P1_k}^{(1)} & \mathbf{h}_{P2_k}^{(1)} & \mathbf{h}_{P1_k}^{(2)} & \mathbf{h}_{P2_k}^{(2)} \end{bmatrix} \begin{bmatrix} \Omega_k(\ell_1) \\ \Omega_k(\ell_2) \\ \Omega_k(\ell_2) \\ \Omega_k(\ell_1) \end{bmatrix} \right\|^2 \right) \\ &= \mathcal{P} \left( \sum_{k=1}^2 \left\| \sqrt{\frac{E_{Tx}}{4E_{\Omega}E_n}} \begin{bmatrix} \mathbf{h}_{P1_k}^{(1)} & \mathbf{h}_{P2_k}^{(1)} & \mathbf{h}_{P1_k}^{(2)} & \mathbf{h}_{P2_k}^{(2)} \end{bmatrix} \begin{bmatrix} \Omega_k(\ell_1) - \Omega_k(l_1) \\ \Omega_k(\ell_2) - \Omega_k(l_2) \\ \Omega_k(\ell_2) - \Omega_k(l_2) \\ \Omega_k(\ell_1) - \Omega_k(l_1) \end{bmatrix} + \mathbf{n}_k \right\|^2 < \|\mathbf{n}_1\|^2 + \|\mathbf{n}_2\|^2 \right), \end{aligned} \quad (4.9)$$

where  $l_2$  is the estimated codeword corresponding to  $\ell_2$  at the receiver. Due to the assumption that only  $\ell_1$  is detected erroneously,  $l_2 = \ell_2$ . Therefore,  $\Omega_k(\ell_2) = \Omega_k(l_2)$  in (4.9). Hence, the conditional PEP may be simplified to:

$$\begin{aligned}
 & \mathcal{P} \left( \ell_1 \rightarrow l_1 \mid \mathbf{h}_{P1_1}^{(1)}, \mathbf{h}_{P2_1}^{(1)}, \mathbf{h}_{P1_1}^{(2)}, \mathbf{h}_{P2_1}^{(2)}, \mathbf{h}_{P1_2}^{(1)}, \mathbf{h}_{P2_2}^{(1)}, \mathbf{h}_{P1_2}^{(2)}, \mathbf{h}_{P2_2}^{(2)} \right) \\
 &= \mathcal{P} \left( \sum_{k=1}^2 \left\| \sqrt{\frac{E_{Tx}}{4E_{\Omega}E_n}} \begin{bmatrix} \mathbf{h}_{P1_k}^{(1)} & \mathbf{h}_{P2_k}^{(1)} & \mathbf{h}_{P1_k}^{(2)} & \mathbf{h}_{P2_k}^{(2)} \end{bmatrix} \begin{bmatrix} \Omega_k(\ell_1) - \Omega_k(l_1) \\ 0 \\ 0 \\ \Omega_k(\ell_1) - \Omega_k(l_1) \end{bmatrix} + \mathbf{n}_k \right\|^2 < \|\mathbf{n}_1\|^2 + \|\mathbf{n}_2\|^2 \right) \\
 &= \mathcal{P} \left( \sum_{k=1}^2 \left\| \sqrt{\frac{E_{Tx}}{4E_{\Omega}E_n}} \left( \mathbf{h}_{P1_k}^{(1)} + \mathbf{h}_{P2_k}^{(2)} \right) \varepsilon_k^{(\ell_1, l_1)} + \mathbf{n}_k \right\|^2 < \|\mathbf{n}_1\|^2 + \|\mathbf{n}_2\|^2 \right). \tag{4.10}
 \end{aligned}$$

In (4.10),  $\varepsilon_k^{(\ell_1, l_1)}$  represents the difference between the constellation points corresponding to labels  $\ell_1$  and  $l_1$  when mapped using  $\Omega_k$ . In general, the difference between labels  $a$  and  $b$  is defined by:

$$\varepsilon_k^{(a, b)} = \Omega_k(a) - \Omega_k(b); \quad k \in [1 : 2], \quad a, b \in [0 : M - 1] \tag{4.11}$$

Using the Equation (5.1.5) from Meyer [52] and simplifying notation by making the substitution  $\mathbf{g}_k = \sqrt{\frac{E_{Tx}}{4E_{\Omega}E_n}} \left( \mathbf{h}_{P1_k}^{(1)} + \mathbf{h}_{P2_k}^{(2)} \right) \varepsilon_k^{(\ell_1, l_1)}$ , the summed terms on the lesser side of the inequality in (4.10) may be written as:

$$\begin{aligned}
 \sum_{k=1}^2 \left\| \sqrt{\frac{E_{Tx}}{4E_{\Omega}E_n}} \left( \mathbf{h}_{P1_k}^{(1)} + \mathbf{h}_{P2_k}^{(2)} \right) \varepsilon_k^{(\ell_1, l_1)} + \mathbf{n}_k \right\|^2 &= \sum_{k=1}^2 \|\mathbf{g}_k + \mathbf{n}_k\|^2 \\
 &= \sum_{k=1}^2 \left[ \|\mathbf{g}_k\|^2 + \|\mathbf{n}_k\|^2 + 2\Re(\bar{\mathbf{n}}_k^T \mathbf{g}_k) \right]. \tag{4.12}
 \end{aligned}$$

Since (4.10) is conditioned on perfect knowledge of all channels,  $\bar{\mathbf{n}}_k^T \mathbf{g}_k$ ,  $k \in [1 : 2]$ , represents the sum of  $2N_{Rx}$  complex Gaussian random variables (GRVs). Each GRV, has zero mean and variance  $|g_{j,k}|^2$ , where  $g_{j,k}$  represents the  $j$ -th element of  $\mathbf{g}_k$  and  $j \in [1 : 2N_{Rx}]$ . Hence, it may be deduced that  $\sum_{k=1}^2 \Re(\bar{\mathbf{n}}_k^T \mathbf{g}_k)$  is a complex GRV with zero mean and variance  $\sigma_{GRV}^2 = \frac{1}{2} \sum_{k=1}^2 \|\mathbf{g}_k\|^2$ .

The conditional PEP in (4.10) may thus be expressed as:

$$\begin{aligned}
& \mathcal{P} \left( \ell_1 \rightarrow l_1 \mid \mathbf{h}_{P1_1}^{(1)}, \mathbf{h}_{P2_1}^{(1)}, \mathbf{h}_{P1_1}^{(2)}, \mathbf{h}_{P2_1}^{(2)}, \mathbf{h}_{P1_2}^{(1)}, \mathbf{h}_{P2_2}^{(1)}, \mathbf{h}_{P1_2}^{(2)}, \mathbf{h}_{P2_2}^{(2)} \right) \\
&= \mathcal{P} \left( \sum_{k=1}^2 \left[ \|\mathbf{g}_k\|^2 + \|\mathbf{n}_k\|^2 + 2\Re(\bar{\mathbf{n}}_k^T \mathbf{g}_k) \right] < \|\mathbf{n}_1\|^2 + \|\mathbf{n}_2\|^2 \right) \\
&= \mathcal{P} \left( \sum_{k=1}^2 \Re(\bar{\mathbf{n}}_k^T \mathbf{g}_k) + \frac{\sum_{k=1}^2 \|\mathbf{g}_k\|^2}{2} < 0 \right) \\
&= \mathcal{Q} \left( \frac{\sum_{k=1}^2 \|\mathbf{g}_k\|^2}{2\sqrt{\sigma_{\text{GRV}}^2}} \right) \\
&= \mathcal{Q} \left( \sqrt{\frac{1}{2} \sum_{k=1}^2 \|\mathbf{g}_k\|^2} \right) \tag{4.13}
\end{aligned}$$

$$= \mathcal{Q} \left( \sqrt{\frac{1}{2} \sum_{j=1}^{2N_{\text{Rx}}} \sum_{k=1}^2 \alpha_{j,k}^2} \right), \tag{4.14}$$

where  $\mathcal{Q}(x) = \frac{1}{\pi} \int_0^{\frac{\pi}{2}} \exp\left(-\frac{x^2}{2\sin^2(y)}\right) dy$  is the Gaussian Q-function in the form presented by Craig [53]. In the penultimate step of the above set of equations, (4.14) is obtained by expanding the vector Frobenius norms in (4.13) and defining the amplitude  $\alpha_{j,k} = |g_{j,k}|$ .

Since the Q-function has finite bounds of integration, it may be solved numerically using a trapezoidal approximation [28, 36]. Hence, (4.14) may be expressed as:

$$\begin{aligned}
\mathcal{Q} \left( \sqrt{\frac{1}{2} \sum_{j=1}^{2N_{\text{Rx}}} \sum_{k=1}^2 \alpha_{j,k}^2} \right) &= \frac{1}{\pi} \int_0^{\frac{\pi}{2}} \exp \left( - \sum_{j=1}^{2N_{\text{Rx}}} \sum_{k=1}^2 \frac{\alpha_{j,k}^2}{4 \sin^2(y)} \right) dy \\
&= \frac{1}{\pi} \prod_{j=1}^{2N_{\text{Rx}}} \prod_{k=1}^2 \int_0^{\frac{\pi}{2}} \exp \left( - \frac{\alpha_{j,k}^2}{4 \sin^2(y)} \right) dy \\
&\approx \frac{1}{4r} \prod_{j=1}^{2N_{\text{Rx}}} \exp \left( - \frac{\alpha_{j,1}^2}{4} \right) \exp \left( - \frac{\alpha_{j,2}^2}{4} \right) \\
&\quad + \frac{1}{2r} \prod_{j=1}^{2N_{\text{Rx}}} \sum_{R=1}^{r-1} \exp \left( - \frac{\alpha_{j,1}^2}{4 \sin^2 \left( \frac{R\pi}{2r} \right)} \right) \exp \left( - \frac{\alpha_{j,2}^2}{4 \sin^2 \left( \frac{R\pi}{2r} \right)} \right), \tag{4.15}
\end{aligned}$$

where  $r$  is a sufficiently large integer to allow the trapezoidal approximation to converge to the integral result.

The next step of this derivation is to obtain the unconditioned PEP,  $\mathcal{P}(\ell_1 \rightarrow l_1)$ , as required by the union bound expression in (4.8). This is done by integrating (4.15) over the probability density function (PDF) of element  $\alpha_{j,k}$ , denoted as  $\mathcal{F}_{\alpha_{j,k}}(\cdot)$ . The resulting expression for the unconditioned

PEP is:

$$\begin{aligned}
\mathcal{P}(\ell_1 \rightarrow \ell_1) &\approx \frac{1}{4r} \prod_{j=1}^{2N_{\text{Rx}}} \int_0^\infty \exp\left(-\frac{\alpha_{j,1}^2}{4}\right) \mathcal{F}_{\alpha_{j,1}}(\alpha_{j,1}) \, d\alpha_{j,1} \int_0^\infty \exp\left(-\frac{\alpha_{j,2}^2}{4}\right) \mathcal{F}_{\alpha_{j,2}}(\alpha_{j,2}) \, d\alpha_{j,2} \\
&+ \frac{1}{2r} \prod_{j=1}^{2N_{\text{Rx}}} \sum_{R=1}^{r-1} \int_0^\infty \exp\left(-\frac{\alpha_{j,1}^2}{4 \sin^2\left(\frac{R\pi}{2r}\right)}\right) \mathcal{F}_{\alpha_{j,1}}(\alpha_{j,1}) \, d\alpha_{j,1} \\
&\quad \times \int_0^\infty \exp\left(-\frac{\alpha_{j,2}^2}{4 \sin^2\left(\frac{R\pi}{2r}\right)}\right) \mathcal{F}_{\alpha_{j,2}}(\alpha_{j,2}) \, d\alpha_{j,2}. \tag{4.16}
\end{aligned}$$

From the earlier definition of  $\mathbf{g}_k$ , it follows that the amplitude  $\alpha_{j,k}$  may be written as  $\alpha_{j,k} = |g_{j,k}| = \left| \sqrt{\frac{E_{\text{Tx}}}{4E_\Omega E_n}} \left( h_{j,\text{P}1_k}^{(1)} + h_{j,\text{P}2_k}^{(2)} \right) \varepsilon_k^{(\ell_1, \ell_1)} \right|$ ,  $j \in [1 : 2N_{\text{Rx}}]$ ,  $k \in [1 : 2]$ , where  $h_{j,\text{P}1_k}^{(1)}$  represents the  $j$ -th element of matrix  $\mathbf{h}_{\text{P}1_k}^{(1)}$ , and similarly for  $h_{j,\text{P}2_k}^{(2)}$ . As per the system model described in Section 4.3, the amplitude of all fading coefficients are assumed to follow a Nakagami- $q$  distribution with zero mean and unit variance. In the case of uncorrelated channels,  $\alpha_{j,k}$  also follows a Nakagami- $q$  distribution with zero mean and variance  $\sigma_{\alpha_{j,k}}^2$ , which is given by:

$$\begin{aligned}
\sigma_{\alpha_{j,k}}^2 &= \mathbb{E} \left\{ \left| \sqrt{\frac{E_{\text{Tx}}}{4E_\Omega E_n}} \left( h_{j,\text{P}1_k}^{(1)} + h_{j,\text{P}2_k}^{(2)} \right) \varepsilon_k^{(\ell_1, \ell_1)} \right|^2 \right\} \\
&= \frac{E_{\text{Tx}}}{4E_\Omega E_n} \left| \varepsilon_k^{(\ell_1, \ell_1)} \right|^2 \times \mathbb{E} \left\{ \left| h_{j,\text{P}1_k}^{(1)} + h_{j,\text{P}2_k}^{(2)} \right|^2 \right\} \\
&= \frac{E_{\text{Tx}}}{4E_\Omega E_n} \left| \varepsilon_k^{(\ell_1, \ell_1)} \right|^2 \times 2 \\
&= \frac{E_{\text{Tx}}}{2E_\Omega E_n} \left| \varepsilon_k^{(\ell_1, \ell_1)} \right|^2. \tag{4.17}
\end{aligned}$$

The expression in (4.17) shows that the variance of  $\alpha_{j,k}$  is independent of  $j$ . Stated differently,  $\sigma_{\alpha_{j,k}}^2 = \sigma_{\alpha_k}^2 \forall j \in [1 : 2N_{\text{Rx}}]$ . Therefore, the PDF of  $\alpha_{j,k}$  may be expressed as [35]:

$$\mathcal{F}_{\alpha_{j,k}}(\alpha_{j,k}) = \frac{\alpha_{j,k} (1 + q^2)}{q \sigma_{\alpha_k}} \exp\left(-\frac{\alpha_{j,k}^2 (1 + q^2)^2}{4q^2 \sigma_{\alpha_k}^2}\right) \text{I}_0\left(\frac{\alpha_{j,k}^2 (1 - q^4)}{4q^2 \sigma_{\alpha_k}^2}\right), \tag{4.18}$$

where  $\text{I}_0(\cdot)$  denotes the zeroth order Bessel function of the first kind. The corresponding moment generating function (MGF) of  $\alpha_{j,k}$  is given by Simon and Alouini [35] as:

$$\mathbf{M}_k(s) = \left[ 1 + 2s\sigma_{\alpha_k}^2 + \left( \frac{2sq\sigma_{\alpha_k}^2}{1 + q^2} \right)^2 \right]^{-\frac{1}{2}}, \tag{4.19}$$

where  $q$  is the Nakagami- $q$  fading parameter, as defined in the system model in Section 4.3.3.

The PEP in (4.16) may then be expressed in terms of the MGF as:

$$\mathcal{P}(\ell_1 \rightarrow l_1) \approx \frac{1}{4r} \prod_{j=1}^{2N_{\text{Rx}}} M_1\left(\frac{1}{4}\right) M_2\left(\frac{1}{4}\right) + \frac{1}{2r} \prod_{j=1}^{2N_{\text{Rx}}} \sum_{R=1}^{r-1} M_1\left(\frac{1}{4 \sin^2\left(\frac{R\pi}{2r}\right)}\right) M_2\left(\frac{1}{4 \sin^2\left(\frac{R\pi}{2r}\right)}\right). \quad (4.20)$$

For uncorrelated channels with identical distributions,  $\alpha_{j,1}$  has the same distribution for all  $j \in [1 : 2N_{\text{Rx}}]$ . The same is true for  $\alpha_{j,2}$ . This is evident as the MGF is independent of  $j$ , as shown in (4.19). Thus, the final expression for the PEP of the STPLD system in uncorrelated Nakagami- $q$  channels, modified from (4.20) and substituting (4.17) and (4.19), is:

$$\begin{aligned} & \mathcal{P}(\ell_1 \rightarrow l_1) \\ & \approx \frac{1}{4r} \left[ M_1\left(\frac{1}{4}\right) M_2\left(\frac{1}{4}\right) \right]^{2N_{\text{Rx}}} + \frac{1}{2r} \sum_{R=1}^{r-1} \left[ M_1\left(\frac{1}{4 \sin^2\left(\frac{R\pi}{2r}\right)}\right) M_2\left(\frac{1}{4 \sin^2\left(\frac{R\pi}{2r}\right)}\right) \right]^{2N_{\text{Rx}}} \\ & \approx \frac{1}{4r} \prod_{k=1}^2 \left[ 1 + \frac{E_{\text{Tx}}}{4E_{\Omega}E_n} \left| \varepsilon_k^{(\ell_1, l_1)} \right|^2 + \left( \frac{qE_{\text{Tx}}}{4E_{\Omega}E_n(1+q^2)} \left| \varepsilon_k^{(\ell_1, l_1)} \right|^2 \right)^2 \right]^{-N_{\text{Rx}}} \\ & \quad + \frac{1}{2r} \prod_{k=1}^2 \sum_{R=1}^{r-1} \left[ 1 + \frac{E_{\text{Tx}}}{4E_{\Omega}E_n \sin^2\left(\frac{R\pi}{2r}\right)} \left| \varepsilon_k^{(\ell_1, l_1)} \right|^2 + \left( \frac{qE_{\text{Tx}} \left| \varepsilon_k^{(\ell_1, l_1)} \right|^2}{4E_{\Omega}E_n(1+q^2) \sin^2\left(\frac{R\pi}{2r}\right)} \right)^2 \right]^{-N_{\text{Rx}}}. \end{aligned} \quad (4.21)$$

The final expression for the ABEP of the uncorrelated STPLD system is obtained by substituting (4.21) in (4.8). This is written in terms of the total average SNR,  $\gamma$ , as defined in Section 4.3 as:

$$\begin{aligned} \mathcal{P}_e \leq & \sum_{\ell_1=0}^{M-1} \sum_{l_1=0}^{M-1} \frac{\Delta(\ell_1, l_1)}{4Mmr} \prod_{k=1}^2 \left[ 1 + \frac{\gamma}{4} \left| \varepsilon_k^{(\ell_1, l_1)} \right|^2 + \left( \frac{q\gamma}{4(1+q^2)} \left| \varepsilon_k^{(\ell_1, l_1)} \right|^2 \right)^2 \right]^{-N_{\text{Rx}}} \\ & + \sum_{\ell_1=0}^{M-1} \sum_{l_1=0}^{M-1} \frac{\Delta(\ell_1, l_1)}{2Mmr} \prod_{k=1}^2 \sum_{R=1}^{r-1} \left[ 1 + \frac{\gamma}{4 \sin^2\left(\frac{R\pi}{2r}\right)} \left| \varepsilon_k^{(\ell_1, l_1)} \right|^2 + \left( \frac{q\gamma \left| \varepsilon_k^{(\ell_1, l_1)} \right|^2}{4(1+q^2) \sin^2\left(\frac{R\pi}{2r}\right)} \right)^2 \right]^{-N_{\text{Rx}}}. \end{aligned} \quad (4.22)$$

#### 4.4.2 Correlated Error Performance

To analyze the error performance of the STPLD system in the presence of correlation, this paper adopts the mathematical framework developed by Hedayet *et al* [45]. To utilise this framework, it is necessary to consider the union bound of the ABEP without making a high-SNR assumptions, as was done in Section 4.4.1. The union bound of the system is then given by:

$$\mathcal{P}_e \leq \frac{1}{M^2} \sum_{\ell_1=0}^{M-1} \sum_{l_1=0}^{M-1} \sum_{\ell_2=0}^{M-1} \sum_{l_2=0}^{M-1} \frac{\Delta(\ell_1, l_1) + \Delta(\ell_2, l_2)}{2m} \mathcal{P}([l_1 \ l_2]^T \rightarrow [\ell_1 \ \ell_2]^T), \quad (4.23)$$

where  $\Delta(\ell_1, l_1)$  is the number of bit errors between  $\ell_1$  and  $l_1$ , as in (4.8). Similarly,  $\Delta(\ell_2, l_2)$  is the number of bit errors between  $\ell_2$  and  $l_2$ .  $\mathcal{P}([\ell_1 \ \ell_2]^T \rightarrow [l_1 \ l_2]^T)$  is the PEP that transmitted codeword vector  $[\ell_1 \ \ell_2]^T$  is incorrectly detected as codeword vector  $[l_1 \ l_2]^T$ .

For correlated analysis, the PEP conditioned on perfect knowledge of all channels is given by:

$$\begin{aligned} & \mathcal{P}([\ell_1 \ \ell_2]^T \rightarrow [l_1 \ l_2]^T \mid \mathbf{h}_{P1_1}^{(1)}, \mathbf{h}_{P2_1}^{(1)}, \mathbf{h}_{P1_1}^{(2)}, \mathbf{h}_{P2_1}^{(2)}, \mathbf{h}_{P1_2}^{(1)}, \mathbf{h}_{P2_2}^{(1)}, \mathbf{h}_{P1_2}^{(2)}, \mathbf{h}_{P2_2}^{(2)}) \\ &= \mathcal{P} \left( \sum_{k=1}^2 \left\| \sqrt{\frac{E_{Tx}}{4E_{\Omega}E_n}} \begin{bmatrix} \mathbf{h}_{P1_k}^{(1)} & \mathbf{h}_{P2_k}^{(1)} & \mathbf{h}_{P1_k}^{(2)} & \mathbf{h}_{P2_k}^{(2)} \end{bmatrix} \begin{bmatrix} \varepsilon_k^{(\ell_1, l_1)} \\ \varepsilon_k^{(\ell_2, l_2)} \\ \varepsilon_k^{(\ell_2, l_2)} \\ \varepsilon_k^{(\ell_1, l_1)} \end{bmatrix} + \mathbf{n}_k \right\|^2 < \|\mathbf{n}_1\|^2 + \|\mathbf{n}_2\|^2 \right) \\ &= \mathcal{P} \left( \sum_{k=1}^2 \left\| \sqrt{\frac{E_{Tx}}{4E_{\Omega}E_n}} \begin{bmatrix} \mathbf{h}_{P1_k}^{(1)} & \mathbf{h}_{P2_k}^{(1)} & \mathbf{h}_{P1_k}^{(2)} & \mathbf{h}_{P2_k}^{(2)} \end{bmatrix} \boldsymbol{\varepsilon}_k + \mathbf{n}_k \right\|^2 < \|\mathbf{n}_1\|^2 + \|\mathbf{n}_2\|^2 \right) \quad (4.24) \end{aligned}$$

$$= \mathcal{P} \left( \sum_{k=1}^2 \left\| \sqrt{\frac{E_{Tx}}{4E_{\Omega}E_n}} \mathbf{C}_{Rx}^{\frac{1}{2}} \begin{bmatrix} \hat{\mathbf{h}}_{P1_k}^{(1)} & \hat{\mathbf{h}}_{P2_k}^{(1)} & \hat{\mathbf{h}}_{P1_k}^{(2)} & \hat{\mathbf{h}}_{P2_k}^{(2)} \end{bmatrix} \left( \mathbf{C}_{Tx}^{\frac{1}{2}} \right)^T \boldsymbol{\varepsilon}_k + \mathbf{n}_k \right\|^2 < \|\mathbf{n}_1\|^2 + \|\mathbf{n}_2\|^2 \right), \quad (4.25)$$

where  $\varepsilon_k^{\ell_k, l_k}, k \in [1 : 2]$ , is defined in (4.11). In the final step, (4.25) is obtained by substituting the Kronecker correlation model given in (4.3) into (4.24). The difference vector,  $\boldsymbol{\varepsilon}_k$ , which was introduced in (4.24) is defined as:

$$\boldsymbol{\varepsilon}_k = \begin{bmatrix} \varepsilon_k^{(\ell_1, l_1)} & \varepsilon_k^{(\ell_2, l_2)} & \varepsilon_k^{(\ell_2, l_2)} & \varepsilon_k^{(\ell_1, l_1)} \end{bmatrix}^T. \quad (4.26)$$

Substituting  $\mathbf{G}_k = \sqrt{\frac{E_{Tx}}{4E_{\Omega}E_n}} \mathbf{C}_{Rx}^{\frac{1}{2}} \begin{bmatrix} \hat{\mathbf{h}}_{P1_k}^{(1)} & \hat{\mathbf{h}}_{P2_k}^{(1)} & \hat{\mathbf{h}}_{P1_k}^{(2)} & \hat{\mathbf{h}}_{P2_k}^{(2)} \end{bmatrix} \left( \mathbf{C}_{Tx}^{\frac{1}{2}} \right)^T \boldsymbol{\varepsilon}_k, k \in [1 : 2]$  in (4.25) and defining the amplitude  $\beta_{j,k} = |G_{j,k}|$ , where  $G_{j,k}$  is the  $j$ -th entry of  $\mathbf{G}_k, j \in [1 : 2N_{Rx}]$ , the unconditioned PEP is obtained by following the same process as given by (4.12)–(4.16). The resulting expression for the unconditioned PEP is:

$$\begin{aligned} & \mathcal{P}([\ell_1 \ \ell_2]^T \rightarrow [l_1 \ l_2]^T) \\ & \approx \frac{1}{4r} \prod_{j=1}^{2N_{Rx}} \int_0^{\infty} \exp\left(-\frac{\beta_{j,1}^2}{4}\right) \mathcal{F}_{\beta_{j,1}}(\beta_{j,1}) \, d\beta_{j,1} \int_0^{\infty} \exp\left(-\frac{\beta_{j,2}^2}{4}\right) \mathcal{F}_{\beta_{j,2}}(\beta_{j,2}) \, d\beta_{j,2} \\ & + \frac{1}{2r} \prod_{j=1}^{2N_{Rx}} \sum_{R=1}^{r-1} \int_0^{\infty} \exp\left(-\frac{\beta_{j,1}^2}{4 \sin^2\left(\frac{R\pi}{2r}\right)}\right) \mathcal{F}_{\beta_{j,1}}(\beta_{j,1}) \, d\beta_{j,1} \\ & \quad \times \int_0^{\infty} \exp\left(-\frac{\beta_{j,2}^2}{4 \sin^2\left(\frac{R\pi}{2r}\right)}\right) \mathcal{F}_{\beta_{j,2}}(\beta_{j,2}) \, d\beta_{j,2}. \quad (4.27) \end{aligned}$$

As was the case in uncorrelated analysis, the random variable  $\beta_{j,k}, j \in [1 : N_{Rx}], k \in [1 : 2]$  follows a Nakagami- $q$  distribution with zero mean and variance  $\sigma_{\beta_{j,k}}^2$ . Thus, similar to (4.18), the PDF of

$\beta_{j,k}$  is given by:

$$\mathcal{F}_{\beta_{j,k}}(\beta_{j,k}) = \frac{\beta_{j,k}(1+q^2)}{q\sigma_{\beta_{j,k}}} \exp\left(-\frac{\beta_{j,k}^2(1+q^2)^2}{4q^2\sigma_{\beta_{j,k}}}\right) \text{I}_0\left(\frac{\beta_{j,k}^2(1-q^4)}{4q^2\sigma_{\beta_{j,k}}}\right). \quad (4.28)$$

The method to calculate the variance of  $\beta_{j,k}$  follows from the analytical framework formulated by Hedayet *et al.* [45]. The starting point of this analysis is to consider the definition of  $\|\mathbf{G}_k\|^2$ , given by:

$$\begin{aligned} \|\mathbf{G}_k\|^2 &= \left\| \sqrt{\frac{E_{\text{Tx}}}{4E_{\Omega}E_{\text{n}}}} \mathbf{C}_{\text{Rx}}^{\frac{1}{2}} \begin{bmatrix} \dot{\mathbf{h}}_{\text{P1}_k}^{(1)} & \dot{\mathbf{h}}_{\text{P2}_k}^{(1)} & \dot{\mathbf{h}}_{\text{P1}_k}^{(2)} & \dot{\mathbf{h}}_{\text{P2}_k}^{(2)} \end{bmatrix} \left(\mathbf{C}_{\text{Tx}}^{\frac{1}{2}}\right)^{\text{T}} \boldsymbol{\varepsilon}_k \right\|^2 \\ &= \frac{E_{\text{Tx}}}{4E_{\Omega}E_{\text{n}}} \text{Tr} \left\{ \mathbf{C}_{\text{Rx}} \begin{bmatrix} \dot{\mathbf{h}}_{\text{P1}_k}^{(1)} & \dot{\mathbf{h}}_{\text{P2}_k}^{(1)} & \dot{\mathbf{h}}_{\text{P1}_k}^{(2)} & \dot{\mathbf{h}}_{\text{P2}_k}^{(2)} \end{bmatrix} \begin{bmatrix} \left(\bar{\mathbf{h}}_{\text{P1}_k}^{(1)}\right)^{\text{T}} \\ \left(\bar{\mathbf{h}}_{\text{P2}_k}^{(1)}\right)^{\text{T}} \\ \left(\bar{\mathbf{h}}_{\text{P1}_k}^{(2)}\right)^{\text{T}} \\ \left(\bar{\mathbf{h}}_{\text{P2}_k}^{(2)}\right)^{\text{T}} \end{bmatrix} \mathbf{C}_{\text{Tx}} \boldsymbol{\varepsilon}_k \bar{\boldsymbol{\varepsilon}}_k^{\text{T}} \right\}. \quad (4.29) \end{aligned}$$

Observing that  $\mathbf{C}_{\text{Rx}}$  is a full rank  $2N_{\text{Rx}} \times 2N_{\text{Rx}}$  square matrix, it may be replaced in (4.29) by a  $2N_{\text{Rx}} \times 2N_{\text{Rx}}$  diagonal matrix consisting of its  $2N_{\text{Rx}}$  distinct eigenvalues. These eigenvalues are denoted  $V_j, j \in [1 : 2N_{\text{Rx}}]$ . Using a similar observation,  $\mathbf{C}_{\text{Tx}} \boldsymbol{\varepsilon}_k \bar{\boldsymbol{\varepsilon}}_k^{\text{T}}$  has rank one, thus it has only one non-zero eigenvalue, denoted  $W_k$ . Thus (4.29) may be simplified to:

$$\begin{aligned} \|\mathbf{G}_k\|^2 &= \frac{E_{\text{Tx}}}{4E_{\Omega}E_{\text{n}}} \text{Tr} \left\{ \begin{bmatrix} |V_1| & \cdots & 0 \\ 0 & \ddots & 0 \\ 0 & \cdots & |V_{2N_{\text{Rx}}}| \end{bmatrix} \begin{bmatrix} \dot{\mathbf{h}}_{\text{P1}_k}^{(1)} & \dot{\mathbf{h}}_{\text{P2}_k}^{(1)} & \dot{\mathbf{h}}_{\text{P1}_k}^{(2)} & \dot{\mathbf{h}}_{\text{P2}_k}^{(2)} \end{bmatrix} \begin{bmatrix} \left(\bar{\mathbf{h}}_{\text{P1}_k}^{(1)}\right)^{\text{T}} \\ \left(\bar{\mathbf{h}}_{\text{P2}_k}^{(1)}\right)^{\text{T}} \\ \left(\bar{\mathbf{h}}_{\text{P1}_k}^{(2)}\right)^{\text{T}} \\ \left(\bar{\mathbf{h}}_{\text{P2}_k}^{(2)}\right)^{\text{T}} \end{bmatrix} |W_k| \right\}. \quad (4.30) \end{aligned}$$

Recalling that  $\beta_{j,k} = |G_{j,k}|$ , the variance of  $\beta_{j,k}$  is obtained by performing elementary manipulation to (4.30) and following a similar process to (4.17). The final result for the variance  $\sigma_{\beta_{j,k}}^2$  is given by:

$$\sigma_{\beta_{j,k}}^2 = \frac{E_{\text{Tx}}}{4E_{\Omega}E_{\text{n}}} |V_j W_k|, \quad j \in [1 : 2N_{\text{Rx}}], k \in [1 : 2]. \quad (4.31)$$

Thus, the MGF for  $\beta_{j,k}$ , which corresponds to the PDF given in (4.28), is defined as [35]:

$$\begin{aligned} \mathbf{M}_{j,k}^{\text{corr.}}(s) &= \left[ 1 + 2s\sigma_{\beta_{j,k}}^2 + \left( \frac{2sq\sigma_{\beta_{j,k}}^2}{1+q^2} \right)^2 \right]^{-\frac{1}{2}} \\ &= \left[ 1 + \frac{E_{\text{Tx}}}{2E_{\Omega}E_n} |V_j W_k| + \left( \frac{qE_{\text{Tx}}}{2E_{\Omega}E_n(1+q^2)} |V_j W_k| \right)^2 \right]^{-\frac{1}{2}}. \end{aligned} \quad (4.32)$$

Finally, the PEP of the STPLD system in the presence of correlation is given by expressing (4.27) in terms of the MGF of  $\beta_{j,k}$ , and then substituting (4.32). The resulting expression is given by:

$$\mathcal{P}([l_1 \ l_2]^T \rightarrow [l_1 \ l_2]^T) \approx \frac{1}{4r} \prod_{j=1}^{2N_{\text{Rx}}} \prod_{k=1}^2 \mathbf{M}_{j,k}^{\text{corr.}} \left( \frac{1}{4} \right) + \frac{1}{2r} \prod_{j=1}^{2N_{\text{Rx}}} \prod_{k=1}^2 \sum_{R=1}^{r-1} \mathbf{M}_{j,k}^{\text{corr.}} \left( \frac{1}{4 \sin^2 \left( \frac{R\pi}{2r} \right)} \right). \quad (4.33)$$

The final ABEP for the correlated STPLD system is then given by substituting (4.32) and (4.33) in (4.23). Writing the result in terms of the total average SNR,  $\gamma$ , yields the expression:

$$\begin{aligned} \mathcal{P}_e &\leq \sum_{\ell_1=0}^{M-1} \sum_{l_1=0}^{M-1} \sum_{\ell_2=0}^{M-1} \sum_{l_2=0}^{M-1} \frac{\Delta(\ell_1, l_1) + \Delta(\ell_2, l_2)}{8M^2mr} \\ &\quad \times \prod_{j=1}^{2N_{\text{Rx}}} \prod_{k=1}^2 \left[ 1 + \frac{\gamma}{8} |V_j W_k| + \left( \frac{q\gamma}{8(1+q^2)} |V_j W_k| \right)^2 \right]^{-\frac{1}{2}} \\ &+ \sum_{\ell_1=0}^{M-1} \sum_{l_1=0}^{M-1} \sum_{\ell_2=0}^{M-1} \sum_{l_2=0}^{M-1} \frac{\Delta(\ell_1, l_1) + \Delta(\ell_2, l_2)}{4M^2mr} \\ &\quad \times \prod_{j=1}^{2N_{\text{Rx}}} \prod_{k=1}^2 \sum_{R=1}^{r-1} \left[ 1 + \frac{\gamma}{8 \sin^2 \left( \frac{R\pi}{2r} \right)} |V_j W_k| + \left( \frac{q\gamma}{8(1+q^2) \sin^2 \left( \frac{R\pi}{2r} \right)} |V_j W_k| \right)^2 \right]^{-\frac{1}{2}}. \end{aligned} \quad (4.34)$$

It is noted that (4.34) may also be used to evaluate uncorrelated STPLD systems, or STPLD systems with either transmit-side or receive-side correlation. To model a system with no transmit-side correlation,  $\mathbf{C}_{\text{Tx}}$  is set to a  $2N_{\text{Tx}} \times 2N_{\text{Tx}}$  identity matrix in (4.25). Similarly, to model a system with no receive-side correlation,  $\mathbf{C}_{\text{Rx}}$  is set to a  $2N_{\text{Rx}} \times 2N_{\text{Rx}}$  identity matrix in (4.25).

## 4.5 Mapper Design to achieve Labelling Diversity

As described in Section 4.3.3, the proposed STPLD system utilises 2 binary mappers,  $\Omega_1$  and  $\Omega_2$ , to encode information codewords to constellation symbols prior to transmission. The design of  $\Omega_1$  and  $\Omega_2$  determines the extent to which labelling diversity is achieved in the system, influencing its error performance.

The design of mappers for labelling diversity systems is an ongoing research problem [28, 29, 38, 54–56]. For a constellation with modulation order  $M$ , there are  $M!$  possible designs for each mapper. Hence, there are  $(M!)^2$  possible designs for the mapper pair  $\Omega_1$  and  $\Omega_2$ . Even for a relatively low modulation order of  $M = 8$ , this results in a joint candidate mapper space of more than  $1.62 \times 10^9$ . Due to the enormity of the joint candidate mapper space, proving the optimality of a pair of mappers remains an open research problem. Recent works on labelling diversity mapper design [28, 29, 38] have focused on the case where the primary mapper is known, and only a secondary mapper needs to be designed. This follows on from the research of Samra *et al.* [54], which indicates that it is optimal to design the primary mapper to perform a Gray coding.

Most of the previous works on labelling diversity mapper design may be classified as either geometric designs or search-based designs. Geometric designs are able to produce secondary mappers that achieve labelling diversity for specific modulation schemes based on heuristics obtained from the geometry of constellation points [28, 29, 55]. The most common heuristics are obtained by considering symmetry within the constellation. There are two key drawbacks of this approach. The first drawback is that the reliance on geometric heuristics, such as symmetry, constrains the modulation schemes that may be considered. The second drawback is that the quality of the secondary mapper is dependent on the choice of heuristic used. Hence, a poorly-selected heuristic may result in a design that fails to achieve labelling diversity. Quazi and Patel [29] study this in more detail using various heuristic designs for circular and rectangular constellations in their related work.

The search-based approach to labelling diversity mapper design [38, 54, 56] is more generic than its geometric counterpart, however it is too computationally expensive to perform exhaustive searches through the  $M!$  candidate secondary mapper space [54]. Samra *et al.* [54] showed that labelling diversity mapper design is an instance of the quadratic assignment problem (QAP), and utilised a branch-and-bound QAP-solver [57] to produce labelling diversity mappers. The QAP-solver produces an optimal labelling diversity secondary mapper for modulation orders  $M \leq 16$ , as stated by Samra *et al.* [54] and verified by Xu *et al.* [28]. However, the computational cost of the QAP solver made this approach unsuitable for modulation orders [54]. A recent work in labelling diversity mapper design by Patel *et al.* [38] utilised a genetic algorithm (GA) to develop secondary mappers for USTLD systems. The GA performs a heuristic search through the candidate mapper space, and is thus unconstrained by possible asymmetry of constellation points. It was also shown by Patel *et al.* [38] that the use of a GA is computationally feasible for modulation orders  $M > 16$ . Therefore,

in this paper, the GA proposed by Patel *et al.* [38] is modified and applied to design secondary mappers that achieve labelling diversity for STPLD systems. The modification is based on the two-stage approach to evaluating and comparing candidate secondary mapper designs in recent literature [29]. Next, this paper presents a description of the original GA [38] and its modifications is presented.

#### 4.5.1 Description of Genetic Algorithm for Secondary Mapper Design

Figure 4.2 provides a high-level illustration of the genetic algorithm for labelling diversity mapper design used in this paper. Candidate secondary mappers are encoded into data structures called ‘chromosomes’, which consists of subunits referred to as ‘genes’. The notation used in this section is to represent genes and chromosomes by variables  $x$  and  $\mathcal{X}$  respectively. The set of candidate secondary mappers considered at in each iteration of the GA is referred to as the ‘population’. In terms of notation,  $\{\mathcal{X}\}^{(n)}$  denotes the population at iteration  $n$ .

During each iteration, the population is modified to model the biological process of ‘evolution’ and ‘natural selection’. This involves the ‘mating’ of ‘parent’ chromosomes from within the population to produce ‘child’ chromosomes, which are added to the population. The entire population is then evaluated using a ‘fitness function’, which requires knowledge of the primary mapper,  $\Omega_1$ . After evaluating the fitness of chromosomes within the population, the least-fit chromosomes are removed. In this paper, the fitness of chromosome  $\mathcal{X}$  is denoted  $\varphi(\mathcal{X})$ . The output of the ‘evolution’ and ‘natural selection’ processes is a modified population at each iteration of the GA.

The GA stops iterating when chromosomes within the population have converged to the same fitness score. If the GA converges, it determines that a locally optimal (but not necessarily globally optimal) candidate mapper exists within the population. All chromosomes in the population are then re-evaluated using a ‘selection function’, which also requires knowledge of  $\Omega_1$ , to identify the locally optimal mapper. The locally optimal mapper is then selected as the output of the GA. The use of the selection function to select the locally optimal mapper from within the converged population is the key difference between the modified GA utilised in this paper and its previous variant [38].

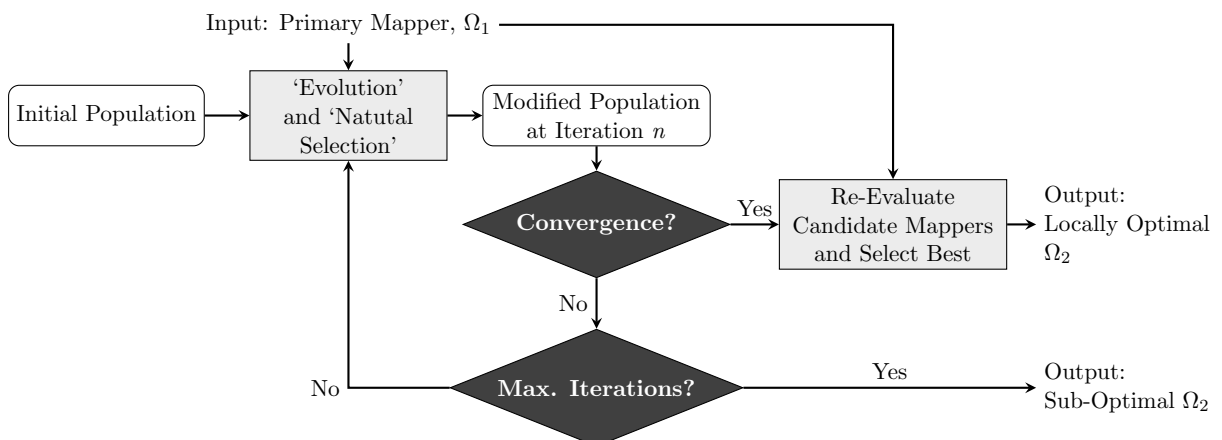


FIGURE 4.2: High-Level Illustration of Genetic Algorithm

To ensure that the GA is not computationally intractable, an upper bound on the number of iterations that may be performed is set. This is denoted  $N_{\max}$ . Patel *et al.* [38] discuss that selecting  $N_{\max} \ll M^5$  ensures that the GA is less computationally expensive than the branch-and-bound QAP-solver used by Samra *et al* [54]. If the GA reaches the maximum number of iterations without converging, then the candidate secondary mapper corresponding to the fittest chromosome (as determined by the fitness function) in the population is selected as the output of the GA. In this case, the output is classified as sub-optimal.

In the rest of this subsection, a more detailed discussion on each stage of the genetic algorithm is provided.

#### 4.5.1.1 Genes, Chromosomes and the Population

##### Genetic Coding

‘Genetic coding’ is the technical term used to describe the representation of each candidate mapper as a chromosome. Each chromosome consists of  $M$  genes,  $x_i, i \in [1 : M]$ , each of which correspond to a symbol from the  $M$ -ary constellation. The value contained within each gene of the chromosome is label associated with that constellation point. Thus, the chromosome  $\mathcal{X}$  is defined by:

$$\mathcal{X} = \begin{bmatrix} x_1 & x_2 & \cdots & x_{M-1} & x_M \end{bmatrix}. \quad (4.35)$$

##### Generating the Initial Population of Chromosomes

The population of chromosomes refers to the set of candidate secondary mappers evaluated by the genetic algorithm at each iteration. Hence, the population during the  $n$ -th iteration,  $\{\mathcal{X}\}^{(n)}$ , is defined as:

$$\{\mathcal{X}\}^{(n)} = \left\{ \mathcal{X}_{1,n} \quad \mathcal{X}_{2,n} \quad \cdots \quad \mathcal{X}_{S-1,n} \quad \mathcal{X}_{S,n} \right\}, \quad (4.36)$$

where  $S$  is the number of chromosomes in the population. As suggested by Patel *et al.* [38], the initial population  $\{\mathcal{X}\}^{(0)}$  should contain any candidate mappers obtained via geometric heuristic designs, if they are available. Thereafter, random chromosomes from the  $M!$  candidate mapper space are added to  $\{\mathcal{X}\}^{(0)}$  until there are  $S$  chromosomes in the population.

#### 4.5.1.2 Imitating ‘Evolution’

##### ‘Mating’ Parent Chromosomes

As mentioned previously, parent chromosomes from the population are ‘mated’ and used to produce ‘child’ chromosomes at each iteration of the GA. The mating of parent chromosomes involves two processes, referred to as ‘crossover’ and ‘mutation’. The crossover process is the most important step of the algorithm [58]. The design of the crossover ensures that desirable properties from the parent chromosomes are passed on to the child chromosomes. The mutation process is a random

event that occurs when a child chromosome undergoes a further change after crossover. The random nature of mutations means that not all child chromosomes undergo this process. Together, crossover and mutation model the biological process of evolution to generate a progressively more optimal population at each iteration of the GA. Hence, the population  $\{\mathcal{X}\}^{(n)}$  is more optimal than  $\{\mathcal{X}\}^{(n-1)}$ ,  $n \in [1 : N_{\max}]$ .

### Crossover

To design labelling diversity mappers, Patel *et al.* [38] developed a new crossover technique called the  $\mathcal{K}$ -point hypersphere swap crossover ( $\mathcal{K}$ -HSX). In summary,  $\mathcal{K}$ -HSX swaps  $\mathcal{K}$  genes in each of the parent chromosomes to produce child chromosomes. The genes to be swapped are chosen such that they fall outside a hypersphere with the 4-dimensional hyperspace defined by the constellation representation of the two parent chromosomes. This ensures that the genes will have different neighbours in the hyperspace after swapping. In other words, the distances between the genes that were swapped and their hyperspace neighbours are greater in the child chromosomes than in the parent chromosomes. The reader is referred to Section III-B2 of the original work [38] for full details of the  $\mathcal{K}$ -HSX, including a procedural example of the swapping process.

All  $\binom{S}{2}$  combinations of parent chromosomes from the population are crossed over, each producing a pair of child chromosomes. Thus, the total size of the population in the  $n$ -th iteration after all crossovers are performed, denoted  $|\{\mathcal{X}\}^{(n)}|$ , is given by:

$$\begin{aligned} |\{\mathcal{X}\}^{(n)}| &= S + 2 \times \binom{S}{2} \\ &= S + \frac{S!}{(S-2)!} \\ &= S^2 \end{aligned} \tag{4.37}$$

### Mutation

As previously mentioned, mutation is a random event that occurs when a child chromosome undergoes further changes after crossover. The probability of a mutation occurring for a given child chromosome is denoted  $\mathcal{P}_m$ . If a mutation occurs, two genes are randomly selected from the child chromosome and swapped. Patel *et al.* [38] highlight that, unlike crossover, no properties from the parent chromosomes are used to inform this swap.

#### 4.5.1.3 Evaluating Candidate Secondary Mappers

As mentioned earlier in this section, the genetic algorithm developed for designing labelling diversity mappers evaluates chromosomes within the candidate mapper population at two points: i) when imitating ‘natural selection’ and ii) when selecting the locally optimal candidate mapper from the converged population. During ‘natural selection’, all chromosomes are evaluated using the fitness function. If the population converges, all chromosomes have the same fitness. Thus, further iterations of the mating process are unlikely to improve the fitness of chromosomes within the population, and

the GA terminates its iterative search. To select the best chromosome from within this converged population, a different metric is required. This metric is computed using the selection function.

The remainder of this subsection focusses on developing the mathematical framework for evaluating candidate secondary mappers, based on recent literature on labelling diversity mapper design [29]. Thereafter, the application of this framework to design the fitness and selection functions in the GA are discussed.

### Mathematical Framework

The genetic algorithm requires an analytical means to compare candidate secondary mappers, and thereby predict the extent to which each mapper achieves labelling diversity. As shown in previous literature [28, 29, 38], the mathematical framework for comparing candidate secondary mappers is developed by taking a high-SNR approximation of the ABEP. Using (4.19), it is observed that as  $\gamma \rightarrow \infty$ , the third term of the MGF dominates. Thus, (4.14) at high-SNR may be approximated as:

$$\begin{aligned} \mathcal{P}(\ell_1 \rightarrow l_1) &\approx \frac{1}{4r} \prod_{k=1}^2 \left( \frac{q\gamma}{4(1+q^2)} \left| \varepsilon_k^{(\ell_1, l_1)} \right|^2 \right)^{-2N_{\text{Rx}}} + \frac{1}{2r} \prod_{k=1}^2 \sum_{R=1}^{r-1} \left( \frac{q\gamma \left| \varepsilon_k^{(\ell_1, l_1)} \right|^2}{4(1+q^2) \sin^2 \left( \frac{R\pi}{2r} \right)} \right)^{-2N_{\text{Rx}}} \\ &\approx \frac{1}{4r} \left[ \left( \frac{q\gamma}{4(1+q^2)} \right)^2 \left| \varepsilon_1^{(\ell_1, l_1)} \right|^2 \left| \varepsilon_2^{(\ell_1, l_1)} \right|^2 \right]^{-2N_{\text{Rx}}} \\ &\quad + \frac{1}{2r} \sum_{R=1}^{r-1} \left[ \left( \frac{q\gamma}{4(1+q^2) \sin^2 \left( \frac{R\pi}{2r} \right)} \right)^2 \left| \varepsilon_1^{(\ell_1, l_1)} \right|^2 \left| \varepsilon_2^{(\ell_1, l_1)} \right|^2 \right]^{-2N_{\text{Rx}}}. \end{aligned} \quad (4.38)$$

The expression in (4.38) indicates that lower values of the product distance  $\left| \varepsilon_1^{(\ell_1, l_1)} \right| \left| \varepsilon_2^{(\ell_1, l_1)} \right|$  result in better error performance. Using this reasoning and substituting (4.38) into (4.8), it is evident that the error floor of the ABEP is set by the minimum product distance. Thus, the objective of secondary mapper design can be formulated as the optimisation problem given by [28, 29]:

$$\Omega_2^{\text{optimal}} = \arg \max_{\substack{\ell_1, l_1 \in [0:M-1] \\ \ell_1 \neq l_1}} \aleph(\ell_1, l_1), \quad (4.39)$$

where  $\aleph$  is the mapper design metric.

Based on the work by Quazi and Patel [29], the expression in (4.38) gives rise to 4 metrics that may be used for comparing labelling diversity mappers: the minimum product distance ( $\aleph_1$ ), the minimum summed product distance ( $\aleph_2$ ), the minimum bit-difference-weighted product distance ( $\aleph_3$ ) and the minimum summed bit-difference-weighted product distance ( $\aleph_4$ ). These metrics are

defined mathematically as:

$$\aleph_1 = \min_{\substack{\ell_1, l_1 \in [0:M-1] \\ \ell_1 \neq l_1}} \left| \varepsilon_1^{(\ell_1, l_1)} \right| \left| \varepsilon_2^{(\ell_1, l_1)} \right|. \quad (4.40)$$

$$\aleph_2 = \min_{\ell_1 \in [0:M-1]} \sum_{l_1=0}^{M-1} \left| \varepsilon_1^{(\ell_1, l_1)} \right| \left| \varepsilon_2^{(\ell_1, l_1)} \right|. \quad (4.41)$$

$$\aleph_3 = \min_{\substack{\ell_1, l_1 \in [0:M-1] \\ \ell_1 \neq l_1}} \frac{1}{\Delta(\ell_1, l_1)} \left| \varepsilon_1^{(\ell_1, l_1)} \right| \left| \varepsilon_2^{(\ell_1, l_1)} \right|. \quad (4.42)$$

$$\aleph_4 = \min_{\ell_1 \in [0:M-1]} \sum_{l_1=0}^{M-1} \frac{1}{\Delta(\ell_1, l_1)} \left| \varepsilon_1^{(\ell_1, l_1)} \right| \left| \varepsilon_2^{(\ell_1, l_1)} \right|. \quad (4.43)$$

The discussion presented by Quazi and Patel [29] shows that the most feasible approach to evaluating candidate secondary mappers is to use a 2-stage approach, considering  $\aleph_1$  and  $\aleph_2$ . In the first stage, candidate secondary mappers are evaluated using  $\aleph_1$ . A larger value of  $\aleph_1$  indicates a more-optimal mapper. It is possible that when evaluating the candidate secondary mappers, multiple candidates may have the same value of  $\aleph_1$  [29]. In this scenario, a second stage is needed to further distinguish these candidate mappers, and do this,  $\aleph_2$  is used. Once again, larger values of  $\aleph_2$  indicate more-optimal mappers in this case.

### Application of Mathematical Framework

As the genetic algorithm evaluates the population of candidate secondary mappers at two points, the 2-stage approach to mapper evaluation is straightforward to apply. When performing ‘natural selection’, the fitness function assigns a value for  $\aleph_1$  to each candidate secondary mapper. This value is used to evaluate the candidate mappers. Thus, if the population converges, all chromosomes have the same value of  $\aleph_1$  and should be re-evaluated to determine  $\aleph_2$ .  $\aleph_2$  is then used to select the locally optimum candidate mapper.

### Further Details on Imitating ‘Natural Selection’

The biological process of ‘natural selection’ is modelled by pruning the population of candidate secondary mappers at the end of each iteration. This is accomplished by determining the fitness of each chromosome, and discarding the least-fit chromosomes from the population. As discussed in Section 4.5.1.2, the mating processes of crossover and mutation result in  $2\binom{S}{2}$  child chromosomes being added to the population. To ensure that the population size at the start of each iteration remains fixed at  $S$ , the  $2\binom{S}{2}$  least-fit candidates are discarded from the population at the end of each iteration. This pruning process has 2 key benefits for the GA:

1. The number of crossovers performed at the next iteration remains constant. Since all possible pairs of parents are crossed over at each iteration, a growth in the population would result in the number of crossovers performed exponentially increasing. This would severely impact the runtime and computational tractability of the genetic algorithm.

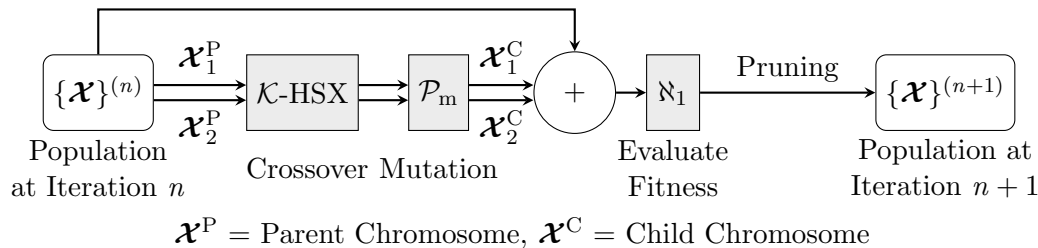


FIGURE 4.3: Simplified Illustration of “Evolution and Natural Selection” during each Iteration of the Genetic Algorithm

2. By discarding the least-fit chromosomes, at the next iteration, there are fitter parent chromosomes to be crossed over. Since child chromosomes inherit desirable properties from their parents, this ensures that the population gets progressively fitter at each iteration.

As mentioned previously, the fitness of chromosomes is determined by (4.40) when pruning the population. Thus, after modelling ‘natural selection’, the  $S$  chromosomes with the highest fitness form the modified population for the next iteration of the GA. For clarity, Figure 4.3 illustrates the processes of crossover, mutation and pruning when modifying the population at each iteration of the GA. For simplicity, the illustration shows the mating of only one pair of parent chromosomes ( $\mathbf{x}_1^P$  and  $\mathbf{x}_2^P$ ), which produces only one pair of child chromosomes ( $\mathbf{x}_1^C$  and  $\mathbf{x}_2^C$ ). The reader is reminded that, in the actual implementation of the GA, all  $\binom{S}{2}$  possible pairs of parent chromosomes are mated.

### Convergence and Termination

As shown in Figure 4.2, there are 2 conditions under which the GA terminates. The first condition occurs when all chromosomes within the population converge to the same fitness score, which indicates that there exists a locally optimal candidate secondary mapper within the population. If this occurs, the selection function is used to compute  $\aleph_2$  (which was defined in (4.41)). The output of the GA is then the chromosome from the converged population with the highest value of  $\aleph_2$ .

The second termination condition which may occur is that the GA reaches the maximum number of permitted iterations,  $N_{\max}$ . As suggested by Patel *et al.* [38], to ensure that it is computationally tractable, this parameter is chosen such that  $N_{\max} \ll M^5$ . If the maximum number of iterations is reached, it is assumed that the genetic algorithm will not converge. In this case, the fittest chromosome from the population, in terms of  $\aleph_1$ , is selected as the output.

### 4.5.2 Designed Mappers for STPLD System

The genetic algorithm for labelling diversity mapper design described in Section 4.5.1 was implemented to produce secondary mappers for the APSK constellations considered in this paper (detailed in Table 4.2, Section 4.3). These are shown in Figures 4.4 to 4.7, and the GA parameters used to design each mapper are detailed in Table 4.3. For readability, Figures 4.4 to 4.7 indicate binary labels

TABLE 4.3: Details of Parameters used in implementing Genetic Algorithm

$M$	$S$	$\mathcal{P}_m$	$N_{\max}$	$\mathcal{K}$	Hypersphere radius for $\mathcal{K}$ -HSX	Convergence Reached
8	7	3%	200	3	1	Yes
16	16	8%	$10^4$	3	1	Yes
32	12	12%	$10^5$	8	5	No
64	10	15%	$10^7$	9	7	Yes

$M$  = Modulation Order,  $S$  = Population Size,  $\mathcal{P}_m$  = Mutation Probability,  $N_{\max}$  = Max. Iterations,  $\mathcal{K}$  = Number of Crossovers,  $\mathcal{K}$ -HSX =  $\mathcal{K}$ -point Hypersphere Swap Crossover [38]

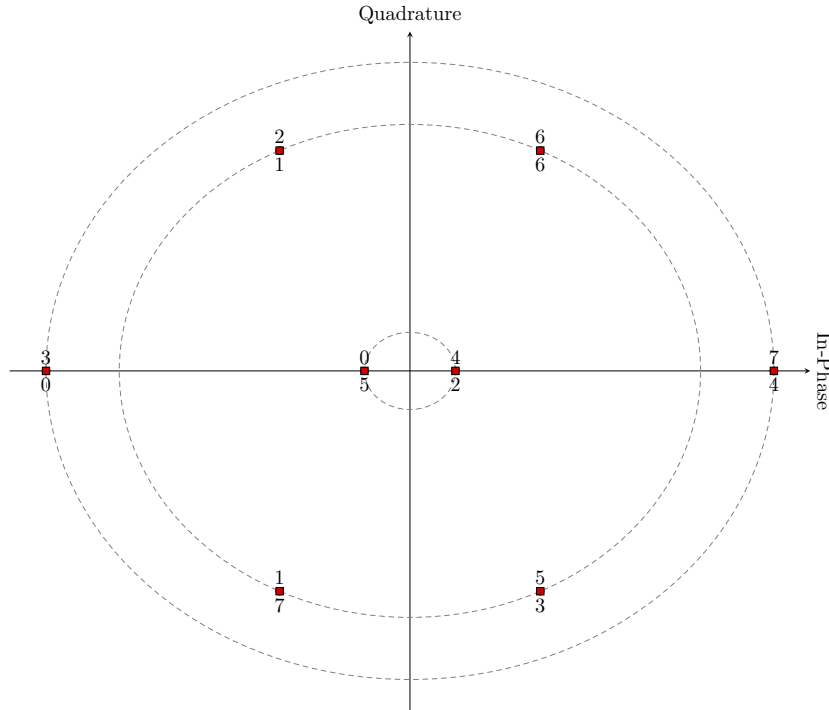


FIGURE 4.4: 8APSK Constellation Mappings

by their decimal equivalent values. The value located below each constellation point indicates label obtained by using mapper  $\Omega_1$ . Similarly, the value located above each constellation point indicates the label obtained by using mapper  $\Omega_2$ , which was produced by the GA.

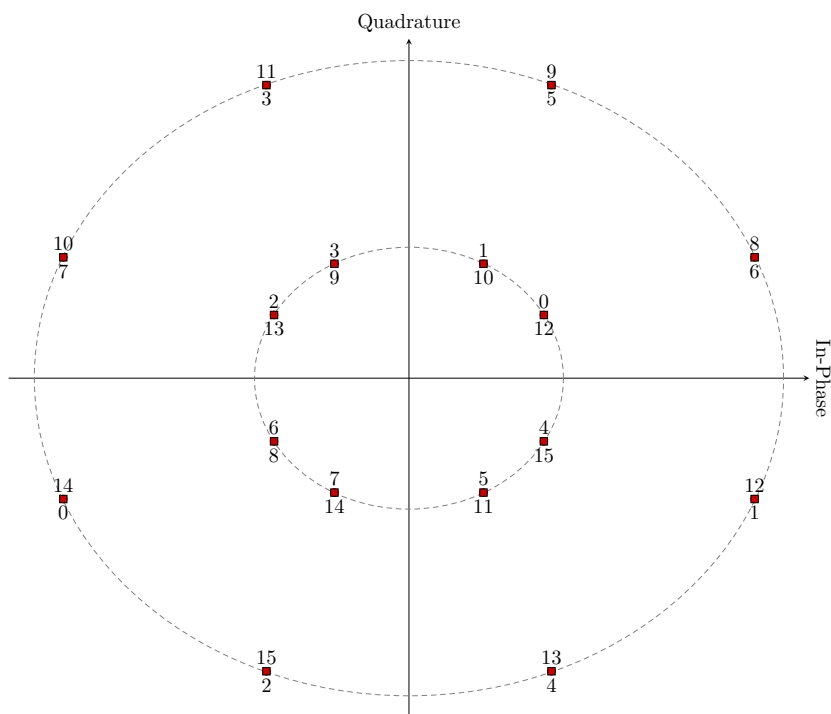


FIGURE 4.5: 16APSK Constellation Mappings

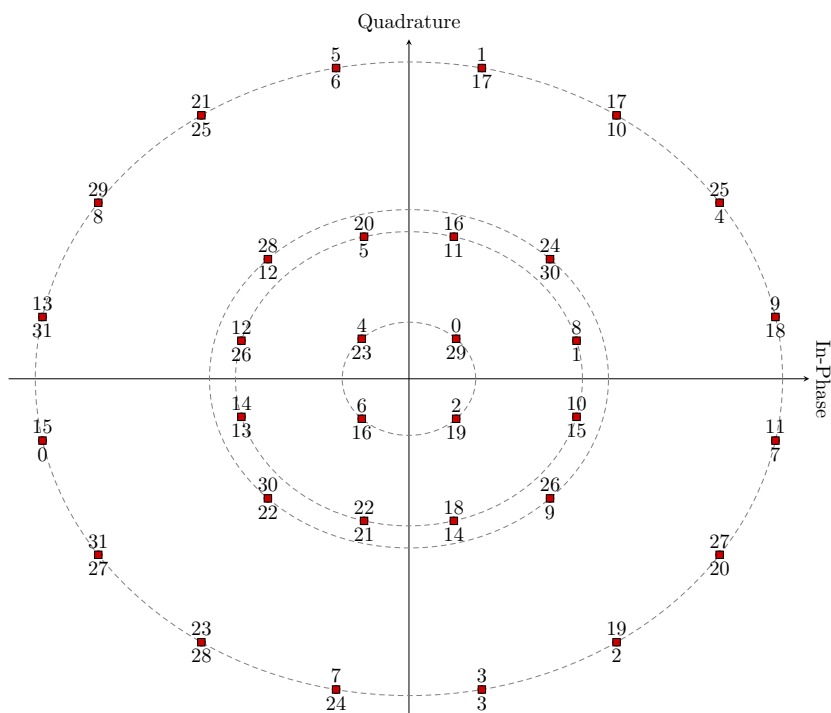


FIGURE 4.6: 32APSK Constellation Mappings

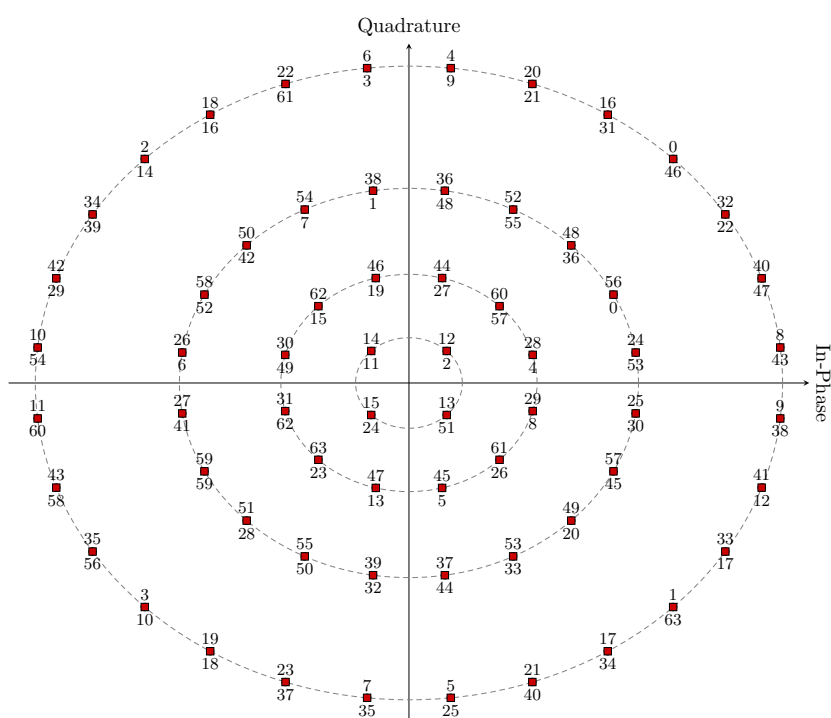


FIGURE 4.7: 64APSK Constellation Mappings

## 4.6 Results and Discussion

### 4.6.1 Error Performance of Proposed System

The first study of the proposed STPLD system compares its error performance to other recent MIMO satellite broadcasting techniques based on terrestrial designs. To ensure a fair comparison, the study is constrained to uncoded systems. Each set of curves shows both the theoretical BER performance of all systems considered, as well as results obtained through the use of Monte Carlo simulations. All systems are assumed to be uncorrelated and subjected to fast-fading. The systems considered are:

1. The orthogonal space-time block code (OSTBC) proposed by Alamouti [25] for terrestrial systems. This was extended to the satellite broadcasting context by Arti *et al.* [26] and Arapoglou *et al.* [17].
2. The orthogonal space-time-polarisation block code (OSTPBC) proposed by Wysocki and Wysocki [27] for terrestrial systems. This was extended to the satellite broadcasting context by Vineetha *et al.* [30] and Aparna *et al.* [31].
3. The USTLD system proposed by Xu *et al.* [28] for terrestrial systems. This was extended to the satellite broadcasting context by Quazi and Patel [29].

To achieve labelling diversity, both the STPLD and USTLD systems utilise the APSK constellation mappings illustrated in Figures 4.4 to 4.7.

The results of the BER performance study are shown in Figures 4.8 to 4.10. The theoretical BER performance curves presented for the OSTBC and USTLD systems are based on analytical expressions which can be found in literature [25, 28, 36]. For the STPLD system, theoretical results are obtained from (4.22). A theoretical expression for the BER performance of the OSTPBC is not explicitly shown in literature [27, 30, 31], however one can be obtained from (4.22) by exploiting the similarity in the structure of the STPLD and OSTPBC systems. This is accomplished by setting  $\Omega_2 = \Omega_1$  in (4.22). Since (4.22) was derived using the union bound, it presents an upper-bound approximation for the BER of the STPLD system. The overlapping of the theoretical and simulated curves for both the STPLD and OSTPBC systems in the high-SNR region indicate that the analytical expression is valid.

As both the USTLD [28] and OSTPBC [27] systems were developed as improvements to the OSTBC [25] system, it is expected that they exhibit better error performance. This is confirmed by the results in Figures 4.8 to 4.10. Quantitatively, at a BER of  $10^{-6}$ , the USTLD scheme improves upon the OSTBC scheme by  $\approx 7$ dB for the  $2 \times 2$  16APSK system, and by  $\approx 5$ dB for both the  $2 \times 4$  32APSK and  $2 \times 2$  64APSK systems. This confirms that the secondary mappers produced by the genetic algorithm in Section 4.5 achieve a significant level of labelling diversity.

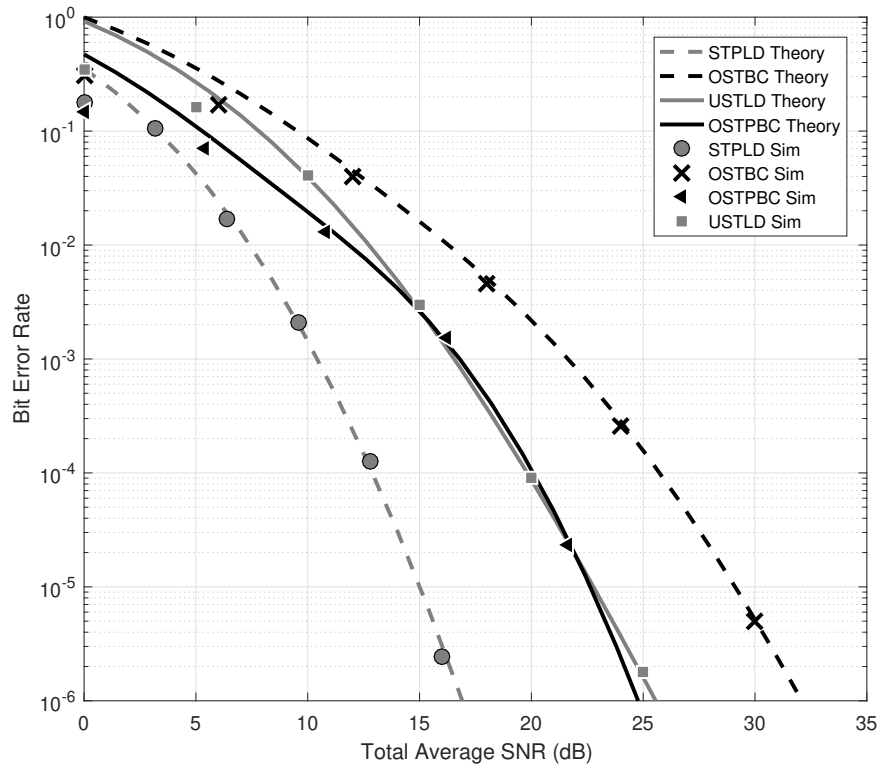


FIGURE 4.8: BER Performance of  $2 \times 2$  16APSK OSTBC, OSTPBC, USTLD and STPLD Systems,  $q = 0.3$

For the 16APSK and 32APSK systems, the OSTPBC scheme shows a marginal improvement of  $<1\text{dB}$  when compared to the USTLD scheme. However, for the 64APSK system, the OSTPBC scheme improves upon the USTLD scheme by  $\approx 2\text{dB}$ . The reason for the OSTPBC scheme outperforming the USTLD scheme is attributed to its diversity. Qualitatively, diversity is indicated by the slope of the BER curves in the high-SNR region. For all three systems presented in Figures 4.8 to 4.10, the OSTPBC has a steeper gradient in the high-SNR region, and hence it achieves more diversity. To quantify this observation, the diversity order (defined in (4.44)) is used [59]. It can be shown that  $\Gamma_{\text{OSTPBC}} = 4N_{\text{Rx}}$ , whereas  $\Gamma_{\text{USTLD}} = \Gamma_{\text{OSTBC}} = 2N_{\text{Rx}}$ .

$$\Gamma = - \lim_{\gamma \rightarrow \infty} \frac{\log \mathcal{P}_e(\gamma)}{\log \gamma} \quad (4.44)$$

The proposed STPLD scheme incorporates the benefits of both labelling and polarisation diversity, and exhibits the best error performance in all systems considered. Using (4.44), it can be shown that the diversity order of the STPLD system is the same as that of the OSTPBC (i.e.  $\Gamma_{\text{STPLD}} = \Gamma_{\text{OSTPBC}} = 4N_{\text{Rx}}$ ). It is also observed that the relative improvement of the STPLD scheme over the OSTPBC scheme is the same as the relative improvement of the USTLD system over the OSTBC scheme at a BER of  $10^{-6}$ .

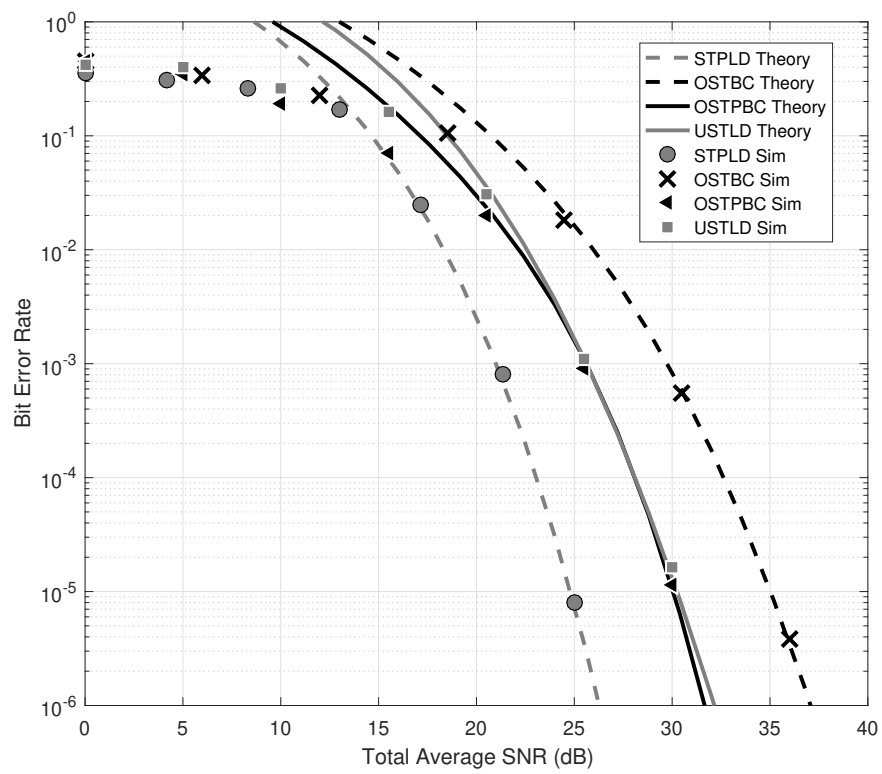


FIGURE 4.9: BER Performance of  $2 \times 4$  32APSK OSTBC, OSTPBC, USTLD and STPLD Systems,  $q = 0.3$

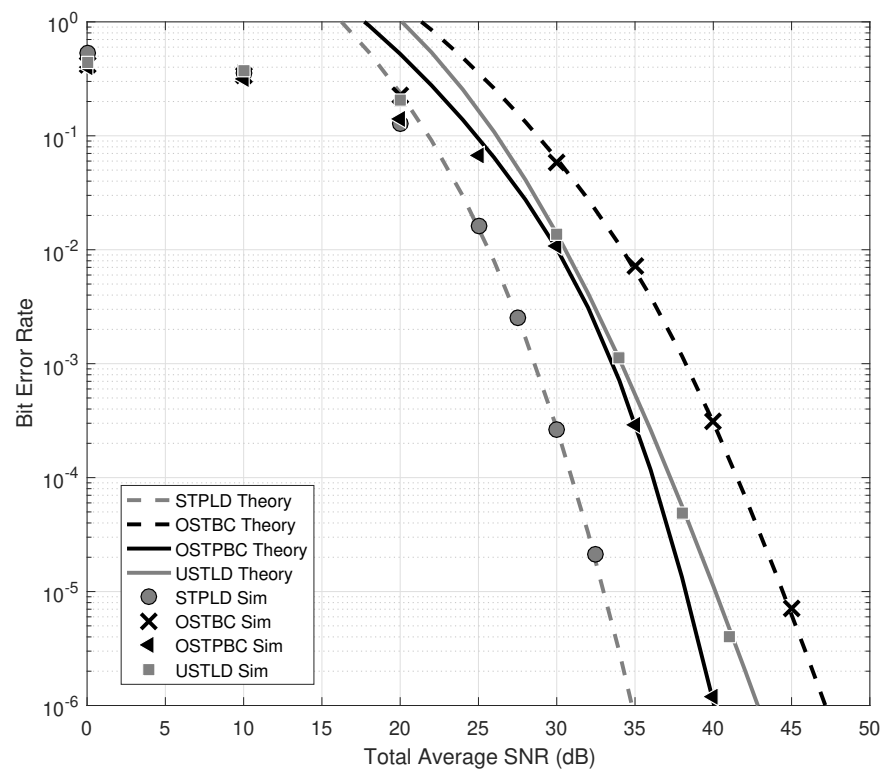


FIGURE 4.10: BER Performance of  $2 \times 2$  64APSK OSTBC, OSTPBC, USTLD and STPLD Systems,  $q = 0.7$

### 4.6.2 Correlation Study

Figures 4.11 and 4.12 show that the analytical bound for the STPLD system, presented in (4.34), converges to results obtained by Monte Carlo simulations. Results are presented for a  $2 \times 3$  8APSK system assuming the correlation models discussed in Section 4.3.4. The IAI and IBI correlation coefficients at both the transmit-side and receive-side were assumed equal, such that  $\rho_{\text{Tx}}^{\text{IAI}} = \rho_{\text{Rx}}^{\text{IAI}} = \rho_{\text{Tx}}^{\text{IBI}} = \rho_{\text{Rx}}^{\text{IBI}} = 0.6$ .

Qualitative inspection of the results in Figure 4.11 shows that the STPLD system configuration with only transmit-side correlation (Tx corr) performs worse than the system subjected to only receive-side correlation (Rx corr). Thus, it is deduced that STPLD systems are more sensitive to correlation at the transmitter than at the receiver. This is in agreement with the findings of other studies on labelling diversity systems, and has been previously explained mathematically by Patel *et al* [36].

Figure 4.12 shows that the analytical model for the correlated STPLD system is valid for systems subject to IAI, IBI and both IAI and IBI. The next study further investigates IAI and IBI to determine which causes a greater degradation in error performance. The analytical results of this study are presented in Figures 4.13 to 4.15. The shading of the surfaces in these Figures corresponds to the BER of the curve.

Figure 4.13 shows the effect of transmit-side IAI and IBI on an STPLD system, assuming no receive-side correlation. The symmetry of the surface plot indicates that error performance of the system

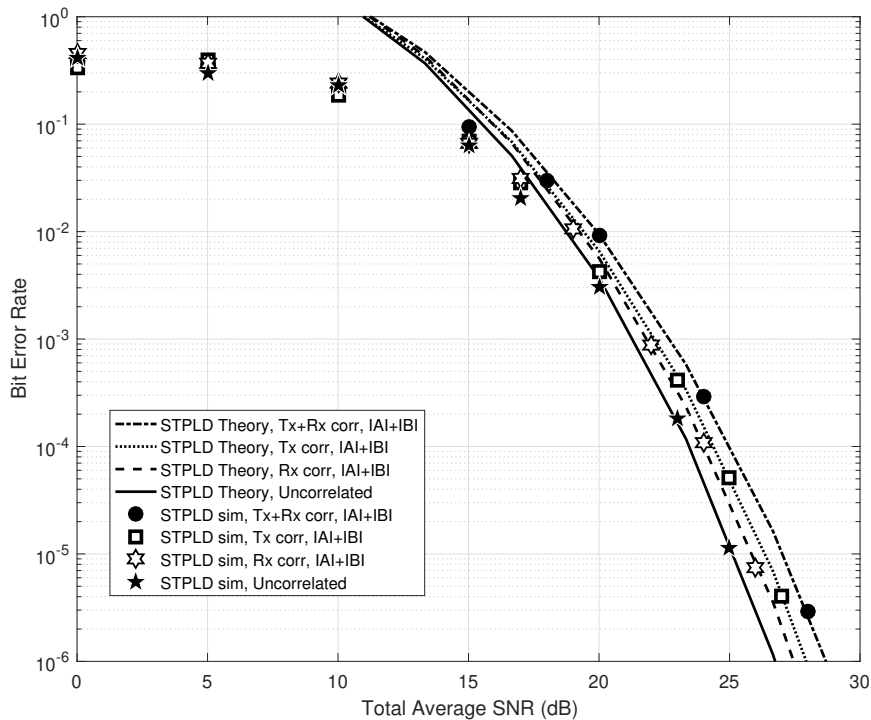


FIGURE 4.11: Validation of (4.34) for  $2 \times 3$  8APSK STPLD Systems with Transmit-Side and Receive-Side Correlation,  $q = 0.5$

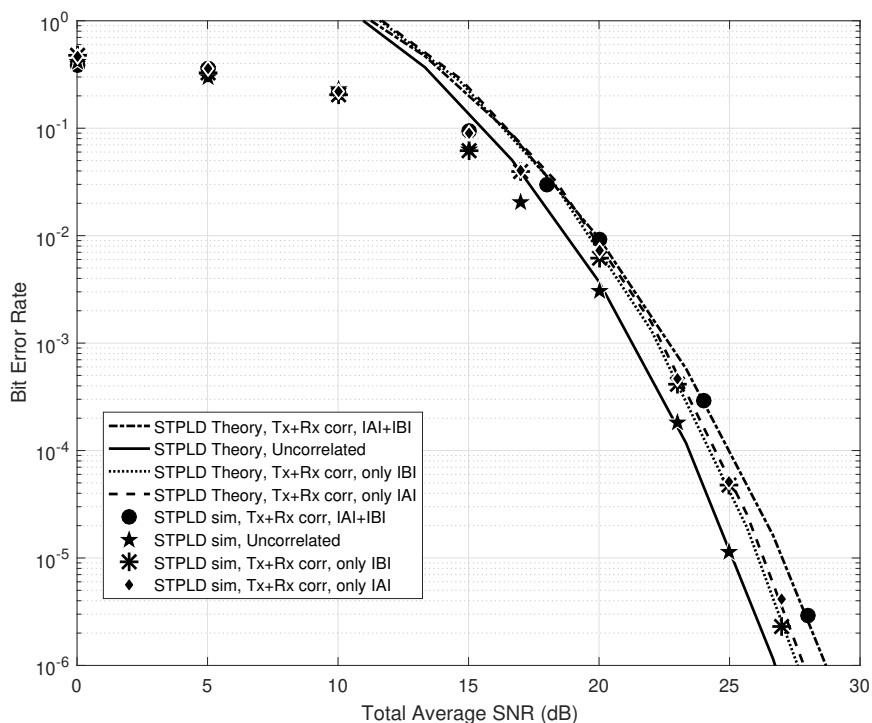


FIGURE 4.12: Validation of (4.34) for  $2 \times 3$  8APSK STPLD Systems with Inter-Antenna and Inter-Beam Interference,  $q = 0.5$

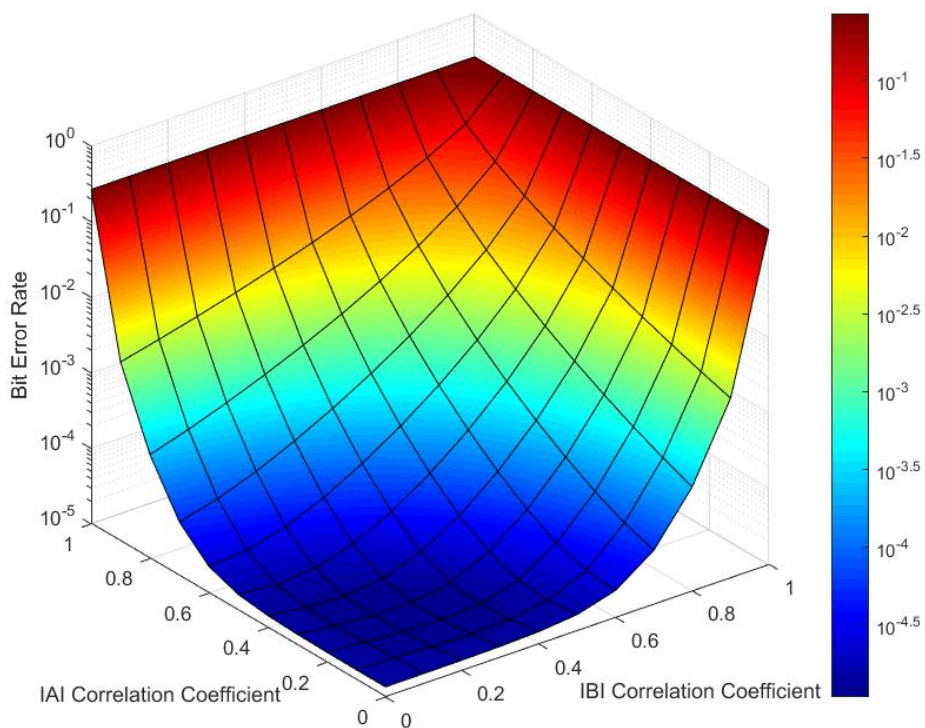


FIGURE 4.13: Effect of Transmit-Side IAI and IBI on  $2 \times 3$  8APSK,  $q = 0.5$ ,  $\gamma = 25$ dB

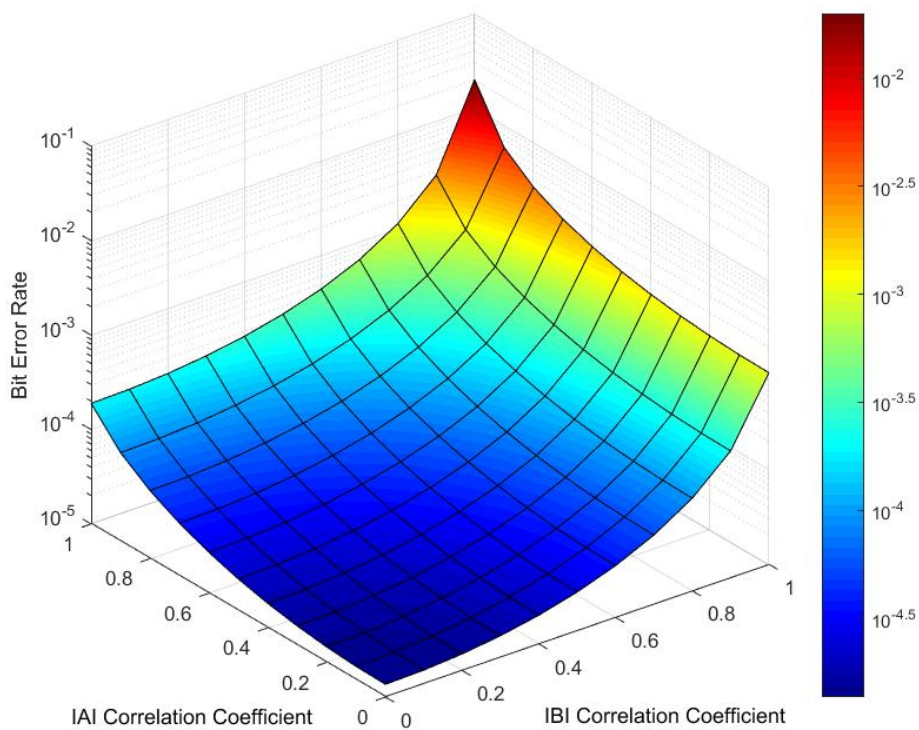


FIGURE 4.14: Effect of Receive-Side IAI and IBI on  $2 \times 3$  8APSK,  $q = 0.5$ ,  $\gamma = 25\text{dB}$

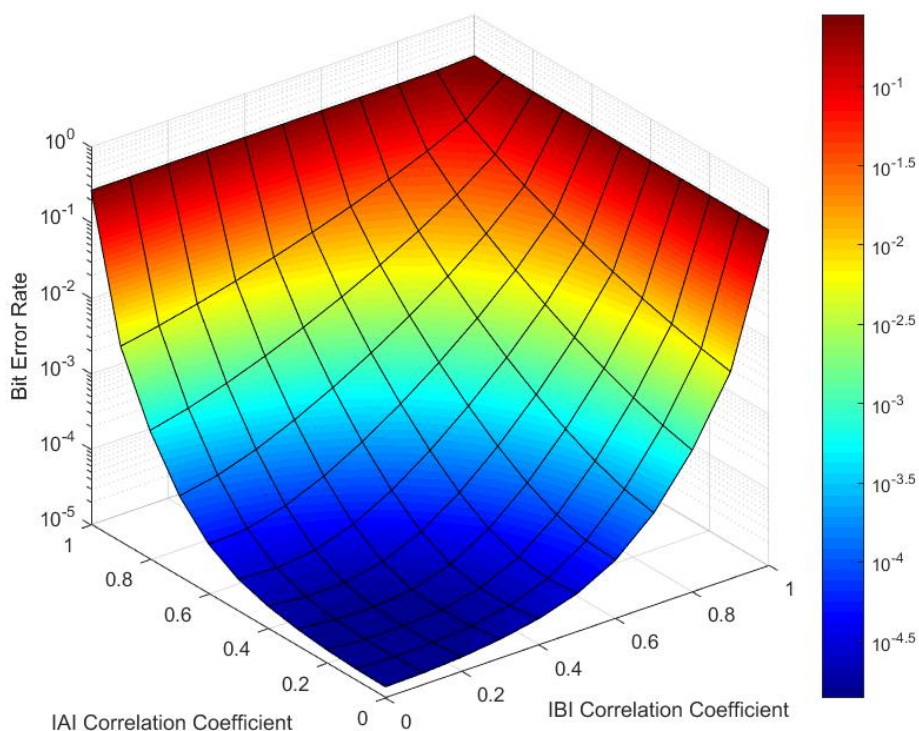


FIGURE 4.15: Effect of Transmit-Side and Receive-Side IAI and IBI on  $2 \times 3$  8APSK,  $q = 0.5$ ,  $\gamma = 25\text{dB}$

is equally susceptible to both IAI and IBI. It is also observed that at low correlation coefficients, the BER performance does not noticeably degrade, as shown by the flat region of the surface with dark blue shading. However, once the correlation coefficients fall outside the bounds of this region, the BER performance rapidly degrades. The worst-case performance of the STPLD system with transmit-side correlation is 4 orders of magnitude worse than the uncorrelated STPLD system. Figure 4.14 presents a similar set of results for receive-side correlation. By observing the contours on the surface, it is evident that as the BER performance of the system degrades more rapidly as the IBI correlation coefficient increases than as the IAI correlation coefficient increases (i.e.  $\frac{\partial \mathcal{P}_e}{\partial \rho^{\text{IAI}}} < \frac{\partial \mathcal{P}_e}{\partial \rho^{\text{IBI}}}$ ). This indicates that the STPLD system is more sensitive to IBI than IAI at the receiver.

Finally, Figure 4.15 shows the effect of IAI and IBI in an STPLD system with both transmit-side and receive-side correlation. For simplicity, it is assumed that  $\rho_{\text{Tx}}^{\text{IAI}} = \rho_{\text{Rx}}^{\text{IAI}} = \rho^{\text{IAI}}$  and  $\rho_{\text{Tx}}^{\text{IBI}} = \rho_{\text{Rx}}^{\text{IBI}} = \rho^{\text{IBI}}$ . The resulting surface plot closely resembles that shown in Figure 4.13. Comparing Figures 4.13 and 4.15, it is observed that the contours along the surface of Figure 4.15 are steeper than in Figure 4.13. This observation reaffirms that transmit-side correlation has a more dominant impact on error performance than receive-side correlation. It is also noted that the flat, dark blue-shaded region in Figure 4.15 extends until  $\rho^{\text{IBI}} \approx 0.4$  when  $\rho^{\text{IAI}} = 0$  and until  $\rho^{\text{IAI}} \approx 0.45$  when  $\rho^{\text{IBI}} = 0$ . Thus, the surface plot presented in Figure 4.15 is slightly asymmetric. This indicates that when there is correlation at both the transmit-side and receive-side, the STPLD system is marginally more susceptible to IBI than IAI. This is expected, given the trends observed for only receive-side correlation discussed previously.

## 4.7 Conclusion

This paper proposes a MIMO satellite broadcasting system that achieves space, time, polarisation and labelling diversity. The proposed STPLD system is modelled under both ideal (uncorrelated) and practical (correlated) conditions, assuming a Nakagami- $q$  fading model. The correlation model provided allows inter-antenna and inter-beam interference to be considered at both the transmitting satellite and the receiving base station. Analytical expressions for both correlated and uncorrelated STPLD systems are derived and corroborated by Monte Carlo simulations.

To design secondary mappers that achieve labelling diversity for the STPLD system, a novel GA is presented. This GA has been designed such that it can be applied to any generic constellation, and in this paper, it is applied to 8APSK, 16APSK, 32APSK and 64APSK constellations from the DVB-S2X satellite broadcasting standard.

Two studies of the STPLD system are presented. In the first study, it is found that STPLD systems achieve a diversity order of  $\Gamma_{\text{STPLD}} = 4N_{\text{RX}}$ . Additionally, the results presented indicate the STPLD system improves performance by  $\approx 7\text{dB}$  for the  $2 \times 2$  16APSK system configuration, and by  $\approx 5\text{dB}$  for both the  $2 \times 4$  32APSK and  $2 \times 2$  64APSK system configurations studied, when compared to the best comparable scheme for MIMO satellite broadcasting (the OSTPBC). The second study of the STPLD system analyses the effects of correlation on BER performance. It is found that STPLD systems are most sensitive to correlation at the transmitting satellite. It is also observed that at the receiving base station, IBI has a more dominant effect on system performance than IAI. These trends were observed when considering a  $2 \times 3$  8APSK STPLD system configuration.

Future works may consider improving the spectral efficiency of the STPLD system, as the large distances between base stations and satellites result in high system latency when transmitting the same information over multiple time slots. It is noted that this problem is common to the OSTBC, OSTPBC and USTLD systems that have previously been adapted for satellite broadcasting. Other relevant topics of interest include studying STPLD systems in other channel models that are relevant to satellite broadcasting, as well as considering the application of STPLD to terrestrial systems.

## References

- [1] The International Telecommunications Union. *ICT Facts and Figures 2017*. [Online Report] 2017. <https://www.itu.int/en/ITU-D/Statistics/Documents/facts/ICTFactsFigures2017.pdf>. Accessed August 4, 2018.
- [2] The Internet Society. *2017 Internet Society Global Internet Report; Paths to our Digital Future*. [Online Report] 2017. <https://future.internetsociety.org/wp-content/uploads/2017/09/2017-Internet-Society-Global-Internet-Report-Paths-to-Our-Digital-Future.pdf>. Accessed August 3, 2018.
- [3] The United Nations General Assembly. *Transforming our world: the 2030 Agenda for Sustainable Development*. [Online Report] A/RES/70/1; 2015. [http://www.un.org/ga/search/view\\_doc.asp?symbol=A/RES/70/1&Lang=E](http://www.un.org/ga/search/view_doc.asp?symbol=A/RES/70/1&Lang=E). Accessed August 5, 2018.
- [4] Cabral A, Moodley L, Yeboah-Amankwah S. *Digital Divide: The impact of closing Africa's Internet gap*. [Online Report] McKinsey & Company; 2018. <https://www.mckinsey.com/business-functions/marketing-and-sales/our-insights/digital-divide-the-impact-of-closing-africas-internet-gap>. Accessed August 5, 2018.
- [5] Nishijima M, Ivanauskas TM, Sarti FM. Evolution and determinants of digital divide in Brazil (2005-2013). *Telecommunications Policy*. 2017; 41: 12–24.
- [6] Scheerder A, van Deursen A, van Dijk J. Determinants of Internet skills, uses and outcomes. A systematic review of the second- and third-level digital divide. *Telematics and Informatics*. 2017; 34: 1607–1624.
- [7] Conte R. Satellite rural communications: telephony and narrowband networks. *Int. J. Satellite Communic. and Networking*. 2005; 23(5): 307–321.
- [8] Iqbal MK, Iqbal MB, Shamoan S, Bhatti M. Future of satellite broadband Internet services and comparison with terrestrial access methods e.g. DSL and cable modem. In: 3rd IEEE Int. Conf. on Computer, Control and Communic., Karachi (Pakistan); 2013: 1–5.
- [9] Yesufu, AK. Possible use of satellites in rural telecommunications in Africa. In: 2nd Int. Conf. on Rural Telecomm., London (England); 1990: 156–159.
- [10] Tomassini D, Ginati A, Feliciani F, Deconick F, Gaudiano V, Cuccarese F, Recchia F, Bove A, Cabanas F, Mathee B, Halloway L, Richardson P, Francis I. Space4edu: Satellite technology for smart rural schools in South Africa. In: 64th Int. Astronautical Congress, Beijing (China); 2013: 4472–4479.
- [11] Olla P. Exploiting satellite radio technology to create an African satellite health education infrastructure. In: 57th Int. Astronautical Congress, Valencia (Spain); 2006: 8955–8961.

- [12] Martín-de-Mercado G, Horsch A, Parentela G, Mancini P, Ginati A. Satellite-enhanced telemedicine and eHealth for sub-saharan Africa: A development opportunity. In: 62nd Int. Astronautical Congress, Cape Town (South Africa); 2011: 4320–4327.
- [13] Bankey V, Upadhyay PK, Da Costa DB, Bithas PS, Kanatas AG, Dias US. Performance Analysis of Multi-Antenna Multiuser Hybrid Satellite-Terrestrial Relay Systems for Mobile Services Delivery. *IEEE Access*. 2018; 6: 24729–24745.
- [14] Aiyetoro G, Takawira F, Walingo T. Near-optimal packet scheduling scheme in satellite LTE networks. *IET Commun.* 2017; 11(15): 2311–2319.
- [15] Peters G. Satellite delivery of next generation broadband access to the UK. In: 5th Adv. Satellite Multimedia Syst. Conf. and the 11th Sig. Process. for Space Communic. Workshop, Cagliari (Italy); 2010: 141–146.
- [16] Kyröläinen J, Hulkkonen A, Ylitalo J, Byman A, Shankar B, Arapoglou P-D, Grotz J. Applicability of MIMO to satellite communications. *Int. J. Satellite Commun. and Networking*. 2014; 32: 343–357.
- [17] Arapoglou P-D, Burzigotti P, Bertinelli M, Bolea Alamanac A, De Gaudenzi R. To MIMO or Not To MIMO in Mobile Satellite Broadcasting Systems. *IEEE Trans. Wireless Commun.* 2011; 10(9): 2807–2811.
- [18] Arapoglou P-D, Liolis K, Bertinelli M, Panagopoulos A, Cottis P, De Gaudenzi R. MIMO over Satellite: A Review. *IEEE Commun. Surveys & Tutorials*. 2011; 13(1): 27–51.
- [19] Goldsmith A. *Wireless Communications*. Cambridge (USA): Cambridge University Press; 2005.
- [20] Schwartz RT, Knopp A, Ogermann D, Hofmann CA, Lankl B. Optimum-capacity MIMO satellite link for fixed and mobile services. In: Int. ITG Workshop on Smart Antennas, Vienna (Austria); 2008: 209–216.
- [21] Zorba N, Realp M, Lagunas MA, Pérez-Neira AI. Dual Polarization for MIMO processing in Multibeam Satellite Systems. In: 10th Int. Workshop on Sig. Process. for Space Commun., Rhodes Island (Greece); 2008: 1–7.
- [22] Arapoglou P-D, Burzigotti P, Bolea Alamanac A, De Gaudenzi R. Capacity potential of mobile satellite broadcasting systems employing dual polarization per beam. In: 5th Adv. Satellite Multimedia Syst. Conf. and the 11th Sig. Process. for Space Communic. Workshop, Cagliari (Italy); 2010: 213–220.
- [23] Hofmann C, Storek K-U, Schwartz RT, Knopp A. Spatial MIMO over Satellite: A Proof of Concept. In: IEEE Int. Conf. on Commun., Kuala Lumpur (Malaysia); 2016: 1–6.
- [24] Byman A, Hulkkonen A, Arapoglou P-D, Bertinelli M, De Gaudenzi R. MIMO for Mobile Satellite Digital Broadcasting: From Theory to Practice. *IEEE Trans. Vehic. Tech.* 2016; 65(7): 4839–4853.

- [25] Alamouti SM. A Simple Transmit Diversity Technique for Wireless Communications. *IEEE J. Sel. Areas in Commun.* 1998; 16(8): 1451–1458.
- [26] Arti MK, Jindal SK. OSTBC Transmission in Shadowed-Rician Land Mobile Satellite Links. *IEEE Trans. Veh. Tech.* 2016; 65(7): 5771–5777.
- [27] Wysocki BJ, Wysocki TA. On an Orthogonal Space-Time-Polarization Block Code. *J. of Commun.* 2009; 4(1): 20–25.
- [28] Xu H, Govindasamy K, Pillay N. Uncoded Space-Time Labeling Diversity. *IEEE Commun. Lett.* 2016; 20(8):1511–1514.
- [29] Quazi T, Patel SS. USTLD Mapper Design for APSK Constellations over Satellite Channels. *Trans. Emerging Telecomm. Tech.* 2019; e3586. DOI: 10.1002/ett.3586
- [30] Vineetha PV, Kirthiga S. Analysis of Polarization Diversity for Land Mobile Satellite System. In: Int. Conf. Wireless Communic., Sig. Process. and Networking, Chennai (India); 2017: 1268–1271.
- [31] Aparna M, Vineetha PV, Kirthiga S. Channel Modeling and Estimation of Polarized MIMO for Land Mobile Satellite Systems. In: Int. Conf. on Advances in Computing, Communic. and Informatics, Udupi (India); 2017: 299–304.
- [32] Patel SS, Quazi T, Xu H. High-Rate Uncoded Space-Time Labelling Diversity with Low-Complexity Detection. *Trans. Emerging Telecomm. Tech.* 2018; under review.
- [33] Digital Video Broadcasting. Second generation framing structure, channel coding and modulation systems for Broadcasting, Interactive Services, News Gathering and other broadband satellite applications; Part 2: DVB-S2 Extensions (DVB-S2X). *European Telecomm. Standards Inst.* 2014; EN 302 307-2 V1.1.1.
- [34] Romero-Jerez JM, Lopez-Martinez FJ. A New Framework for the Performance Analysis of Wireless Communications Under Hoyt (Nakagami-q) Fading. *IEEE Trans. Inf. Theory.* 2017; 63(3): 1693–1702.
- [35] Simon MK, Alouini M-S. *Digital Communication over Fading Channels: A Unified Approach to Performance Analysis.* New York (USA): John Wiley & Sons, Inc.; 2000.
- [36] Patel SS, Quazi T, Xu H. Error performance of Uncoded Space Time Labelling Diversity in spatially correlated Nakagami-q channels. *Int. J. Commun. Syst.* 2018; 31(12): e3720. <https://doi.org/10.1002/dac.3720>.
- [37] Chytil B. The distribution of amplitude scintillation and the conversion of scintillation indices. *J. Atmospheric and Terrestrial Phys.* 1967; 29(9): 1175–1177.

- [38] Patel SS, Quazi T, Xu H. A Genetic Algorithm for Uncoded Space-Time Labelling Diversity Mapper Design. In: Proc. IEEE Int. Workshop on Signal Process. Syst., Cape Town (South Africa); 2018: 77–82.
- [39] Huang Y, Ritcey JA. Improved 16-QAM constellation labeling for BI-STCM-ID with the Alamouti scheme. *IEEE Commun. Letters*. 2005; 9(2): 157–159.
- [40] Huang Y, Ritcey JA. Optimal constellation labeling for iteratively decoded bit-interleaved space-time coded modulation. *IEEE Trans. Inf. Theory*. 2005; 51(5): 1865–1871.
- [41] Quazi T, Xu H. BER Performance of a Hierarchical APSK UEP System over Nakagami-m fading channels. 2016; 107(4):230–236
- [42] Park B, Jin S, Jeong D, Kim J, Cho Y, Moon K, Kim B. Highly Linear mm-Wave CMOS Power Amplifier. *IEEE Trans. Microwave Theory and Techniques*. 2016; 64(12): 4535–4544.
- [43] Cormen TH, Leiserson CE, Rivest RL, Stein C. *Introduction to Algorithms*. Cambridge (USA): The MIT Press; 2009. ISBN 978-0-262-03384-8.
- [44] Kermoal JP, Schumacher L, Pedersen KI, Mogensen PE, Frederiksen F. A stochastic MIMO radio channel model with experimental validation. *IEEE J. Sel. Areas in Commun.* 2002; 20(6): 1211–1226.
- [45] Hedayat A, Shah H, Nosratinia A. Analysis of Space-Time Coding in Correlated Fading Channels. *IEEE Trans. Wireless Commun.* 2005; 4(6): 2882–2891.
- [46] Reşat MA, Özyurt S. Performance of Zero-Forcing MIMO Systems with Signal Space Diversity under Transmit Antenna Correlation. In: 10th Int. Conf. on Elec. and Electron. Eng.(ELECO), Bursa (Turkey); 2017: 700–704.
- [47] Aalo VA. Performance of Maximal-Ratio Diversity Systems in a Correlated Nakagami-Fading Environment. *IEEE Trans. Commun.* 1995; 43(8): 2360–2369.
- [48] Albdran S, Alshammari A, Matin MA. Spectral and energy efficiency for massive MIMO systems using exponential correlation model. In: IEEE 7th Annual Comp. and Commun. Workshop and Conf. (CCWC), Las Vegas, NV (USA); 2017.
- [49] Loyka, SL. Channel capacity of MIMO architecture using the exponential correlation matrix. *IEEE Commun. Lett.* 2001; 5(9): 369–371.
- [50] Patel SS, Quazi T, Xu H. Optimal Antenna Spacings for Uncoded Space-Time Labelling Diversity Systems with Linear and Non-Linear Antenna Configurations. In: Proc. Southern Africa Telecom. Networks and Applications Conf. (SATNAC), Arabella, Hermanus (South Africa); 2018: 86–91.
- [51] Akoun PO, Xu H. Optimal error analysis of receive diversity schemes on arbitrarily correlated Rayleigh fading channels. *IET Commun.* 2016; 10(7): 854–861.

- 
- [52] Meyer CD. *Matrix Analysis and Applied Linear Algebra*. Philadelphia (USA): Society for Industrial and Applied Mathematics; 2000. ISBN: 978-0-898714-54-8
- [53] Craig JW. A new, simple, and exact result for calculating the probability of error for two-dimensional signal constellations. In: IEEE Military Commun. Conf. (MILCOM), McLean, VA (USA); 1991: 571–575.
- [54] Samra H, Ding Z, Hahn P. Symbol Mapping Diversity Design for Multiple Packet Transmissions. *IEEE Trans. Commun.* 2005; 53(5): 810–817.
- [55] Seddik KG, Ibrahim AS, Liu KJR. Trans-Modulation in Wireless Relay Networks. *IEEE Commun. Lett.* 2008; 12(3): 170–172.
- [56] Krasicki M. Essence of 16-QAM labelling diversity. *IET Electronics Lett.* 2013; 49(8): 567–569.
- [57] Hahn PM, Grant TL. Lower Bounds for the Quadratic Assignment Problem based upon a Dual Formulation. *Oper. Res.* 1998; 46(6): 912–922.
- [58] Ahmed ZH. An Improved Genetic Algorithm using Adaptive Mutation Operator for the Quadratic Assignment Problem. In Proc. 38th Int. Conf. Telecomm. and Sig. Process., Prague (Czech Republic); 2015. DOI: 10.1109/TSP.2015.7296481.
- [59] Zhang H, Dai H, Zhou Q, Hughes BL. On the Diversity Order of Spatial Multiplexing Systems With Transmit Antenna Selection: A Geometrical Approach. *IEEE Trans. Inf. Theory.* 2006; 52(12): 5297–5311.

## Chapter 5

# Concluding Remarks

In this thesis, USTLD model has been enhanced to increase its spectral efficiency and link reliability. One of the enhanced USTLD systems has been specifically developed for satellite broadcasting. Furthermore, the practical considerations of detection complexity and correlation have been studied for the proposed systems. Table 5.1 provides a summary of the key results obtained from the research presented.

In Chapter 2, the HR-USTLD system was proposed. HR-USTLD enhanced the spectral efficiency of the USTLD system by drawing inspiration from the V-BLAST architecture and adding more transmission streams to the transmitter. This was achieved by extending the USTLD model to allow for  $N_{Tx} \geq 2$  transmit antennas and performing spatial multiplexing. This allows an HR-USTLD system utilising an  $M$ -ary modulation scheme to achieve a data rate of  $0.5N_{Tx} \log_2 M$  bits/sec/Hz. An analytical bound for the bit error performance of HR-USTLD systems was derived and verified by simulated results. When comparing the error performance of USTLD-based systems with a 6 bits/sec/Hz data rate, results showed that HR-USTLD achieves a 4dB performance improvement over the closest other scheme considered.

The computational complexity when performing MLD on the HR-USTLD system increases exponentially with the number of transmit antennas used. Thus, Chapter 2 also studied the adaptation of existing QRD-based LCDAs for HR-USTLD. Direct adaptation of the existing LCDAs was found not to achieve optimal detection accuracy, therefore a new LCDA designed specifically for USTLD systems (MSRSD-USTLD) was developed. MSRSD-USTLD was shown to achieve detection accuracy comparable to MLD for the  $4 \times 4$  16QAM and  $4 \times 5$  16PSK systems considered. Additionally, when compared to MLD, MSRSD-USTLD reduced the number of effective real operations performed during the detection by 79.75% and 92.53% for the respective 16QAM and 16PSK systems.

A further consequence of increasing the number of transmit antennas in the USTLD system is that limited available space on devices results in antennas being positioned closer together. It is thus pertinent to study the effect of antenna correlation on USTLD systems. Chapter 3 presented an analysis of the error performance of USTLD systems in both uncorrelated and correlated Nakagami- $q$

TABLE 5.1: Summary of Key Results

Chapter 2	<p>The proposed HR-USTLD system is able to achieve higher data rates than the original USTLD system.</p> <p>The data rate of a HR-USTLD system increases linearly with the number of transmit antennas used.</p> <p>The complexity of performing MLD on a HR-USTLD system increases exponentially with the number of transmit antennas used and is <math>\mathcal{O}(N_{\text{Tx}}N_{\text{Rx}}M^{N_{\text{Tx}}})</math>.</p> <p>When compared to similar USTLD systems of the same data rate, HR-USTLD achieves superior error performance (for all systems tested).</p> <p>The proposed MSRSD-USTLD low-complexity detection algorithm is able to achieve MLD detection accuracy, and reduces complexity by more than 79% for all systems tested.</p>
Chapter 3	<p>Antenna correlation causes a degradation in the error performance of USTLD systems.</p> <p>USTLD systems are more sensitive to antenna correlation at the transmitter than at the receiver.</p> <p>It is theoretically optimal to space antennas <math>0.4\lambda</math> apart in a USTLD system, where <math>\lambda</math> is the wavelength of the transmission carrier.</p>
Chapter 4	<p>The proposed STPLD system achieves twice the diversity order of USTLD systems.</p> <p>STPLD systems are more sensitive to transmit antenna correlation than receive antenna correlation.</p> <p>IBI has a dominant effect on error performance at the STPLD receiver.</p> <p>Neither IAI nor IBI have a dominant effect on error performance at the STPLD transmitter.</p> <p>A genetic algorithm that is able to design labelling diversity mappers for any generic constellation is designed.</p> <p>The MLD detection complexity of the STPLD system is <math>\mathcal{O}(4N_{\text{Rx}}M^2)</math>.</p>

fading environments. Analytical expressions for the error performance of these systems were derived and corroborated by Monte Carlo simulations. The study concluded that USTLD systems are more sensitive to antenna correlation at the transmitter than at the receiver. Results indicated that an antenna spacing of  $0.4\lambda$  is theoretically optimal, where  $\lambda$  is the transmission carrier wavelength. It was also shown that USTLD systems are more susceptible to the effects of antenna correlation than the comparable Alamouti space-time block coded system.

Chapter 4 proposed the STPLD system, which improves upon USTLD through the inclusion of polarisation diversity. The STPLD system was designed for satellite broadcasting and utilised APSK constellations to encode data from the latest DVB-S2X satellite broadcasting standard. Previous works on labelling diversity systems did not include mapper designs for these APSK constellations. Additionally, the approaches to mapper design presented in literature were constrained by the size and shape of the considered constellations. To overcome these challenges, a genetic algorithm capable of designing mappers for any generic constellation was developed. The genetic algorithm was implemented to design labelling diversity mappers for the APSK constellations studied. The use of

these mappers were able to contribute gains of between 5dB and 7dB due to labelling diversity for the  $2 \times 2$  16APSK,  $2 \times 4$  32APSK and  $2 \times 2$  64APSK systems considered.

Due to polarisation diversity, it was shown that STPLD systems achieve twice the diversity order of USTLD systems. However, the implementation of polarisation diversity would result in the problem of inter-beam interference in a real-world system. To this end, analytical expressions for the STPLD system considering both uncorrelated and correlated conditions were derived and verified using simulated results. Thereafter, a correlation study of the STPLD system considering both inter-beam and inter-antenna interference was presented. By studying a  $2 \times 3$  8APSK STPLD system, it was concluded that STPLD systems are more susceptible to correlation at the transmitter than at the receiver, It was also concluded that IAI and IBI are equally important to consider at the transmitter, whereas IBI has a dominant effect on error performance at the receiver.